

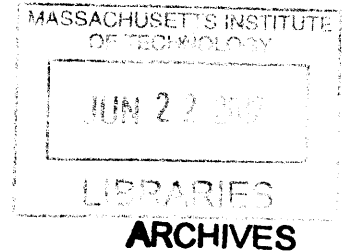
The Effect of Geometry and Topology on the Mechanics of Grid Shells

by

Samar Rula Malek

B.S. Civil Engineering
Johns Hopkins University, 2002

S.M. Civil and Environmental Engineering
Massachusetts Institute of Technology, 2007



Submitted to the Department of Civil and Environmental Engineering
in Partial Fulfillment of the Requirements for the Degree of

Doctor of Philosophy in the Field of Structures and Materials
at the Massachusetts Institute of Technology

June 2012

© 2012 Massachusetts Institute of Technology. All rights reserved.

Signature of Author: _____
Department of Civil and Environmental Engineering
May 1 2012

Certified by: _____
John A. Ochsendorf
Associate Professor of Building Technology and Civil and Environmental Engineering
Thesis Co-Supervisor

Certified by: _____
Tomasz Wierzbicki
Professor of Applied Mechanics
Thesis Co-Supervisor

Certified by: _____
Pedro M. Reis
Assistant Professor of Civil and Environmental Engineering and Mechanical Engineering
Thesis Reader

Accepted by: _____
Pedro M. Reis
Chair, Departmental Committee for Graduate Students

The Effect of Geometry and Topology on the Mechanics of Grid Shells

by

Samar Rula Malek

Submitted to the Department of Civil and Environmental Engineering
on May 1, 2012 in Partial Fulfillment of the Requirements for the Degree of
Doctor of Philosophy in the Field of Structures and Materials

Abstract

The use of grid shell structures in architecture and structural engineering has risen in the past decade, yet fundamental research on the mechanics of such structures is lacking. Grid shells are long span structures comprised of a lattice of single layer members forming a curved surface. Grid shells can be made of a wide range of materials from steel to wood. They have potential to be used in readapting existing spaces or in new aesthetically pleasing structures. By studying their mechanics, engineers can be more effective at the schematic phase of design so that the potential of grid shells can be maximized.

This research conducts a parametric study that varies the topology and topography of grid shells. The parametric space is framed around real-world design constraints including the grid spacing, panel shape, span-to-height ratio and the use of double curvature.

In this thesis, the buckling capacity is evaluated using finite element analysis for two typical grid shell geometries: the spherical cap and the corrugated vault. First, a spherical cap is considered for which an analytical solution exists and therefore the accuracy of the numerical procedure is validated. Simple closed-form solutions are derived using the concept of the equivalent continuum and compared to the numerical models. Then, the parametric study of the spherical cap is performed including variations of the grid spacing, the span to height ratio and the panel shape (triangles and quadrilaterals).

Having determined the efficiency of the computational tool the study is extended to the barrel vault. Here the new features of the analysis are the use of double curvature by introducing corrugation along the edge and the crown. By understanding the fundamental mechanical behavior of grid shells, design guidelines aimed to maximize their capacity and efficiency and intended to facilitate the discussion between architect and engineer are proposed.

Thesis Co-Supervisor: John A. Ochsendorf

Title: Associate Professor of Building Technology and Civil and Environmental Engineering

Thesis Co-Supervisor: Tomasz Wierzbicki

Title: Professor of Applied Mechanics

Thesis Reader: Pedro M. Reis

Title: Assistant Professor of Civil and Environmental Engineering and Mechanical Engineering

Acknowledgments

I am most grateful to the guidance I have received from my co-supervisors, Professors Wierzbicki and Ochsendorf. Thank you John for setting the example on how to pursue research passions, how to empower students and how kindness can be an incredible motivating force. I cannot thank you enough for giving me the generous opportunity to teach your class and for extending your network of amazing scholars, engineers and architects.

Thank you Professor Wierzbicki for teaching me mechanics! For allowing me to be your teaching assistant and your officemate. More importantly thank you for the countless hours of discussion and advice on this dissertation, mechanics, academia, ... and classical music. Thank you Professor Pedro Reis for your sincere enthusiasm, encouragement, advice and for serving on my committee.

A heartfelt thank you to my undergraduate mentor Professor Roger Ghanem who introduced me to research starting my freshman year of college and whose guidance opened the door to MIT. Thank you for your generosity with all the research and academic opportunities.

Thank you to my sources of funding and support and people who have influenced my professional development: The Martin Family Fellowship for Sustainability; Professor John Fernandez & the Building Technology Program; Kris Kipp & Department of Civil and Environmental Engineering; Duncan Kincaid & CRON; the Department of Mechanical Engineering; ODGE & MSRP; the GSC Travel Grant; Kim Bernard, Professor Linn Hobbs & GECD.

Thank you to my students - from JHU to Teach for America to CMHS to TutoringPlus to MIT, and to my friends and colleagues who have supported me along the way: Tia Letras, Bryna Chen, Mira Chokshi, Dr. David Quinn, Marcia, Diana Chien, Caitlin Mueller, Rory Clune, Dr. Jenn Zessin, and Dr. Elham Sahraei.

A special thank you to Dr. Alejandra Menchaca-Brandan and Monica Orta for being amazing, smart, funny people. Thank you Alex for the years of so many good memories and for always being there. Thank you Monica for introducing me to MSRP - the best part of my MIT experience - and for being my 'rock'.

Lastly, thank you to my family. To mom and dad, for leaving their country and sacrificing their families to give their kids a better opportunity. To my sister Alia for being the first to set the example to follow. To my brother Hussam for giving me the childhood memories to reminisce on. To my brother-in-law Nilesh for being the '4th' sibling to read my essays, but more importantly for being a great dad to my niece. To my sister Rana whose love and unconditional support I could not live without, but most especially for bringing Manal into this world. To the joy of my life and my reason to persevere, Manal (and my future second niece) - I love you!

Table of Contents

List of Figures	8
List of Tables	12
1 Introduction	14
1.1 Motivation	14
1.1.1 Definition of Grid Shell	14
1.1.2 Advantages of Grid Shells	15
1.1.3 Unresolved Questions	18
1.2 Problem Statement	21
1.2.1 Current Design of Grid Shells	21
1.2.2 Thesis Goals	21
1.2.3 Approach	22
1.3 Outline of Chapters	23
2 Literature Review	25
2.1 Introduction	25
2.2 Structural Design	25
2.2.1 Design Constraints	26
2.2.2 Design Analysis	28
2.3 Structural Mechanics	29
2.3.1 Numerical Methods	29
2.3.2 Analytical Methods	30
2.4 Summary	32
3 Methodology	34
3.1 Procedure for Parametric Study	34
3.1.1 Parameters and Test Geometries	35
3.1.2 Numerical and Analytical Methods	35
3.2 Computational Model Verification	37
3.2.1 2D Arch Study	39
3.2.2 Grillage Study	45

Table of Contents

3.3	Summary	47
4	Spherical Cap Grid Shell Study	48
4.1	Introduction	48
4.2	Problem Definition	49
4.2.1	Parameters	50
4.2.2	Numerical Approach	50
4.2.3	Analytical Approach	51
4.3	Results	54
4.3.1	Model Verification	54
4.3.2	Collapse Analysis	55
4.3.3	Numerical Results	56
4.3.4	Analytical Results	58
4.3.5	Numerical and Analytical Results	59
4.4	Discussion	60
4.5	Summary	62
5	Corrugated Vault Study	64
5.1	Introduction	64
5.2	Problem Definition	65
5.2.1	Geometry	65
5.2.2	Parameters	66
5.2.3	Methodology	68
5.2.4	Analytical Models	70
5.2.5	Numerical Models	72
5.3	Results	75
5.3.1	Model Validation	76
5.3.2	Continuous Shell	76
5.3.3	Grid Shell	84
5.4	Discussion	92
5.5	Summary	93
6	Conclusions	94
6.1	Summary of Contributions	94
6.2	Future Work	95
A	MATLAB Code	97
A.1	Spherical Cap - Quadrilateral Grid	97
A.2	Spherical Cap - Triangular Grid	105
A.3	Corrugated Vault - Continuous Shell	112
A.4	Corrugated Vault - Quadrilateral Grid	116
A.5	Corrugated Vault - Triangular Grid	121

Table of Contents

B Equivalent Continuum 126

Bibliography 128

List of Figures

1.1	The Great Court grid shell at the British Museum.	15
1.2	Examples of grid shells.	17
1.3	Quadrilateral grid at the National Portrait Gallery (left); triangular grid at the Great Court (right).	19
1.4	Coarse grid at the National Portrait Gallery (left); dense grid at the Mannheim Multihalle (right).	20
1.5	Shallow shell at the Odeon in Munich (left); steeper shell at the Museum for Hamburg History (right).	20
1.6	The Japan Pavilion (left); the National Portrait Gallery (right).	21
1.7	The current design process of grid shells (two figures reproduced from (Harris et al., 2008)).	22
1.8	Proposed contributions of this dissertation to the design process of grid shells.	23
2.1	The British Museum.	26
2.2	External view of the Kogod Courtyard grid shell at the National Portrait Gallery.	27
2.3	External view of the Neckarsulm Swimming Arena.	27
2.4	Equivalent continuum example defined by an equivalent volume.	31
3.1	Values and illustration of the varied parameters.	36
3.2	Examples of the spherical cap and the corrugated barrel vault as grid shells.	36
3.3	Examples of the continuous shell and the grid shell finite element model for the spherical cap and the barrel vault.	37
3.4	Examples of the inputted undeformed finite element model and the ADINA output of the first buckling mode (magnified at a maximum factor of 4500).	38
3.5	2D geometry of the pinned-pinned arch.	40
3.6	The three competing failure modes (buckling, snap-through, yielding) of an arch as a function of the span-to-height ratio.	40
3.7	Monotonic convergence of the strain energy for a simply supported beam with a distributed load.	42
3.8	The strain energy convergence of a pinned-pinned arch with a normally distributed load.	42
3.9	Comparison of the arch deflection under uniform distributed loading between a coarse and a dense mesh.	42

List of Figures

3.10	Force displacement plot as a function of increasing mesh density.	42
3.11	Comparison of the theoretical buckling load (Equation 3.1c) to the numerical linearized buckling analysis.	44
3.12	Comparison of linear and nonlinear buckling analysis for two scaled magnitudes (ϕ) of imperfection.	44
3.13	Comparison of the buckling load for the circular (C) and parabolic (P) arch with a normally (N) and vertically (V) distributed load.	45
3.14	Comparison of the theoretical buckling load for a distributed load and the numerical buckling load for point loading.	45
3.15	Finite element representation of rigid ends.	46
3.16	Grillage case study.	46
4.1	Spherical cap grid shell.	49
4.2	A hierarchal tree illustrating the number of models for the spherical cap study.	50
4.3	Illustration of the six combinations of the panel shape and spacing.	51
4.4	Example of the spherical cap grid shell finite element model with $\frac{L}{h}=6$	52
4.5	The quadrilateral and triangular topology and their repeating units (the cruciform and the hexagon).	53
4.6	Comparison of the numerical and the theoretical buckling load of a continuous spherical cap using axisymmetric shell elements.	55
4.7	Error in the numerical buckling load to the analytical when the loading is applied as a point load and a pressure load.	55
4.8	Comparison of the collapse load to the linearized buckling load for a spherical cap of $\frac{L}{h} = 20$	56
4.9	The buckling capacity of the spherical cap as a function of the grid spacing for the quadrilateral grid (left) and the triangular grid (right).	57
4.10	First buckling mode of spherical cap with $\frac{L}{h} = 20$ and a spacing of $s = 30in$: quadrilateral topology (left), and triangular topology (right) (magnified by a factor of 5000).	57
4.11	Structural efficiency of the spherical cap grid shell (Equation 4.2).	58
4.12	Comparison of the buckling load (Equation 4.1) for the four equivalent continuum definitions for a quadrilateral grid with $\frac{L}{h}=20$	59
4.13	Comparison of analytical and numerical results for the spherical cap grid shell study. The rows from top to bottom represent the topologies quadrilateral and triangular, respectively. The columns from left to right represent decreasing span-to-height ratios.	61
4.14	Design guidelines for a spherical cap grid shell. Columns from left to right represent decreasing span-to-height ratio.	62
5.1	Examples of grid shells with corrugation at the edge and the crown.	64
5.2	The four groups of parameters: corrugation location, aspect ratio, span-to-height ratio, and grid spacing (left to right).	65
5.3	Straight edge barrel vault geometry and boundary conditions	66

List of Figures

5.4	The hierarchal tree illustrating the number of corrugated grid shell models.	67
5.5	Corrugated barrel vault geometry.	68
5.6	Illustration of the eight combinations of n and β_i for the corrugated edge.	69
5.7	Geometric representation of the corrugated edge as a function of $\frac{\lambda}{a_1}$	69
5.8	Plane strain condition.	71
5.9	Corrugated shell cross-section.	71
5.10	The effect of a varied moment of inertia on the numerical factor m for the buckling load.	73
5.11	The three grid shell densities used in the corrugated vault study (10x10, 20x20, 30x30).	74
5.12	Dimensions of the grid spacing and the overlay of the repeating unit of the grid shell cruciform and the square continuous shell.	75
5.13	Plane strain validation for the continuous shell.	76
5.14	The buckling mode for the continuous shells magnified by a factor of 400.	76
5.15	Plane strain validation for the grid shell.	77
5.16	The first buckling mode of the straight vault for each of the three grid shell densities (magnified by a factor of 1000).	77
5.17	Gain in capacity from the straight barrel vault by corrugating the edge of the continuous shell.	78
5.18	Gain in capacity from the straight barrel vault by corrugating the crown for the continuous shell.	78
5.19	First buckling mode for the corrugated edge case with increasing corrugation from top to bottom (magnified by a factor of 500).	79
5.20	Illustration of the effective arclength α_{eff}	80
5.21	A matrix of plots highlighting the gain in capacity from the straight barrel vault by using in-phase corrugation for the continuous shell. The rows represent the increase in corrugation amplitude by β_i and the columns represent the number of waves n	82
5.22	Comparison of the numerical results of the corrugated crown and the in-phase to the analytical (Equation 5.8) for the continuous shell.	83
5.23	Comparison of the gain in capacity in terms of the percent volume increase from the straight vault for the continuous shell.	85
5.24	Comparison of the collapse load and the buckling load for a normally distributed load (N) and a vertically distributed load (V) for the in-phase continuous shell.	86
5.25	Gain in capacity by corrugating the edge of the 30x30 grid shell.	86
5.26	The effect of varying the grid density for the corrugated edge grid shell.	88
5.27	Gain in capacity by corrugating the crown of the 30x30 grid shell.	89
5.28	Gain in capacity by in-phase corrugation of the 30x30 grid shell.	90
5.29	Comparison of the gain in capacity in terms of percent volume increase from straight vault for the grid shell for all three corrugation locations (edge, crown and in-phase).	91

List of Figures

5.30 Set of design guidelines to be used in the early stages of design of a corrugated
grid shell vault. 93

List of Tables

1.1	Some grid shells built in the past 30 years.	16
1.2	Examples showing the range of the size and materials of grid shells.	18
2.1	Summary of previous research on the equivalent continuum.	32
3.1	Comparison of the analytical and numerical tip deflection w_o using both the beam and plate models for the grillage.	47
4.1	The equivalent thickness (t_{eq}) relations for the quadrilateral and the triangle using the four equivalent definitions.	54
5.1	Equations for calculating α_{eff} given a span-to-height ratio and an aspect ratio of corrugation.	81
5.2	Maximum value of $\frac{\lambda}{a_1}$ to increase the capacity of thte corrugated edge by at least 50%.	87
5.3	Maximum values of $\frac{\lambda}{a_1}$ and $\frac{\lambda}{a_2}$ to increase the capacity by 50% for the 30x30 grid shell.	89

Chapter 1

Introduction

The objective of this work is to evaluate the mechanical performance of grid shells and to provide design guidelines to facilitate the discussion between the architect and the engineer during schematic design. A parametric study is conducted by varying the topology and topography and calculating the change in the load-bearing capacity using both numerical and analytical methods. The parameters are studied using two key grid shell geometries: the spherical cap and the barrel vault.

1.1 Motivation

In the year 2000 the Great Court grid shell at the British Museum (Figure 1.1) opened and quickly became one of the most photographed, and visited public spaces in London. While it was not the first grid shell, its popularity and success propelled grid shells into both the public and the professional architectural and engineering conscience. Since then there has been a rise in the number of grid shells built. Table 1.1 lists grid shells that have built since the year 1975.

1.1.1 Definition of Grid Shell

The term *grid shell* is defined more recently as “a structure with the shape and strength of a double curvature shell, but made of a grid instead of a solid surface. These structures can cross large spans with very few material. They can be made of any kind of material - steel, aluminum, wood or even cardboard tubes” (Douthe et al., 2006). The terms “lattice shell” and “reticulated shell” have also been used to describe grid shells but more by the

1.1. Motivation



Figure 1.1 – The Great Court grid shell at the British Museum.

academic community and not practicing engineers. There is a debate if a grid shell is defined by its structural action, or by its construction process. For example, grid shells made from wood are formed by laying the lattice flat and then either pushing or dropping the shell into place as was done in the Mannheim Multihalle (Happold and Liddell, 1975), and the Weald and Downland Museum (Wells, 2001), respectively. For this thesis, a grid shell is defined to be a long span structure comprised of a network of members creating the single layer “grid” that forms the curved surface “shell”.

1.1.2 Advantages of Grid Shells

Grid shells are an efficient means of spanning space. They have been used to cover both existing spaces such as the Cabot Circus (Figure 1.2a) and new spaces like the Savill Garden Visitor Center (Figure 1.2b). They have been used as stand-alone structures as seen in the Weald and Downland Museum (Figure 1.2c).

The benefits of using a grid shell compared to either the conventional slab and frame system or the continuous shell are both aesthetical and structural. Grid shells create dramatic spaces by pulling the eye to heights higher than the building top, and by articulating the space with its discretized topology. They create beautiful spaces because they

Chapter 1. Introduction

Table 1.1 – Some grid shells built in the past 30 years.

Year	Structure	Location
1975	Mannheim Multihalle	Mannheim, Germany
1989	Museum for Hamburg History	Hamburg, Germany
1989	Swimming Arena Neckarsulm	Neckarsulm, Germany
1994	Meeting Hall Flemish Council	Brussels, Belgium
1996	Zoo Berlin Hippo House	Berlin, Germany
1998	DZ-Bank	Berlin, Germany
2000	Great Court	London, United Kingdom
2000	Japan Pavilion Hanover Expo	Hanover, Germany
2001	Porticullis House	London, United Kingdom
2002	Weald and Downland Museum	West Sussex, United Kingdom
2002	German Historical Museum	Berlin, Germany
2005	Fiera Milano	Milan, Italy
2006	Berlin Main Train Station	Berlin, Germany
2007	Kogod Courtyard	Washington DC, USA
2007	Savill Gardens	Egham, UK
2007	Odeon Courtyard	Munich, Germany
2007	Golden Terraces	Warsaw, Poland
2008	Cabot Circus Roof	Bristol, United Kingdom
2009	Palacio de Comunicaciones	Madrid, Spain
2011	Centre Pompidou-Metz	Metz, France
2011	National Maritime Museum	Amsterdam, Netherlands

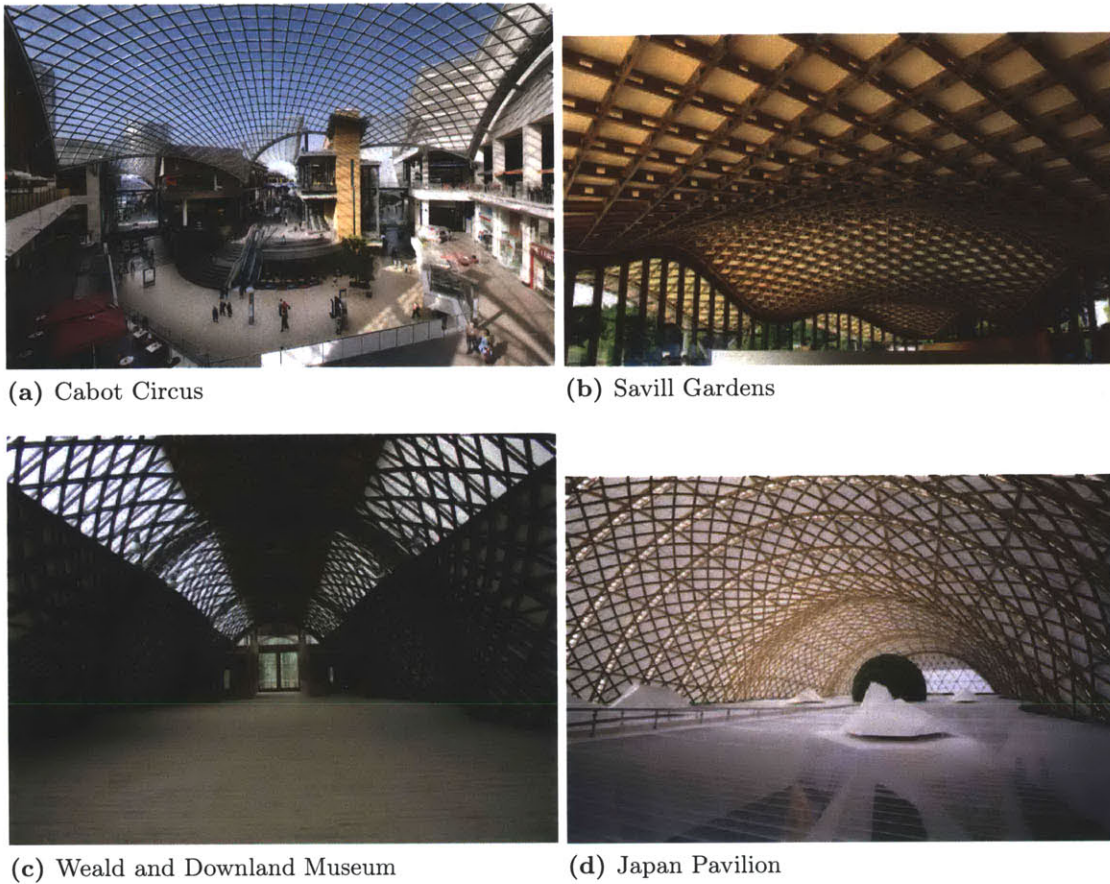


Figure 1.2 – Examples of grid shells.

are light and airy due to their efficient use of material, single layer members, and openings. Their fairly simple construction of members and nodes create shell-like structures without the arduous process of form work and pouring.

Grid shells also differ from conventional frame systems and continuous shells in that they can create more sustainable design by lowering embodied energy and by reducing operating energy. In 2008, the UK adopted the Climate Change Act which calls for an 80% reduction in CO₂ emission by 2050 (Parliament, 2008). Further, all new public buildings are to have zero carbon emissions by 2018. However, 60% of existing buildings in the UK will exist in 2050 and they will represent 45% of the total floor space (Delay et al., 2009). Thus effort to reduced carbon emissions is by both the refurbishments of existing buildings and the design of new ones. Further, lighting, heating and ventilation were found to be the predominant consumers of energy in UK buildings.

Chapter 1. Introduction

Grid shells facilitate sustainable development in three major ways. *(i)* They enable adaptive reuse of historic buildings, allowing open spaces to become enclosed, offering shelter, commercial, or recreational possibilities. *(ii)* They save structural material needs by over 50% compared to conventional framed structures and can be constructed of a variety of materials with lower embodied energy such as wood or cardboard tubes (Ref, 2007). *(iii)* They also admit greater natural light, harnessing the natural elements to create heating and cooling environments that are comfortable (Pople, 2002a).

Grid shells also have an unexplored potential for use as temporary buildings. For example they can be used at the Olympics, fulfilling the need for temporary large structures. Grid shells can also be used for disaster relief situations or for exhibition spaces.

Examples of grid shells that demonstrate their vast range of material, shape and function are the Great Court in London (Figure 1.1), the Weald and Downland in West Sussex (Figure 1.2c), and the Japanese Pavilion from the Hanover Exposition (Figure 1.2d). Their range of material include steel, wood and cardboard and Table 1.2 lists the range of panel shape, footprint, function and cladding seen in grid shells.

Table 1.2 – Examples showing the range of the size and materials of grid shells.

	The Great Court	Weald and Downland	Japan Pavilion
member material	steel	wood	cardboard
panel shape	triangle	triangle	quadrilateral
panel material	glass	wood & glazing	paper membrane
shell footprint	320ft x 230ft	164ft x 50ft	236ft x 114ft
function	roof	building	temporary structure

1.1.3 Unresolved Questions

Grid shells are highly complex structures as are their mechanics. For example, there is no clear understanding if a quadrilateral grid is better than a triangular. Figure 1.3 are magnified views of the National Portrait Gallery and the Great Court grid shells. In the National Portrait Gallery the members become increasingly larger as they approach the support. Whereas in the Great Court, the members are slender and not noticeably varying in size. Are grid shells bending or membrane dominated and what is the trade-off between using the quadrilateral grid versus the triangular?

1.1. Motivation

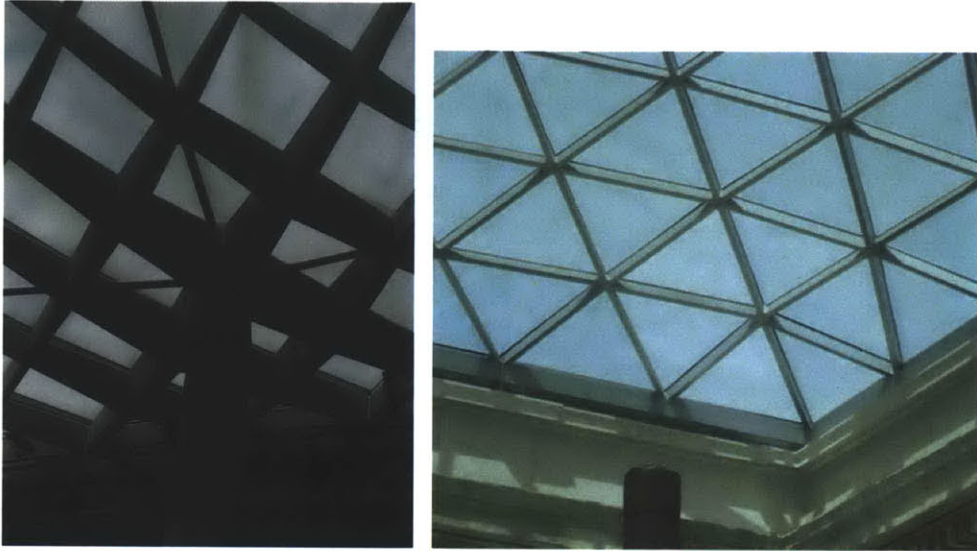


Figure 1.3 – Quadrilateral grid at the National Portrait Gallery (left); triangular grid at the Great Court (right).

The effect of topology is also dependent on the spacing. The benefit of shell structures is the additional stiffness due to curvature. Figure 1.4 juxtaposes the aerial view of the National Portrait Gallery on the left and the Mannheim Multihalle on the right. For the coarse grid on the left, the surface is more faceted, whereas on the right, the denser grid is a smoother surface. Thus, how dense must the grid be to exhibit geometric stiffness? And how does grid spacing affect the capacity?

Because geometric stiffness results from curvature, how does the span-to-height ratio affect the load bearing capacity? In Figure 1.5 the shallower shell at the Odeon in Munich is compared to the steeper shell on the right at the Museum of Hamburg History. So which structure is stronger? How does the span-to-height ratio affect the load bearing capacity and the weight required?

Chapter 1. Introduction

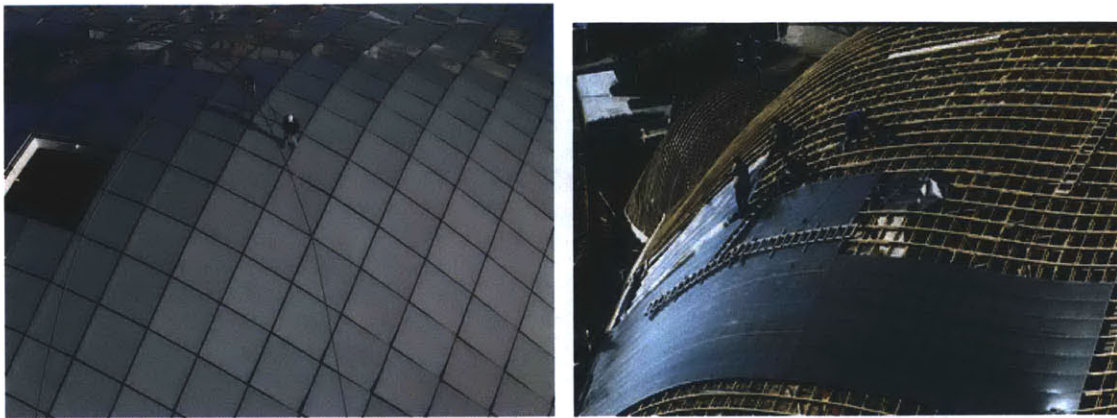


Figure 1.4 – Coarse grid at the National Portrait Gallery (left); dense grid at the Mannheim Multihalle (right).



Figure 1.5 – Shallow shell at the Odeon in Munich (left); steeper shell at the Museum for Hamburg History (right).

In addition to considering the curvature along the cross section, curvature can also be introduced along the length. In Figure 1.6, the Japan Pavilion on the left has corrugation at the crown and the edge, but at the National Portrait Gallery the corrugation is only at the crown and flattens at the perimeter. Where is the best location for corrugation to maximize the vault strength and how much corrugation is needed?

1.2. Problem Statement

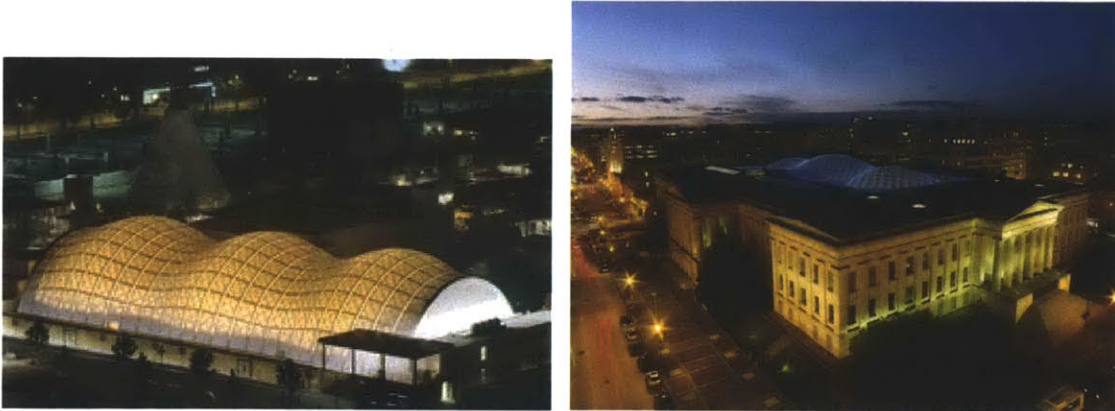


Figure 1.6 – The Japan Pavilion (left); the National Portrait Gallery (right).

1.2 Problem Statement

1.2.1 Current Design of Grid Shells

Grid shells have been designed on a case by case basis and have not been studied as a structural type. In the schematic phase of design, the key players are the architect and the client where they start the design from the architect's sketch; here the global geometry is defined purely on the aesthetics. Figure 1.7 illustrates the progression of design from schematic design (SD) to design development (DD). Currently, the engineers come in the design development phase to refine the details of the previously selected shape. The engineer at this stage has no power to make any major changes to a proposed structure.

It is therefore imperative that the questions regarding the main aspects of grid shell geometry posed in the previous section be addressed during early design stages. In order to do that there is a need to build an intuition and to develop simple expressions that can allow engineers to do back of the envelope calculations. Thus, the improved design process of grid shells will include the engineers as a key player in SD and the use of “back of the envelope” calculations in SD.

1.2.2 Thesis Goals

There is a need to evaluate the mechanical performance of grid shells during schematic design and to provide design guidelines to facilitate discussion between architect and

Chapter 1. Introduction

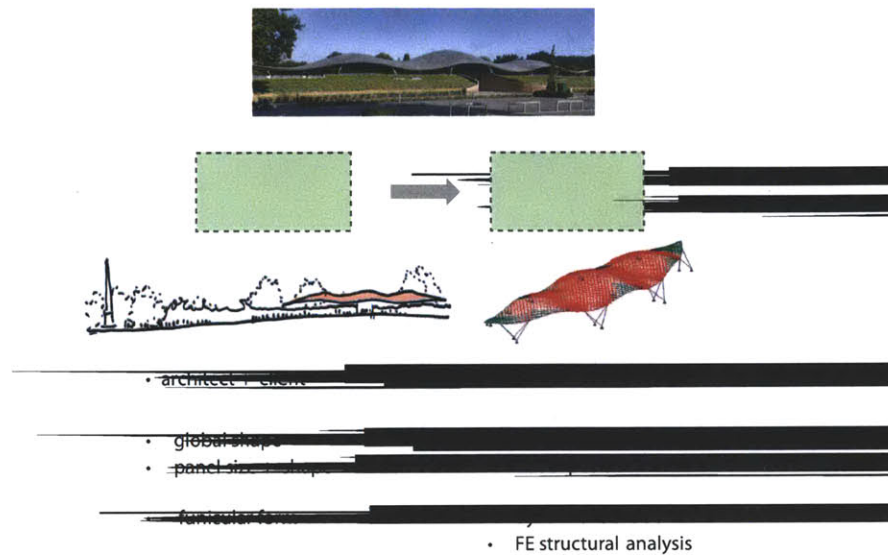


Figure 1.7 – The current design process of grid shells (two figures reproduced from (Harris et al., 2008)).

engineer (Figure 1.8). Therefore the goals of this dissertation are:

- to develop a methodology to calculate the change in load-bearing capacity of grid shells due to their curvature and topology using numerical and analytical methods;
- to provide a set of design guidelines that can contribute to maximize the mechanical performance of grid shells during early design stages.

The thesis goals can be summarized into the following three questions.

1. How do the curvature and topology affect the load-bearing capacity of grid shells?
2. How to best describe the mechanics of these structures?
3. What are the design rules of thumb to maximize grid shell performance?

1.2.3 Approach

The approach used in this thesis is to conduct a parametric study varying the topology and topography and to calculate the change in load-bearing capacity using numerical and analytical methods. Normally intuition is built from theory, experiments and case

1.3. Outline of Chapters

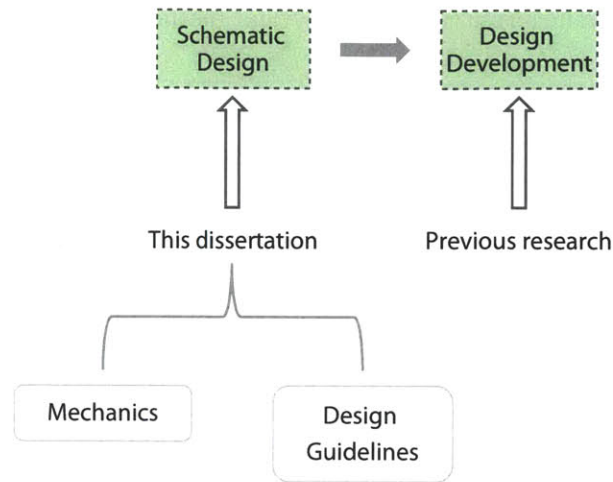


Figure 1.8 – Proposed contributions of this dissertation to the design process of grid shells.

studies. Because these structures are complex and few have been built, identifying the structural trends must rely on computational models. A parametric study is conducted on two structural shapes: the spherical cap and the barrel vault. The parameters perturbed are identified in the following Chapter as those that often drive the design process and affect both the engineering and the aesthetics of the grid shell.

1.3 Outline of Chapters

In Chapter 2 published research on grid shells from the communities of structural design and structural mechanics is presented. The literature review provides the context of this dissertation and establishes the need for this original research. It also identifies the design parameters and constraints that have the most impact on the global shape and topology that will be used in the following chapters.

In Chapter 3, the methodology for achieving the thesis goals is presented. All computational methods and modeling assumptions are also explained and verified using the commercial finite element package ADINA (Engineering, 2010).

The first of the parametric studies, the spherical cap grid shell, is presented in Chapter 4. Both analytical and numerical methods are used to determine the load-bearing capacity of the spherical cap grid shell. New equivalent continuum techniques are derived and compared. The coupling of the numerical and analytical work provides an understanding

Chapter 1. Introduction

of the mechanics of the structures. Simple analytical methods to estimate the capacity of a grid shell are also derived and presented.

In Chapter 5 the parametric study is extended to a barrel vault. The role of curvature on the load-bearing capacity is investigated by corrugating the vault. In both studies a continuous shell is first modeled so to validate the methods used. Chapter 6 concludes with the original contributions of this dissertation.

Chapter 2

Literature Review

2.1 Introduction

The objectives of this chapter are to present the key contributions of previous research done on grid shells and to provide the context for the contributions herein. There are two communities that directly and indirectly work on grid shells: the structural design community and the structural mechanics community. The structural design community consists of practicing engineers and consultants who provide firsthand experience of the design process of existing grid shells. The structural mechanics community are academics who focus more on the nonlinear analysis techniques of shells like imperfection sensitivity. First the work of the structural design community will be presented, followed by the mechanics community and conclude with a summary of the remaining open problems that this dissertation solves.

2.2 Structural Design

The structural design community provides both the overview of the design process and the detailed analysis of existing grid shells. The publications on the overall design process are authored by the structural engineers of the grid shells and describe specifically the design constraints, challenges and solutions. The more detailed papers on the mathematical progression of the grid geometry are then provided by the consultants who are tasked with writing the specific codes that map out the grid.

Chapter 2. Literature Review

2.2.1 Design Constraints

Based on the literature on built grid shells, there are three main design constraints that govern their global shape and topology: the shell height, the grid spacing, and the panel shape. In both the design of the Great Court and the Dutch Maritime Museum, the height of the shell was governed by the constraint that the shell was not to be seen from the ground (Figure 2.1a) (Anderson, 2000; Adriaenssens et al., 2010). The Great Court's shell height was further constrained because it could not be taller than the dome of the Reading Room and obstruct the view of the dome in the London skyline (Figure 2.1b).

The second and third constraints are the panel shape and subsequently its size. The topology of grid shells has differed from quadrilaterals to triangles to irregularly shaped polygons. In the case of the Great Court, the selection of the triangular grid came from the constraint that the glazing must produce a smooth flat surface (Williams, 2001). Whereas for the Kogod Courtyard grid shell at the National Portrait Gallery, the use of the quadrilateral grid and double curvature created a jagged external surface (Figure 2.2). In one built grid shell, the Neckarsulm Swimming Arena, the cladding was made of curved quadrilateral glazing so to make the surface smooth (Figure 2.3) (Schlaich and Schober, 1996).

In some cases the panel size has been determined by the panel shape and in other cases by the required strength of the grid shell. For the Great Court, the average triangular panel is seven feet because the glass triangular panels could not be manufactured at a



(a) Entrance



(b) Skyline view

Figure 2.1 – The British Museum.

2.2. Structural Design

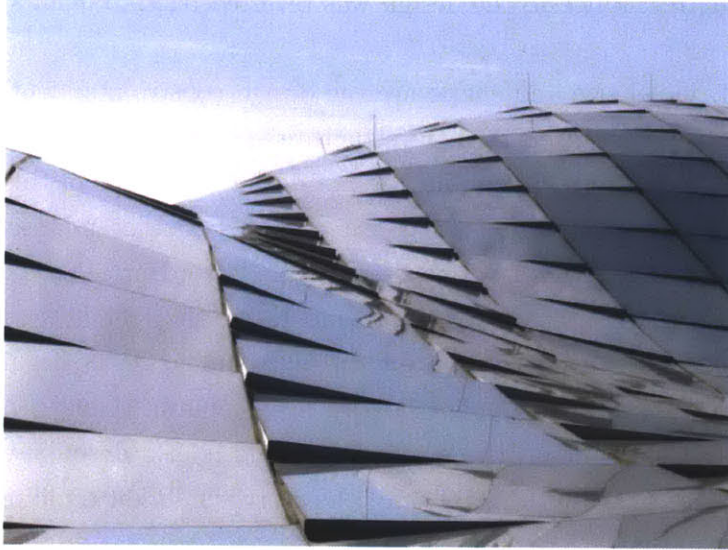


Figure 2.2 – External view of the Kogod Courtyard grid shell at the National Portrait Gallery.



Figure 2.3 – External view of the Neckarsulm Swimming Arena.

Chapter 2. Literature Review

larger size (Anderson, 2000). In the case of the Weald and Downland grid shell, the grid spacing was first varied from $0.5m$ to $1m$. However, the $1m$ spacing could not provide the required buckling resistance so the design was reverted back to $0.5m$ spacing (Harris et al., 2003).

The shell height, panel size and shape are the design constraints identified here that impact the aesthetics and engineering of the structure. There are other design constraints that are also described in these papers but are not within the scope of this thesis.

For example, another constraint is that the grid shell cannot impose any loads on the existing structures they touch (Adriaenssens et al., 2010; Hart, 2001). All the forces must be transferred to vertically supporting members. In the Dutch Maritime Museum all the loads are transferred to the courtyard corners (Keuning, 2011) and in the National Portrait Gallery the grid shell rests on a series of visible columns (Ouroussoff, 2007). The restriction to not impose loads on the existing building is also described in the design of the Portcullis House (Thornton, 2000) and the Norwich Union buildings (Stansfield, 2007).

2.2.2 Design Analysis

Grid shells are currently designed on a case by case basis. Computer codes are specifically written to define the geometry of each grid shell and to perform the structural analysis. The main method employed for mapping a grid to a surface is dynamic relaxation (Day, 1965). This method modifies the shape by monitoring the kinetic energy as the model is forced to move.

As mentioned earlier, the starting point from which the engineer is involved is after the global shape and topology have been established. For example, in the Great Court (Williams, 2001) the process of generating the final geometry began from the input of a triangular grid shell with the maximum shell height being reached between the perimeter and the Reading Room dome. A similar process was done on both the Savill Gardens and the Weald and Downland Museum (Harris et al., 2008, 2003). After Dr. Williams performed the initial form-finding analysis on the initial geometry, the edited shape was imported into a structural analysis program for the buckling analysis.

Because the global shape is established before the engineer is involved with the design, the structural design community has also looked at other ways to map the grid onto a surface by using also dynamic explicit finite element simulations (Bouhaya et al., 2010)

2.3. Structural Mechanics

or by applying fractal geometry (Vyzantiadou et al., 2007).

The geometry and structural analysis of grid shells is tedious and complex and not every design option can be investigated. Over 3000 lines of code were written specifically for the Great Court's geometry definition and structural analysis, and it took over 5000 cycles for the model to converge (Williams, 2001). There is a need for more simplified tools that can inform the engineer and architect during the Schematic Design phase.

2.3 Structural Mechanics

In the structural mechanics community it is well established that buckling is the dominant failure mode for reticulated shells (Gioncu, 1985). Research on grid shells has subsequently focused mainly on the factors influencing the buckling load like coupled instabilities, the rigidity of joints (Lpez et al., 2007), and the effect of imperfections (Balut and Gioncu, 2000; Buchert, 1965; Calladine, 1995; Hanaor, 1995; Singer and Abramovich, 1995; Sumec and Sumec, 1990). A more detailed overview of the state of the art on reticulated shells has been presented (Gioncu, 1995).

2.3.1 Numerical Methods

For example, one paper studied the effects of imperfection on the stability of barrel vaults and domes (Bulenda and Knippers, 2001). The first challenge was to define the imperfect shape. Both the static deflected shape and the first buckling mode were considered with various magnitudes. The varied parameters were the span-to-height ratio, the boundary conditions from hinged to fixed and the loading from symmetric to asymmetric.

While the span-to-height ratio was varied, the range only considered steep shells. As shown earlier in the many roof examples of grid shells, the shells are shallow. They also did not consider the effect of other design parameters mentioned in Section 2.2.1. In addition, they studied the effects on basic barrel vaults when in reality grid shells are built as corrugated vaults. In fact, until this dissertation, there has not been research on the mechanics of corrugated vault grid shells though that is what is actually built.

The main contributions of the structural mechanics community are most useful in the Design Development phase of grid shells when the nonlinear structural analysis needs to be completed. The numerical studies did not investigate the effects of the parameters (shell height, panel size and shape) most influential in the design process. There has yet

Chapter 2. Literature Review

to be an extensive parametric study that considers those parameters and also chooses realistic ranges of their values. Lastly, the majority of the research is of a numerical nature and does not provide an analytical explanation into the behavior of grid shells.

2.3.2 Analytical Methods

In Chapter 3, the analytical derivation will employ the equivalent continuum technique. The concept of equivalent thickness has been around since the 60's (Wright, 1965; Forman and Hutchinson, 1970). Previous shell mechanics research focused on assessing the buckling capacity of grid shells using an equivalent continuum idea and discrete methods. But the validation and exploration of those methods were limited to the technology of their time. The researchers also did not compare multiple equivalent continuum definitions.

First the concept of equivalent thickness is illustrated with a simple example. Given a volume of material V , the volume can be “smeared” into the shape of a spherical cap as either a thin continuous shell or into a network of bars shown in Figure 2.4.

For example, in a grid shell with a quadrilateral topology the repeating unit is a cruciform as shown in Figure 2.4. The cross sectional area $A = t_1 t_2$ is kept constant and the network of bars is equally spaced in both directions at a value of s . The equivalent thickness for a continuous shell and a grid shell to have the same volume is derived in Equation 2.1. The volumes are approximately equal because there are two negligible sources of error: the partial cruciform units at the perimeter are neglected and the volume where the members intersect is counted twice.

$$\begin{aligned} Volume_{continuous} &\approx Volume_{gridshell} \\ t_{eq} s^2 &\approx 2st_1 t_2 \\ t_{eq} &\approx \frac{2t_1 t_2}{s} \end{aligned} \tag{2.1}$$

The previous example considers an equivalence defined by volume only. However, other equivalences have been and can be established. The three previously researched methods for equivalence include equivalent stiffness, equivalent split rigidity, and orthotropic equivalence (Gioncu, 1995).

One method of equivalence is defined by an equivalent depth and an equivalent Young's Modulus (Wright, 1965; Chriss and Wright, 1978). Two cases of a spherical shell, discretized with equilateral triangles are considered: one where the members have the same

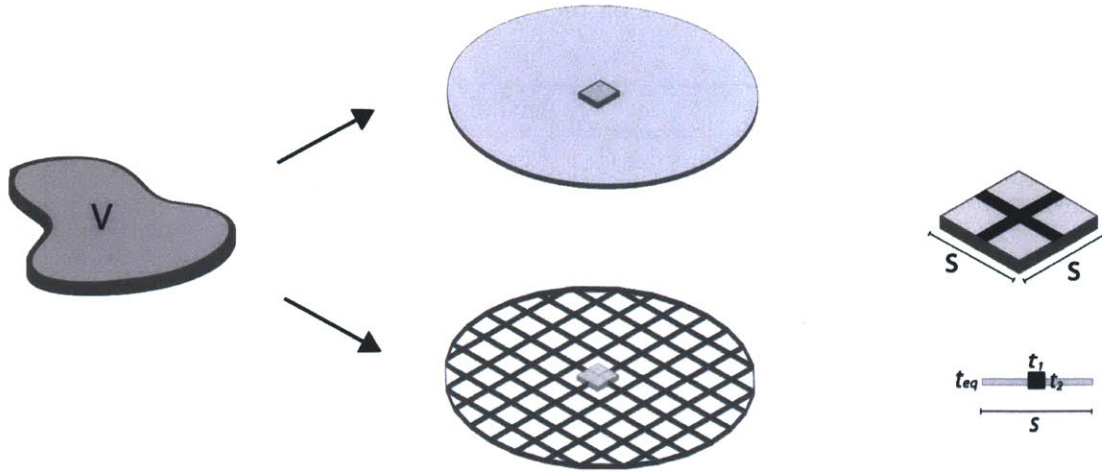


Figure 2.4 – Equivalent continuum example defined by an equivalent volume.

cross-section and another where the cross-sections are different. The methodology includes developing a relationship between the shell and bar forces, the elastic properties and the buckling criteria. After establishing an equivalent thickness, the buckling load is calculated. The proposed method was then compared to the known existing collapse loads of domes such as the Bucharest dome (Wright, 1965).

Another equivalence definition used two different thicknesses for each of the rigidities (axial and bending) (Forman and Hutchinson, 1970). The authors tested their method on a spherical cap with an equilateral triangular grid. The equivalent continuum results were compared to that of a discrete model and it was found that the accuracy had a 3-6% error depending on the slenderness of the members. For more slender members the equivalent continuum became more inaccurate. The authors called for a need of further theoretical and experimental comparisons.

Lastly, equivalence has been defined using orthotropic equivalence (Kollar and Dulacska, 1984). Here the shell buckling equation is derived for an orthotropic continuum where the orthotropic property mimics the placement of ribs in the x and y direction. While this method was proposed it was not validated on any case studies.

Table 2.1 summarizes the methods and their respective researchers. In all the works mentioned only one technique in each case was considered; the researchers did not compare their methods with each other nor tested their methods with different topologies or as a function of either the grid spacing or the shell height as is done in this dissertation.

Chapter 2. Literature Review

Table 2.1 – Summary of previous research on the equivalent continuum.

Method	Approach	Authors	Time Frame
Equivalent Stiffness	uses an equivalent depth and modulus of elasticity	(Wright, 1965; Sumec and Sumec, 1990)	1970-1990
Split Rigidity	defines two thicknesses defined by extensional and flexural deformations	(Buchert, 1965; Forman and Hutchinson, 1970)	1970
Orthotropic	derives the differential equations and rigidities	(Gioncu, 1985; Kollar and Dulacska, 1984)	1975-1985

2.4 Summary

This chapter has provided the context of this dissertation by identifying the previous research done on grid shells from two communities: the structural design and the structural mechanics communities. This chapter reviewed what research been done, the topics of interest and has highlighted the areas in which contributions need to be made. This literature review allows the following conclusions to be drawn, and motivates the corresponding contributions of this dissertation:

- The main design constraints that govern the global shape of the grid shell are the shell height, the panel size and the panel shape.
- Having established buckling as the main failure mode, research within the structural mechanics community focuses on nonlinear effects like imperfections. The implications of these effects is used in the Design Development phase when the final structural analysis is performed and not in the Schematic Design.
- While academic research on grid shells has considered the effect of some parameters on the stability of the structure, the parameters are not framed within the real design constraints nor described in a language useful for practicing architects and engineers. An extensive parametric study is needed to study the effect of real

2.4. Summary

design parameters on the load-bearing capacity of grid shells and to help build the engineer's intuition on the mechanical behavior of grid shells.

- The analysis of built grid shells is complicated and requires computer codes written specifically to the geometry of the shell. Simpler analytical methods are needed for back of the envelope calculations used by practicing structural engineers.

Chapter 3

Methodology

The methodology used to answer the research questions posed in Chapter 1 and stated again below will be presented in this chapter.

1. How do the curvature and topology affect the load-bearing capacity of grid shells?
2. How to best describe the mechanics of these structures?
3. What are the design rules of thumb to maximize grid shell performance?

The thesis goals are to conduct a parametric study varying the topology and topography and to calculate the change in the load-bearing capacity using numerical and analytical methods.

3.1 Procedure for Parametric Study

In order to achieve the thesis goals, an outline of the steps required are listed below and explained in the following subsections.

1. Identify the parameters influencing the design as defined by the real design constraints.
2. Define two geometries based on typical grid shell footprints.
3. Build a finite element model for each permutation for both the continuous shell and the grid shell.

3.1. Procedure for Parametric Study

4. Use the commercial finite element software ADINA to run a linearized buckling analysis and post-process the results.
5. Derive new analytical expressions to calculate the buckling load and compare with the numerical results.

3.1.1 Parameters and Test Geometries

The first step is to identify the parameters that drive the global shape in the design process. The parameters are the grid spacing, the panel shape, the span-to-height ratio and the use of double curvature by corrugation. All the parameters were identified and explained in Sections 1.1.3 and 2.2.1. In Figure 3.1 the parameters and their ranges are listed and illustrated.

The grid spacing is varied between 30in, 60in, and 120in. The two shapes considered are the quadrilateral grid and the triangular grid. The three span-to-height ratios considered are $\frac{L}{h} = 6, 11, 20$ representing fairly shallow shells. The use of double curvature is implemented at either the edge, the crown, or simultaneously at the crown and edge.

The effect of changing the parameters is tested on two key geometries - the spherical cap and the barrel vault and the results are presented in Chapters 4 and 5 respectively. These geometries were selected because they are often used as grid shells (Figure 3.2). The geometry, member properties, loading and boundary conditions of the spherical cap and the barrel vault will be defined later in their respective chapters.

3.1.2 Numerical and Analytical Methods

The thesis goals are achieved using both numerical and analytical methods. Engineering problems cannot always be solved with a closed-form derivation. Thus the mathematical formulation is often solved using numerical (discrete) methods. A powerful method used in engineering is the finite element method where engineering bodies are represented as discrete elements that satisfy equilibrium, compatibility, and constitutive relations. In this thesis, complex, doubly-curved structures are studied numerically using finite element modeling (FEM).

A finite element model is built for each permutation of the parameters for both a continuous shell and a grid shell. A continuous shell was modeled first to validate the computational modeling techniques and to help build the understanding of the mechanics

Chapter 3. Methodology

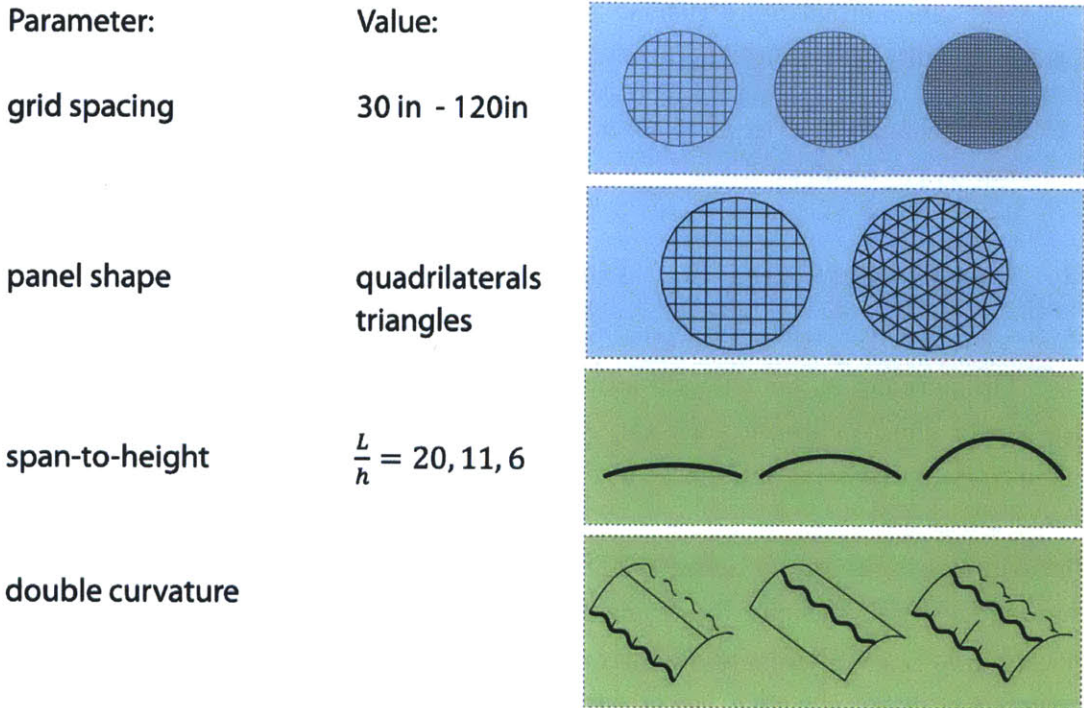


Figure 3.1 – Values and illustration of the varied parameters.

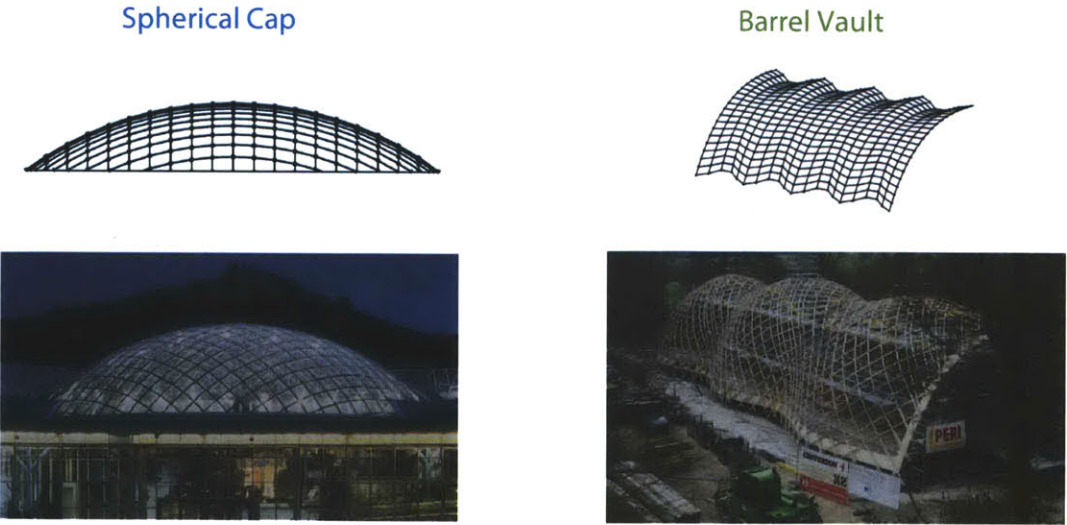


Figure 3.2 – Examples of the spherical cap and the corrugated barrel vault as grid shells.

3.2. Computational Model Verification

before complicating them further as grid shells (Figure 3.3).

The finite element models are generated using a program written by the author and provided in Appendix A. The user inputs the parameter values defined earlier and the geometry of the structure, and outputs the finite element model input file to be used in ADINA. The linearized buckling analysis is then run and the buckling load and mode are calculated. An example of the undeformed finite element model and the post-processed buckled shape are shown in Figure 3.4. The linearized buckling analysis does not account for prebuckling rotations. The linear analysis is chosen over the nonlinear analysis because it is computationally faster and similar to the predicted collapse load as will be verified in later sections. Lastly, new analytical expressions are derived to calculate the buckling load and compared with numerical results.

3.2 Computational Model Verification

In order to proceed with more complicated problems, the computational modeling techniques are validated by studying the failure modes of a 2D arch and the bending of a grillage. In establishing the accuracy of the models, the following technical questions are answered:

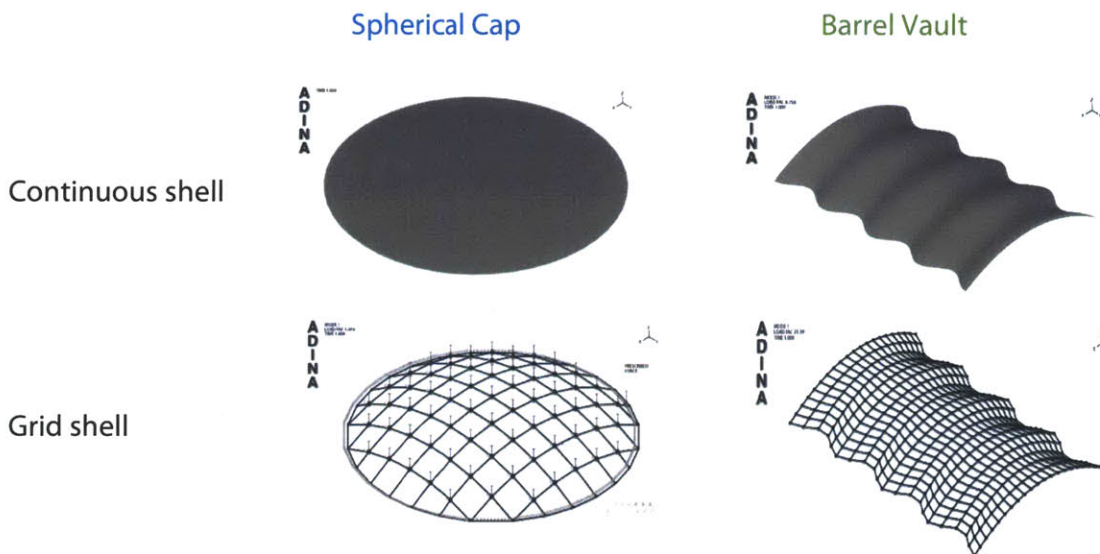


Figure 3.3 – Examples of the continuous shell and the grid shell finite element model for the spherical cap and the barrel vault.

Chapter 3. Methodology

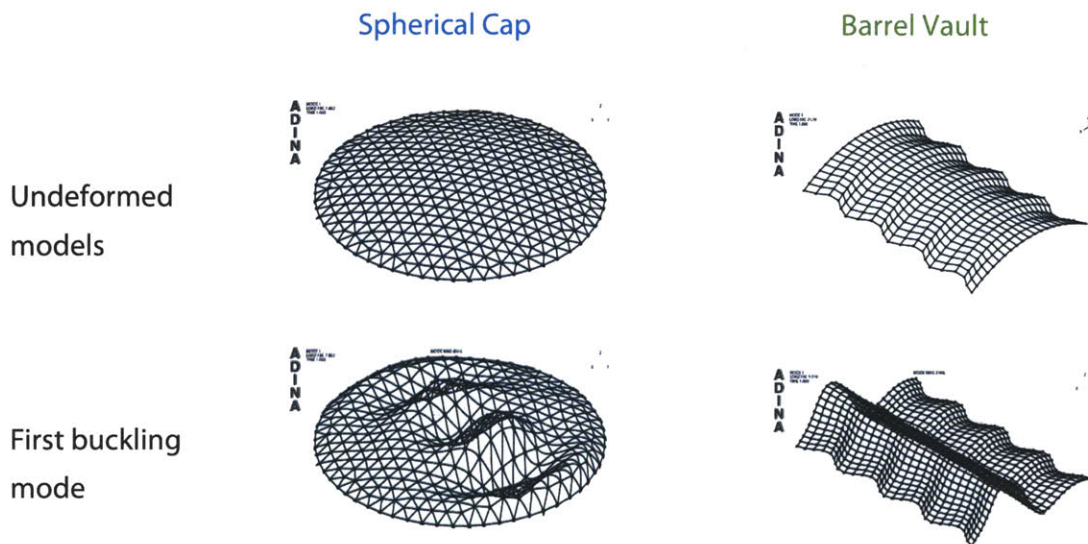


Figure 3.4 – Examples of the inputted undeformed finite element model and the ADINA output of the first buckling mode (magnified at a maximum factor of 4500).

- What are the failure modes of an arch and the corresponding critical loads?
- What closed form solutions exist and what are their limitations?
- How fine of a mesh is needed to accurately predict the failure load?
- Is there a difference in capacity between a circular and parabolic arch or between a normally distributed load and a vertically distributed load?
- What are the limitations of the linear eigenvalue solution for determining the critical buckling load?
- Can the distributed load be represented by an equivalent point load?
- For the grillage model, how should the joints be modeled?

Options for validating research questions include experimental, analytical and numerical techniques. For grid shells, because they are large structures and few have been built, full scale experimental studies were not a valid option. Where appropriate, analytical solutions were employed and derived. However, the bulk of this research uses numerical models. Even though computational methods have advanced, it is still necessary to validate the modeling assumptions and techniques using benchmark studies.

3.2. Computational Model Verification

3.2.1 2D Arch Study

A 2D arch is a good prototype structure on which various methods and approximations can be tested. All the complications resulting from the interplay between bending and membrane action are present in the arch. Therefore attention is focused first on the analysis of the arch comparing the analytical to the numerical solution.

Consider a shallow, circular arch of radius R , height h , span L and angle α shown in Figure 3.5. The arch is pinned-pinned supported with a uniformly distributed normal load q . There are three competing failure modes derived by Timoshenko (Timoshenko, 1961): yielding, snap-through and buckling (Equations 3.1), where E is Young's Modulus of Elasticity, I is the moment of inertia, A is the cross sectional area, σ_y is the yield stress.

$$q_{cr}|_{yielding} = \frac{\sigma_y A}{\sqrt{\left(\frac{L^2}{8h}\right)^2 + \left(\frac{L}{2}\right)^2}} \quad (3.1a)$$

$$q_{cr}|_{snap-through} = \frac{384EIh}{5L^4} \left(1 + \sqrt{\frac{4\left(1 - \frac{4I}{AR^2}\right)^3}{27\frac{4I}{AR^2}}} \right) \quad (3.1b)$$

$$q_{cr}|_{buckling} = \frac{EI}{R^3} \left(\frac{\pi^2}{\alpha^2} - 1 \right) \quad (3.1c)$$

Failure by yielding is self-explanatory and less likely to happen, whereas the other two failure modes require further explanation and are most likely to happen. In the case of the shallow arch, the theory assumes that the arch is inextensional, no axial deformation is allowed and the buckled shape has an inflection point at the center of the arch. The failure mode of snap through is for an arch of small curvature (essentially flat). In this case, axial strain must be considered.

In order to determine the failure mode of the arch, first the variable that governs the transition from one failure mode to another is established. Though there are four geometrical parameters of the arch (R, α, h, L) two are sufficient to uniquely define the arch and in this study the span-to-height ratio $\frac{L}{h}$ becomes the independent variable. By plotting the failure load versus the span-to-height ratio (Figure 3.6), the dominant failure mode in a given range of the independent variable can be found.

As $\frac{L}{h} \rightarrow \infty$ the arch becomes flat. It can be seen that the range of L/h for which the dominant failure mode is buckling is $L/h < 135$. The practical range of interest in this dissertation is $L/h < 20$, thus the arch fails first by buckling. While the above is a simple

Chapter 3. Methodology

analysis of a 2D arch, the lessons learned can be expanded to the failure modes of a 3D shell. Previous research described in Chapter 2 has also concluded that global buckling is the governing failure mode of shells.

Strain Energy Convergence

Having established the analytical solution to the failure of an arch, next the numerical model is discussed. In verifying the accuracy of the FEM both the strain energy and mesh convergence are checked. The limits of Timoshenko's small angle assumption is numerically checked by calculating the difference in the buckling load between a circular and a parabolic arch and between a normally and vertically distributed load. The current studies use a steel arch of a span-to-height ratio of $\frac{L}{h} = 8$ and a square cross-section of $5in \times 5in$.

The sufficiency of the finite element mesh is evaluated by plotting the rate of convergence of the strain energy to mesh refinement measured by $\frac{1}{l_h}$ where l_h is the element length. The strain energy in both the continuum and the discrete model is given in Equations 3.2 and 3.3, respectively. Typically, the finite element model exhibits monotonic convergence where the error decreases as the mesh is refined and converges from below to

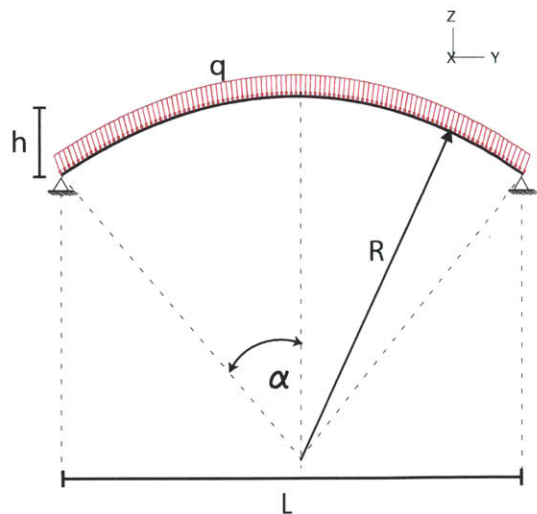


Figure 3.5 – 2D geometry of the pinned-arch.

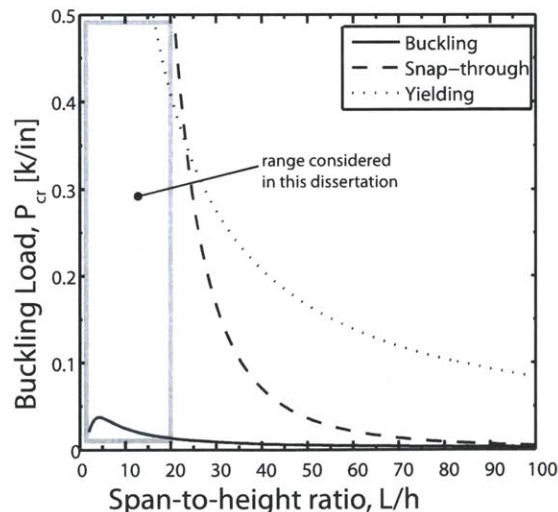


Figure 3.6 – The three competing failure modes (buckling, snap-through, yielding) of an arch as a function of the span-to-height ratio.

3.2. Computational Model Verification

the exact strain energy.

$$E_h = \frac{1}{2} \int_V \underline{\epsilon}_h \underline{\mathcal{I}}_h dV \quad (3.2)$$

$$E_h = \frac{1}{2} \underline{\mathbf{U}}^T \underline{\mathbf{K}} \underline{\mathbf{U}} \quad (3.3)$$

To illustrate monotonic convergence consider the strain energy plot of a simply supported beam with a distributed load (Figure 3.7). As the mesh is refined (increasing on the x-axis), the strain energy quickly converges to the reference energy E_{ref} . The reference energy is either calculated by the exact solution, if available, or by the FEM of a highly refined mesh. Because the plot shows that both a coarse mesh and a fine mesh converge to the reference strain energy, then the coarse mesh is sufficient and the computational expense of a finer mesh can be avoided.

For monotonic convergence the strain energy for coarser meshes cannot be greater than E_{ref} as a consequence of the FEM being “stiffer” than the continuum. Interestingly, in performing the convergence study for the arch, a curved structure, the opposite is witnessed; the strain energy converges from above.

In Figure 3.8 the strain energy convergence is plotted for an arch with a normally distributed load. The reference mesh density was 1200 elements. For curved structures, a coarser mesh is the equivalent to having a faceted curve where depending on the density, the additional stiffness due to curvature is not captured. The coarser mesh will displace more than the finer and, as a result, have a higher strain energy and converge from above. The results from the strain energy convergence study reinforce that a continuous curve can be represented as a faceted curve as is done in real structures. But how many faceted elements are needed to accurately exhibit the geometric stiffness resulting from curvature? The more coarse the mesh the less the structure exhibits geometric stiffness. Figure 3.9 plots the deformed arch for both the coarse and the fine mesh. The less stiff structure (the coarser mesh) displaces more for the same load. This is further seen in the force-displacement plot in Figure 3.10 where the displacement at the middle of the arch is measured as the mesh is refined, further explaining why the strain energy in Figure 3.8 converges from above.

Collapse Analysis

The conventional approach to determine buckling failure is to perform an eigenvalue analysis. There are two limitations to this approach. One is that buckling of shallow shells

Chapter 3. Methodology

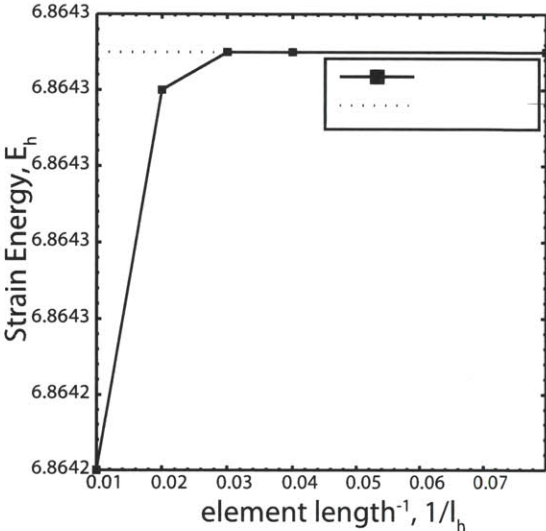


Figure 3.7 – Monotonic convergence of the strain energy for a simply supported beam with a distributed load.

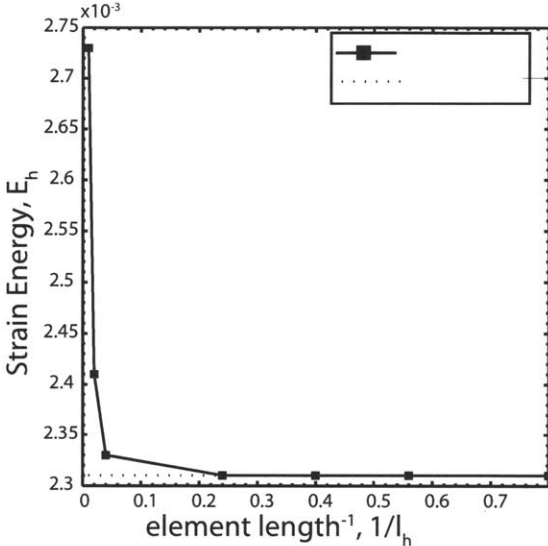


Figure 3.8 – The strain energy convergence of a pinned-pinned arch with a normally distributed load.

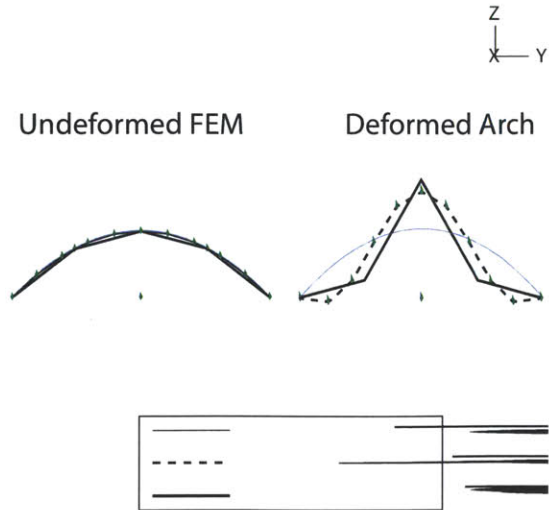


Figure 3.9 – Comparison of the arch deflection under uniform distributed loading between a coarse and a dense mesh.

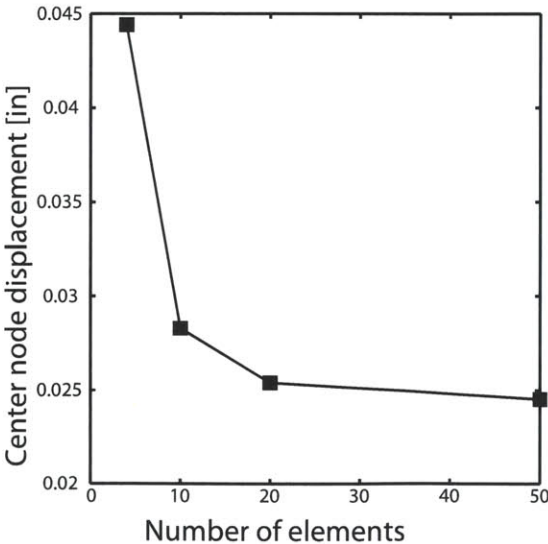


Figure 3.10 – Force displacement plot as a function of increasing mesh density.

3.2. Computational Model Verification

is preceded by a nonlinear prebuckling phase; the eigenvalue analysis disregards the nonlinearity of the prebuckling phase. Secondly, the eigenvalue analysis cannot incorporate structural imperfections. At the same time the equilibrium approach predicts the growth of the initial imperfection and the magnitude of the ultimate load followed by a postbuckling weakening phase. The differences between the equilibrium and eigenvalue approach are studied on the 2D arch.

The theoretical buckling solution is compared with the linearized buckling analysis as a function of the span to height ratio $\frac{L}{h}$ (Figure 3.11). Though Timoshenko's derivation is based on shallow arches (small angle approximation), the buckling loads for steep arches are calculated as well. For steep arches Timoshenko's theory has an error of less than 10% compared to the numerical solutions.

Because a FEM is stiffer than the continuum, the numerical frequencies are greater than the theoretical. A continuum has an infinite number of natural frequencies because every particle can move in infinite directions; whereas a FEM has only N natural frequencies corresponding to the N degrees of freedom in the mesh. While the predicted FEM frequencies are greater than the theoretical in Figure 3.11, within the range of shallow arches number $\frac{L}{h} \leq 20$, the error is insignificant at a maximum of 3%.

The collapse load is next calculating using a Load-Displacement Constraint (LDC) method to solve for the non-equilibrium path of the collapse and post-collapse responses (Bathe, 1996). This method requires specifying the amount of geometrical imperfections. As a common practice, the shape of imperfection used was the first buckling mode. Two scales of the imperfect shape were considered: $\phi = 0.05$ and 1. The comparison between the analytical, and both the linear eigenvalue and the nonlinear analysis is shown in Figure 3.12. There is a qualitative agreement between all three solutions. In particular, the linear eigenvalue estimate is as accurate as both the analytical and the rigorous non-linear prebuckling analysis. It can be concluded that for practical applications the accuracy of either the analytical or linear numerical solution is sufficient.

Small Angle Approximation

The small angle approximation of the Timoshenko closed-form solution is checked by comparing a circular arch to a parabolic arch and a normally distributed load to a vertically distributed load. For shallow arches ($\frac{L}{h} > 6$) there is little geometric difference between a circle and a parabola as well as little difference in their buckling capacity (Figure 3.13). This figure also compares the buckling load between the normal and vertical distributed

Chapter 3. Methodology

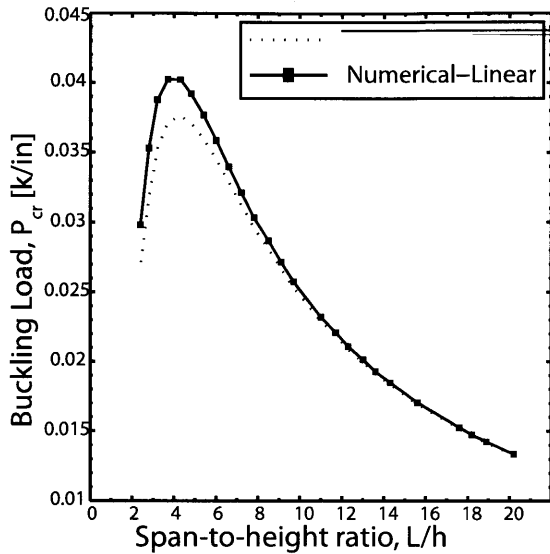


Figure 3.11 – Comparison of the theoretical buckling load (Equation 3.1c) to the numerical linearized buckling analysis.

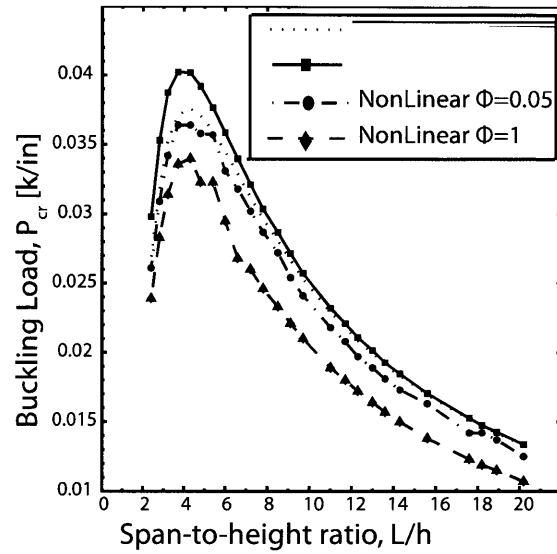


Figure 3.12 – Comparison of linear and non-linear buckling analysis for two scaled magnitudes (ϕ) of imperfection.

load. For both the circular geometry with either a normally distributed or vertical loading and for the parabolic geometry with either the normally distributed or vertical loading, there is little difference.

Load Equivalence

In preparation for modeling grid shell structures, it is important to confirm that the analytical solution that assumes a pressure load can still be used for a grid shell when the loading becomes point loads at the joints. The calculation of an equivalent pressure is provided in Equation 3.4 where P is the point load in kips, N is the number of nodes, and S is the arclength in inches. In Figure 3.14, the theoretical buckling load for a uniformly distributed load is compared to the numerical prediction where the loading is applied as point loads at the joint. The distributed load is accurately represented with point loads at a mesh density of 50 elements for an error of 9%.

$$q_{cr|equivalent} = \frac{P \times N}{S} \quad (3.4)$$

3.2. Computational Model Verification

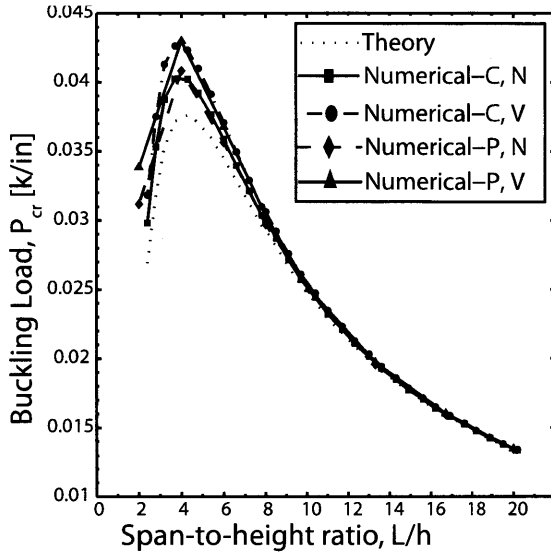


Figure 3.13 – Comparison of the buckling load for the circular (C) and parabolic (P) arch with a normally (N) and vertically (V) distributed load.

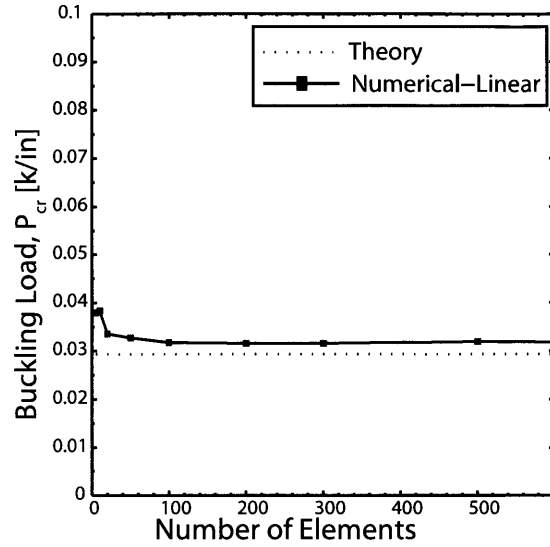


Figure 3.14 – Comparison of the theoretical buckling load for a distributed load and the numerical buckling load for point loading.

3.2.2 Grillage Study

In addition to the finite element modeling concerns investigated earlier on the 2D arch, a grillage is also studied to clarify how to model rigid connections so to transfer moments. Rigid ends are modeled within ADINA by identifying the location of the connection based on the element number, and inputting the rigid connection's length and stiffness. The physical model and the finite element representation of a rigid joint is illustrated in Figure 3.15. The rigid end option assumes the the rigid ends will never undergo plasticity and that the element is formulated as one single element. The rigid end lengths used in all the models of this dissertation are equal to the thickness of the members which is a typical length used for welded connections.

A simple bending case study is done to verify the modeling of the joints. A $1200in \times 1200in$ steel cantilever plate with a tip load is modeled as an assemblage of beams forming a quadrilateral grid (Figure 3.16). Two analytical models are used to calculate the deflection. The first assumes the grid to deflect as one cantilevered beam by making the connections rigid (Figure 3.16a). The second assumes the assemblage becomes a wide plate with a thickness of $0.8in$ defined by having an equivalent moment of inertia to the beam model (Figure 3.16b). The beam has a point load of $1kip$ and a square cross section

Chapter 3. Methodology

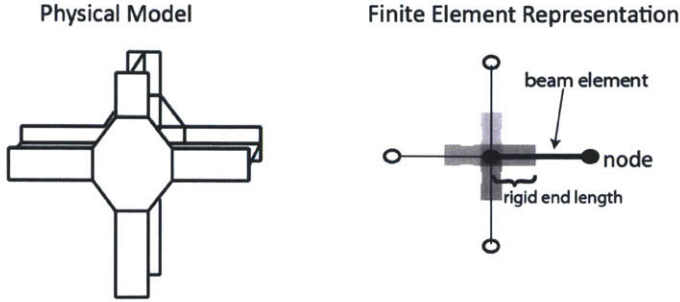


Figure 3.15 – Finite element representation of rigid ends.

of $25in^2$. The plate has a distributed line load of $0.025k/in^2$ with a thickness of $0.8in$. Using the deflection of a cantilevered beam with a tip load (Equation 3.5), the analytical deflection is calculated and compared to the numerical results for both the beam and plate models in Table 3.1. There is good agreement which verifies that the plate/shell is an assemblage of beams with moment connections at the joints.

$$w_o = \frac{PL^3}{3EI} \tag{3.5}$$

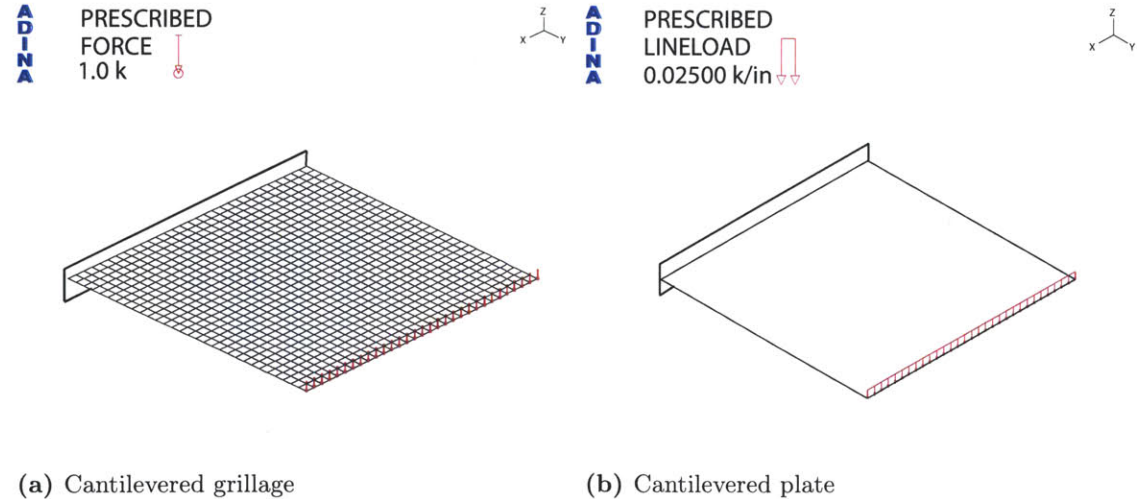


Figure 3.16 – Grillage case study.

3.3. Summary

Table 3.1 – Comparison of the analytical and numerical tip deflection w_o using both the beam and plate models for the grillage.

	Beam	Plate
Analytical [in]	381	11,460
Numerical [in]	300	11,035

3.3 Summary

This chapter outlined the methodology for calculating the change in load-bearing capacity of grid shells due to their curvature and topology using numerical and analytical methods. In preparation for the grid shell parametric studies a mathematical model for which an analytical exact solution is known, the 2D arch, was first studied and compared using numerical methods. This builds confidence and validates the methods that will be used as the models have more complicated features introduced to them. The computational model verification studies confirmed that:

- the geometric stiffness of an arch is accurately represented by a faceted arch with a mesh density of $\frac{1}{50}$ the arclength.
- a linearized buckling analysis is sufficient for predicting the collapse load.
- moment connections can be accurately modeled using rigid ends in ADINA.

In the next chapter, the computational techniques verified here will be employed in the parametric study of a spherical cap grid shell where the effect of curvature and topology on the load-bearing capacity will be studied and quantified.

Chapter 4

Spherical Cap Grid Shell Study

4.1 Introduction

There is a vast body of literature touching upon the failure mode and ultimate carrying capacity of grid shells. However there is a lack of simplified tools that would assist in early design of such structures for maximizing their strength and/or minimizing their weight and in facilitating the design discussion between architects and engineers. Previous works reviewed in Chapter 2 solve only specific boundary value problems and thus fail to contribute to the understanding of the underlying physics.

Specifically, the mechanics of lattice structures are controlled by the transition between pure membrane response in the prebuckling domain to the combined bending/membrane response at the point of buckling and in the post-buckling range. This chapter identifies groups of parameters that are responsible for a given lattice structure reaching its critical load and studies their influence using both analytical and numerical techniques. In this connection the following global questions from Chapter 1 are revisited for spherical caps:

- How do the curvature and topology affect the load-bearing capacity of grid shells?
- How to best describe the mechanics of these structures?
- What are the design rules of thumb to maximize grid shell performance?

More specifically, here it is asked:

- What is the effect of topology, span-to-height ratio and grid spacing on the load-bearing capacity?

4.2. Problem Definition

- Can a closed-form solution be derived that accounts for the varied parameters?

4.2 Problem Definition

In order to understand how grid shells behave and to find a fast and simple analytical estimation on the buckling capacity, a case study on a spherical cap grid shell is performed. A spherical cap shape is a natural choice because it is a simple geometry from which more complicated shapes can grow and because it has been seen in existing grid shells (as shown earlier) such as the Swimming Arena in Neckarsulm, Germany (Holgate, 1997).

The buckling load is calculated analytically and numerically for a pinned supported spherical cap under uniform pressure (Figure 4.1a). The members have a solid square cross-section, are made from steel and have rigid connections at the joints. The load is applied as vertical point loads at the joints (Figure 4.1b). The parametric case study is framed around the parameters that influence most the architectural design (aesthetics) and the engineering design (capacity). The analytical and numerical buckling loads are then analyzed and compared.

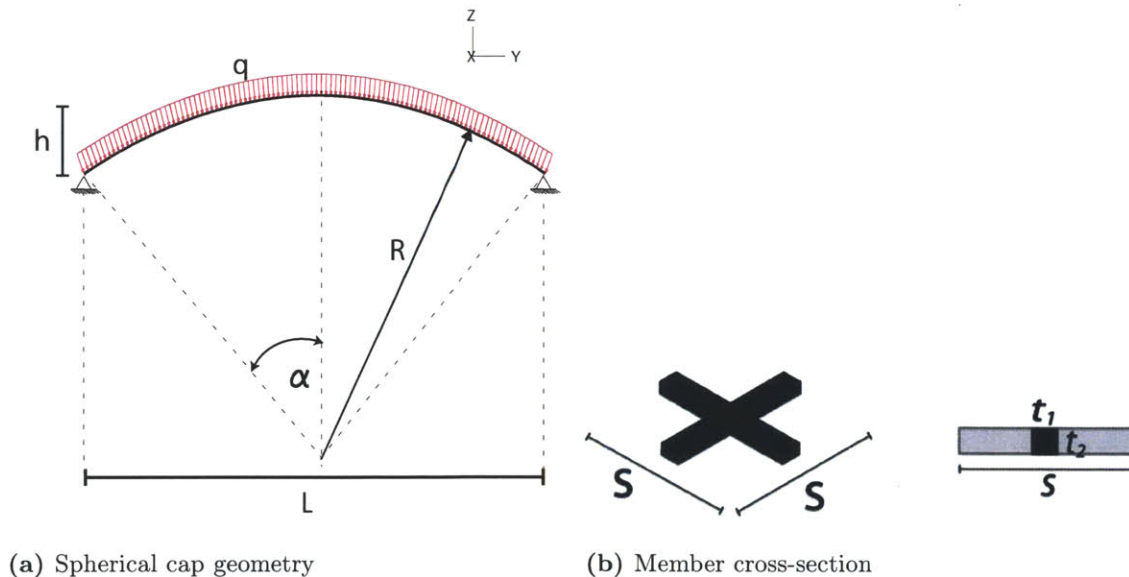


Figure 4.1 – Spherical cap grid shell.

Chapter 4. Spherical Cap Grid Shell Study

4.2.1 Parameters

The three selected parameters that frame the spherical cap study are the panel shape, the panel spacing, and the span-to-height ratio. These parameters are selected based on the main design constraints explained in Chapter 2. The panel shapes considered are the quadrilateral and the triangle with a spacing of $s=30, 60, 120$ in. The span-to-height ratios are $\frac{L}{h}=20, 11, 6$. The member's square cross-sectional area is $A = t_1 t_2$ and is kept constant in this study at $25in^2$. Every permutation of the parameters, schematically shown by the hierarchal tree of Figure 4.2, is considered, resulting in a total of 30 grid shell models. Figure 4.3 shows more clearly all the combinations of the panel shapes and spacing.

4.2.2 Numerical Approach

The finite element models for every permutation is created by a Matlab program written by the author and provided in Appendix A. The grid shell models for the triangular topology are partially built using a Matlab mesh generator code (Persson and Strang, 2004). The mesh generator uses a force-based method and Delaunay triangulation to create an equally spaced grid. All 30 models are imported into ADINA where a linearized buckling analysis is used to calculate the buckling load and mode.

Each member is modeled as an ADINA beam element (a 2-node Hermitian beam

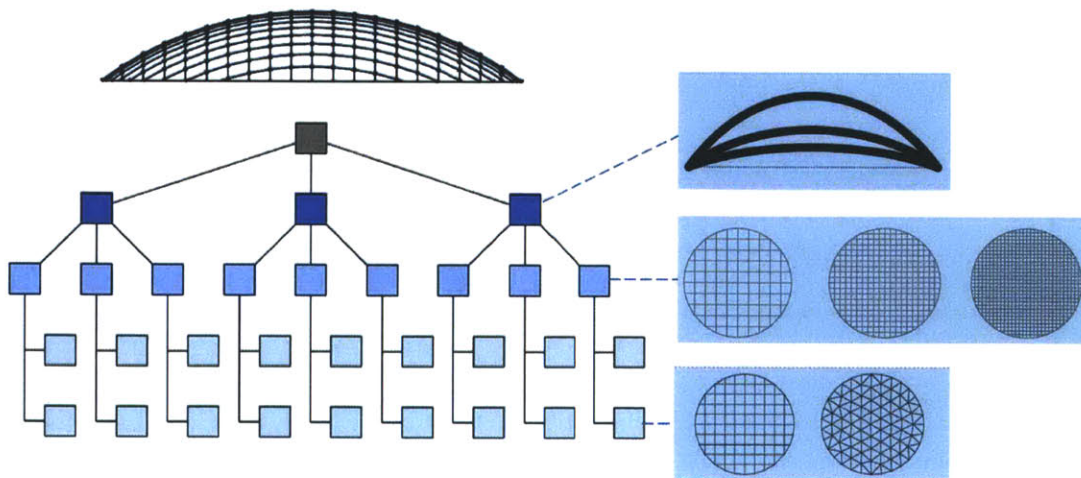


Figure 4.2 – A hierarchal tree illustrating the number of models for the spherical cap study.

4.2. Problem Definition

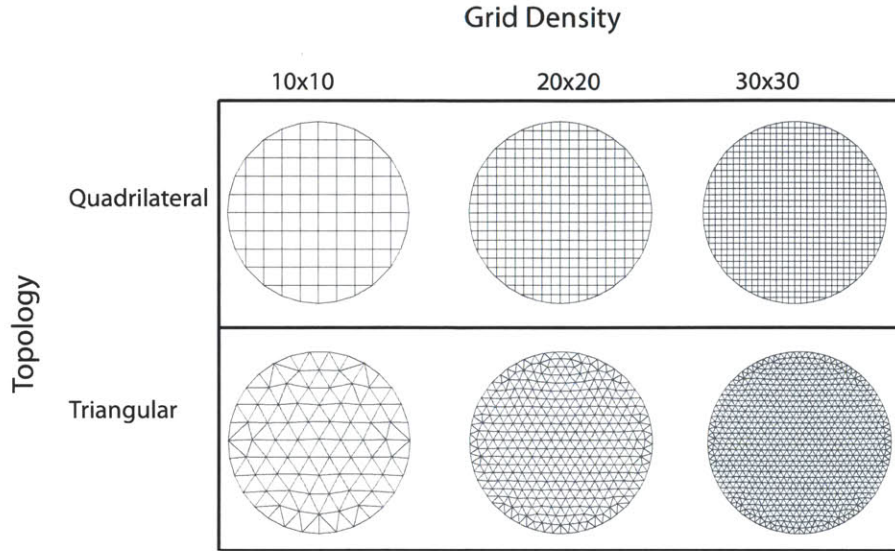


Figure 4.3 – Illustration of the six combinations of the panel shape and spacing.

with 6 degrees of freedom at each node 3 translations and 3 rotations). Each member has a mesh density of five. The joints are modeled as rigid connections as explained in Section 3.2.2. Lastly, the perimeter members are pinned, and the loading is applied vertically to the joints. One of the 30 models is shown in Figure 4.4, highlighting the mesh density, boundary conditions and the loading.

In addition to the grid shell finite element models, a continuous shell is also created in order to validate both analytical and numerical techniques. Two types of continuous shells are defined: one employs the axisymmetric beam, and the other uses shell elements. The models and their results will be described further in the Model Verification section.

4.2.3 Analytical Approach

One way to converge fast to an optimized solution is to make better use of existing analytical solutions for axisymmetric shells that have uniform thickness. Therefore, the key issue in using the analytical solution, for the purpose of establishing a practical design tool, is a proper definition of the equivalent thickness describing the transition from the discrete grid shell to the continuous shell. The difficulty in defining the equivalent thickness is in understanding the interplay between the in-plane membrane response and the out-of-plane bending response because the bending and axial stiffness include shell

Chapter 4. Spherical Cap Grid Shell Study

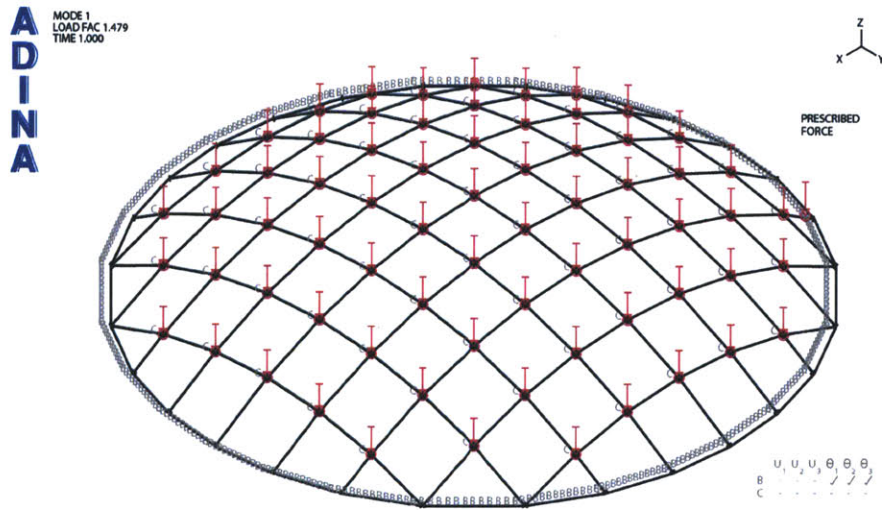


Figure 4.4 – Example of the spherical cap grid shell finite element model with $\frac{L}{h}=6$.

thickness raised to a different power. The issue is to decide what is more necessary to have: sufficient cross-sectional area to withstand the membrane forces or enough moment of inertia to withstand the bending?

Consider the spherical shallow shell with pin supports and a uniformly distributed pressure shown earlier in Figure 4.1a. The closed form solution of the buckling load by Timoshenko, given in Equation 4.1, is obtained assuming an axisymmetric buckling mode (Timoshenko, 1961). The radius of the spherical cap is defined by R and ν is Poisson's ratio. In the present application of this equation, t_{eq} is a thickness of an equivalent uniform shell understood in a certain sense to be equivalent to the grid shell.

$$q_{cr} = \frac{2E}{\sqrt{3(1-\nu^2)}} \left(\frac{t_{eq}}{R} \right)^2 \quad (4.1)$$

In this research multiple definitions of the equivalent continuum are compared which not only facilitate finding simpler approximate solutions, but also fills the knowledge gap in understanding how these structures are behaving; specifically, their transition from bending to membrane action. Developing this understanding helps to better design structures in terms of weight efficiency.

In addition, the concepts reviewed in Chapter 2 and reviewed in Chapter 2 are extended here by validating various equivalent thickness methods with discrete models (Wright, 1965; Forman and Hutchinson, 1970; Kollar and Dulacska, 1984). While one

4.2. Problem Definition

paper uses discrete analysis to evaluate their equivalent continuum buckling prediction, it was limited to the tools available in 1970 (Forman and Hutchinson, 1970). The authors acknowledged that their method was to be further validated by experiments. Today computational software facilitates completing this much needed parametric study.

Furthermore, the results in this thesis are uniquely presented in a form applicable for design. This is done by including the parameters that influence the design in the simplest form so as to be accessible to both architects and engineers. The previous works also did not validate the equivalent continuum technique in terms of the design parameters like topology. It can be concluded that there is a lack of well validated methods for a rapid estimation of the failure of grid shells needed for preliminary design.

There is no unique method to calculate the equivalent thickness based on the topology of the grid shell, the spacing and the member cross-section. Figure 4.5 highlights the geometry of the repeating grid shell unit for a quadrilateral and triangular topology. Equivalent thickness could be determined on the bases of *(i)* area equivalence, *(ii)* moment of inertia equivalence, *(iii)* volume equivalence or *(iv)* a combination of area and moment of inertia. The area, moment of inertia and volume equivalence are self-explanatory. In the case of the concept of area and moment of inertia, the Timoshenko solution is valid; however, the derivation of the final expression is more complicated. It requires rederiving the spherical cap buckling load while keeping the thickness due to the axial rigidity and to the bending rigidity separate. The derivation is provided in Appendix B. The summary of the equivalence thicknesses derived in this dissertation using the above four methods is listed in Table 4.1. Note similar expressions can be derived for different cross-section geometries.

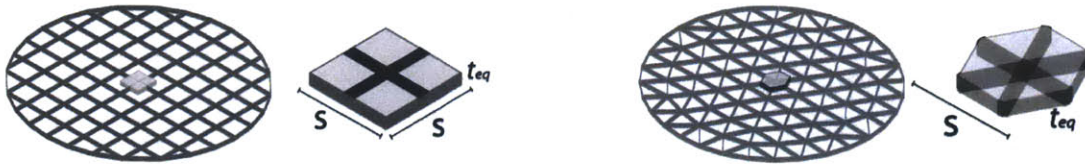


Figure 4.5 – The quadrilateral and triangular topology and their repeating units (the cruciform and the hexagon).

Chapter 4. Spherical Cap Grid Shell Study

Table 4.1 – The equivalent thickness (t_{eq}) relations for the quadrilateral and the triangle using the four equivalent definitions.

Definition of Equivalence	Quadrilateral Topology	Triangular Topology
Area (A_{eq})	$\frac{t_1 t_2}{s}$	$\frac{2t_1 t_2}{s}$
Moment of Inertia (I_{eq})	$\left(\frac{t_1 t_2^3}{s}\right)^{\frac{1}{3}}$	$\left(\frac{2t_1 t_2^3}{s}\right)^{\frac{1}{3}}$
Area & Moment of Inertia ($A_{eq} + I_{eq}$)	$t_2 \sqrt{\frac{t_1}{s}}$	$t_2 \sqrt{\frac{2t_1}{s}}$
Volume (V_{eq})	$\frac{2t_1 t_2}{s}$	$\frac{8t_1 t_2}{\sqrt{3}s}$

4.3 Results

4.3.1 Model Verification

Before proceeding with the grid shell FEM, the computational model and the range of analytical validity is verified first by modeling a continuous shell. The analytical model is Timoshenko's buckling equation for a shallow spherical cap (Equation 4.1). Two numerical models are considered: one using axisymmetric isobeam elements for $\frac{L}{h} \leq 20$, and the other using shell elements for only $\frac{L}{h} = 20$. The latter model was used primarily to check the load equivalence method described in Section 3.2.1. Both models have a thickness $t = 3in$.

For the range of shallowness established in Chapter 3 ($\frac{L}{h} \leq 20$), the numerical results have a maximum of 2% error at $\frac{L}{h} = 15$ (Figure 4.6). In Chapter 3, the sources of error between the finite element solution and the analytical were already discussed. Here, another source of error is that the first buckling mode is assumed to be axisymmetric in the analytical solution; however, the axisymmetric shell element predicts a symmetric buckling mode. Because the corresponding buckling load is only 0.3% error from the analytical this error is negligible. In the model that uses shell elements the first buckling mode is axisymmetric and has with a 0.3% error for the buckling load.

In Section 3.2.1 the load equivalence method is checked where the buckling load is calculated by applying point loads instead of a distributed. Here, that study is repeated for the spherical cap. In Figure 4.7, the buckling load for the continuous shell using distributed loading and point loading is compared. For an inverse element length of 0.025 the point load predicts the theoretical buckling load with a 5% error.

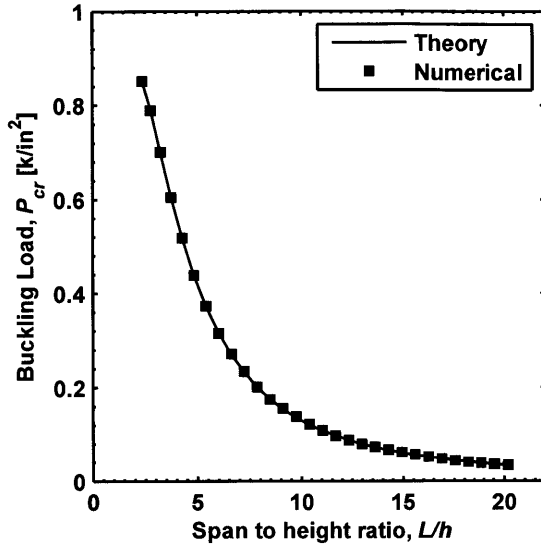


Figure 4.6 – Comparison of the numerical and the theoretical buckling load of a continuous spherical cap using axisymmetric shell elements.

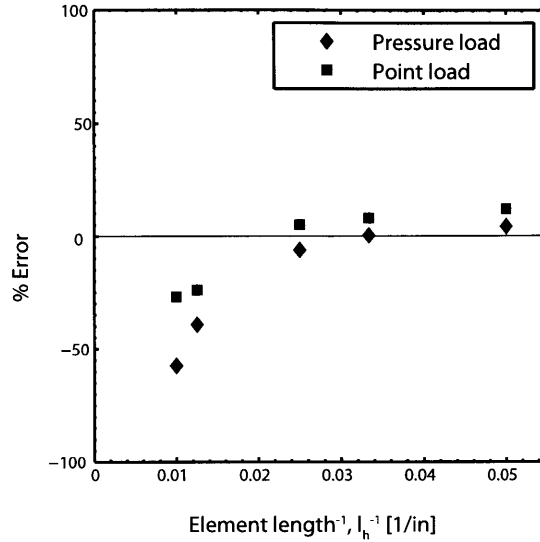


Figure 4.7 – Error in the numerical buckling load to the analytical when the loading is applied as a point load and a pressure load.

4.3.2 Collapse Analysis

As explained in Section 3.2.1 the linearized buckling analysis does not account for prebuckling rotations. In this section the critical load is calculated using the nonlinear collapse analysis and is compared to the linearized buckling analysis for a spherical cap of $\frac{L}{h} = 20$. The concern is if the linearized buckling load prediction overestimates the collapse or if the grid shell's collapse load is negligible because the deformed shape gains more stiffness.

In this study the collapse analysis is induced by an imperfection in the z-direction at the center equal to $0.1in$ or $\delta_z = \frac{t}{3}$. In Figure 4.8, the pressure versus displacement curve is plotted. The collapse load is 15% less than the predicted linearized buckling load. Because the error can vary as seen in Section 3.2.1, a linearized buckling analysis is still used in this case study because it is computationally faster to both set up and run. Also by doing a collapse analysis other complications arise, for example like what and where should the imperfection be and how large? Previous research has looked at imperfection sensitivity for shell buckling analysis (Singer and Abramovich, 1995; Calladine, 1995; Blachut and Galletly, 1995; Bernard et al., 1999). After using the trends concluded in this thesis to guide the schematic design of a grid shell, the research on imperfection studies can be used in the robust analysis needed for the final design.

Chapter 4. Spherical Cap Grid Shell Study

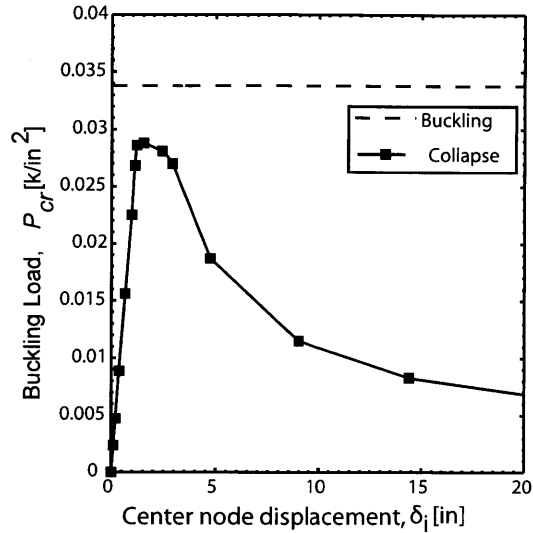


Figure 4.8 – Comparison of the collapse load to the linearized buckling load for a spherical cap of $\frac{L}{h} = 20$.

4.3.3 Numerical Results

Recall that the objective is to study the change in buckling capacity as a function of the shell height, the panel shape and spacing and the shell height. As an example of the FEM output of the mode shape, the buckling mode for both the quadrilateral and triangular grid shell are shown in Figure 4.10.

The change in the buckling load for both the quadrilateral and the triangular grids is plotted as a function of the grid spacing in Figure 4.9. The three span-to-height ratios heights are distinguished by their markers. For both the quadrilateral and triangular grids, as the spacing increases the capacity decreases and all the models converge to the same capacity regardless of their height.

As expected, the steeper the shell the higher the capacity because the buckling load is proportional to $\frac{1}{R^2}$. The triangular grid is stronger than the quadrilateral especially as the shell gets steeper. However to properly account for the trade-off between the triangle and the quadrilateral, the volume of material is accounted for next.

A metric of performance is defined as the structural efficiency η to measure how much a structure can carry of its own weight q_{sw} (force per unit area) (Equation 4.2). In Figure 4.11 the structural efficiency of each structure is plotted. Note that for all models the structural efficiency is always greater than one; the grid shell spherical cap can always

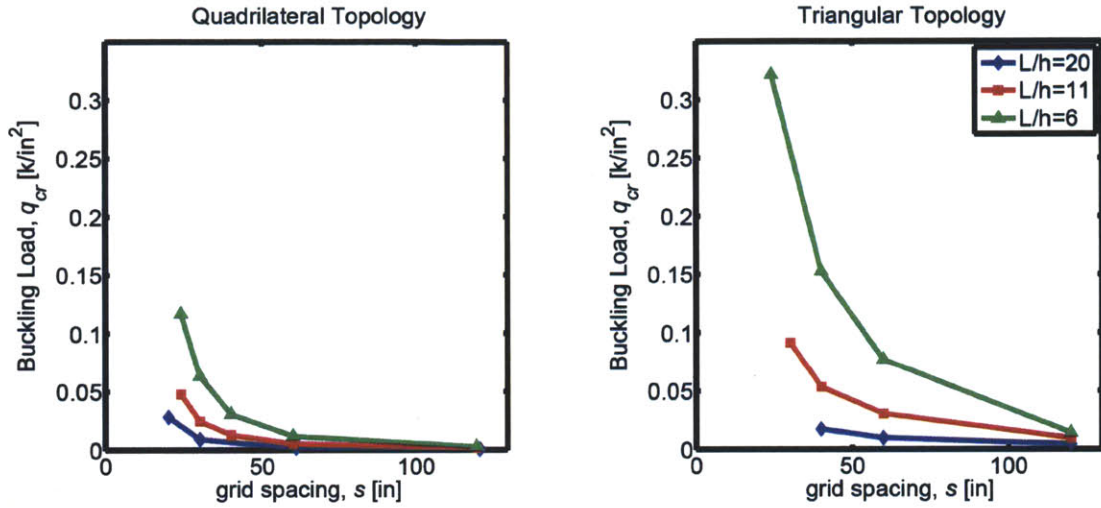


Figure 4.9 – The buckling capacity of the spherical cap as a function of the grid spacing for the quadrilateral grid (left) and the triangular grid (right).

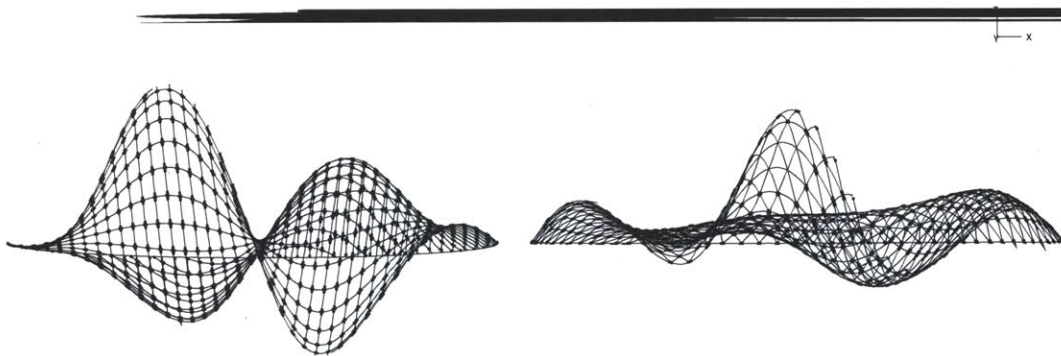


Figure 4.10 – First buckling mode of spherical cap with $\frac{L}{h} = 20$ and a spacing of $s = 30in$: quadrilateral topology (left), and triangular topology (right) (magnified by a factor of 5000).

Chapter 4. Spherical Cap Grid Shell Study

carry more than its weight.

$$\eta = \frac{q_{cr}}{q_{sw}} \quad (4.2)$$

Figure 4.11 also shows that for shallow caps a quadrilateral grid is as efficient as the triangle. However, as the shell becomes steeper, the triangle grid is up to two times more efficient than the quadrilateral. The plot indicates that different design configurations can have the same structural efficiency. For example, for the structure to carry 50 times its own weight, there are four different grid shell geometries. Two options include either a shallow, quadrilateral, dense grid or a steep, triangular, coarse grid. Therefore a designer can consider more options when trying to achieve an efficient shell structure.

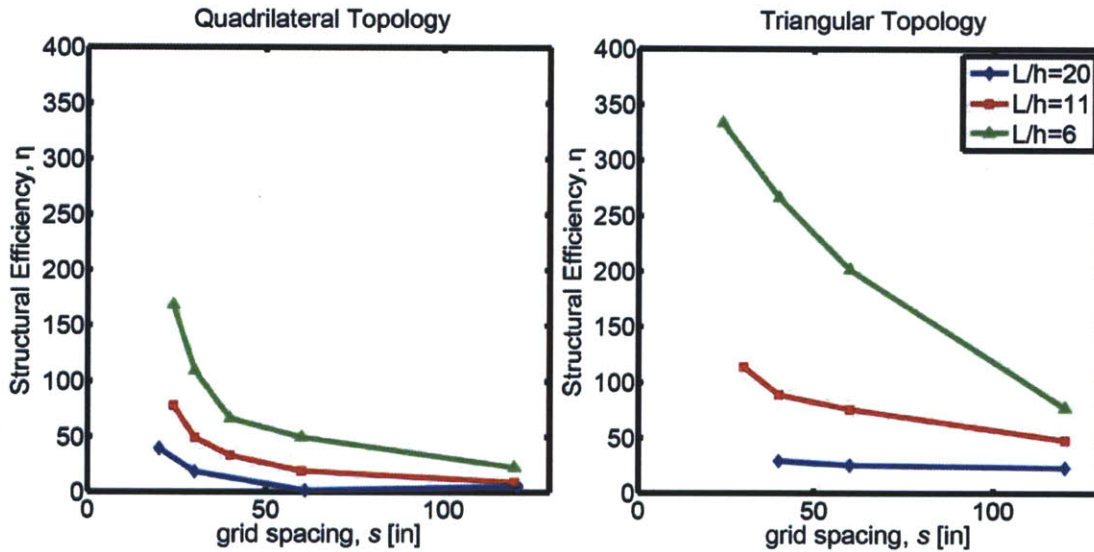


Figure 4.11 – Structural efficiency of the spherical cap grid shell (Equation 4.2).

4.3.4 Analytical Results

The analytical solution using Equation 4.1 for a quadrilateral grid of $\frac{L}{h} = 20$ is plotted in Figure 4.12. The four lines represent each of the four different equivalent thickness definitions (area, moment of inertia, area and moment of inertia, volume) in Table 4.1. The buckling load calculated from the four equivalent continuum methods are compared as a function of the grid spacing s .

The figure shows that the upper and lower bound of the buckling load correspond to the equivalent moment of inertia approach and the equivalent area approach, respectively.

It is expected for the extremes to indicate whether a structure is bending dominated or membrane dominated. In between the bounds are the volume equivalent and the area and bending equivalence. As shown more clearly in the figure, the area and bending equivalent is not the average of the area equivalence and the bending equivalence.

4.3.5 Numerical and Analytical Results

Figure 4.13 plots both the numerical and analytical solutions for all three $\frac{L}{h}$ ratios and for the two topologies. The matrix of plots is organized from left to right by decreasing span-to-height ratio, and from top to bottom as the quadrilateral and the triangular topology. As explained earlier, the analytical solution for the area and for the moment of inertia equivalence will always give, respectively, the lower and upper bound solution. Here all the numerical results fall within those bounds. Placing the results within the context of those bounds, the shallow shells are seen to be more membrane dominated while the steeper shells are more bending dominated. This is clearly seen on the figure where the numerical solution is closer to either the moment of inertia or area equivalence depending on the height.

The plots also show that for quadrilaterals the equivalent volume is best and for

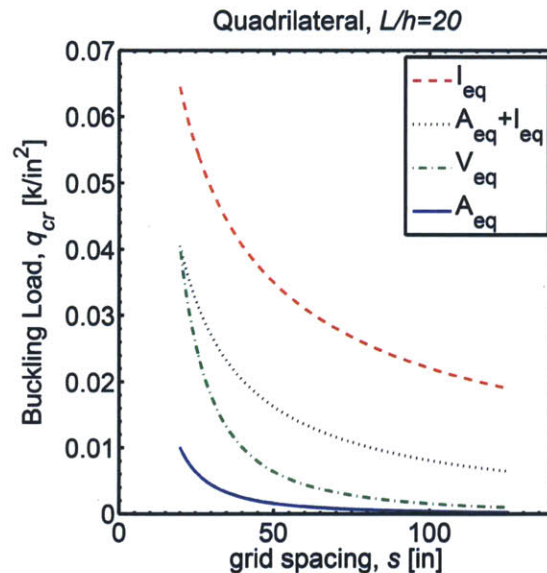


Figure 4.12 – Comparison of the buckling load (Equation 4.1) for the four equivalent continuum definitions for a quadrilateral grid with $\frac{L}{h}=20$.

Chapter 4. Spherical Cap Grid Shell Study

triangles the best approach goes from area to area/bending to bending as the shell becomes more steep. It is expected that the shallower shells trend toward membrane action, requiring more axial rigidity because the axial force is greater the more shallow the shell. The denser grid has a stronger buckling capacity which is expected because a more dense grid converges to a continuous shell. It should also be noted that although the buckling mode shape of the theoretical solution is axisymmetric and that the buckling mode in the numerical solution for the triangle is symmetric, the corresponding buckling loads are quite close to each other. This leads to the conclusion that the simple axisymmetric Timoshenko equation, modified to account for an equivalent thickness, can be used to estimate of the buckling load of grid shells. For quadrilaterals, the upper bound is best defined by using the equivalent volume. For the triangle the volume equivalence is used up to a spacing of 40in. For spacing less than 40in the combined area and moment of inertia equivalence provides the best upper bound.

4.4 Discussion

The opportunity for architects and engineers to create weight efficient elegant structures is in the preliminary stages of design. Here a framework is presented for a fast assessment of grid shell performance in terms of the main design constraints (grid spacing, shell height and span). The results of the parametric study performed on those variables are combined into a set of design guidelines presented in Figure 4.14.

The guidelines are organized into three categories based on the three span-to-height ratios. For the more shallow shells (the left column), it is more effective to decrease the grid spacing than to change topology. Whereas for the steeper shells (the right column) it is best to change the topology. In between those two extremes, the effect of changing the grid spacing or the topology is similar and one can do either. The design guidelines provide an immediate answer on how to improve the buckling capacity of the spherical cap grid shell.

The notion of the equivalent thickness is not uniquely defined. The best equivalent continuum approach varies between topology and curvature. There are significant differences in buckling prediction between the four equivalent continuum approaches. While a simple bending and area equivalence give an upper and lower bound, the spread is very wide. This further illustrates that grid shells respond both in membrane and bending action. At the same time the volume equivalence and the combined area/bending equiva-

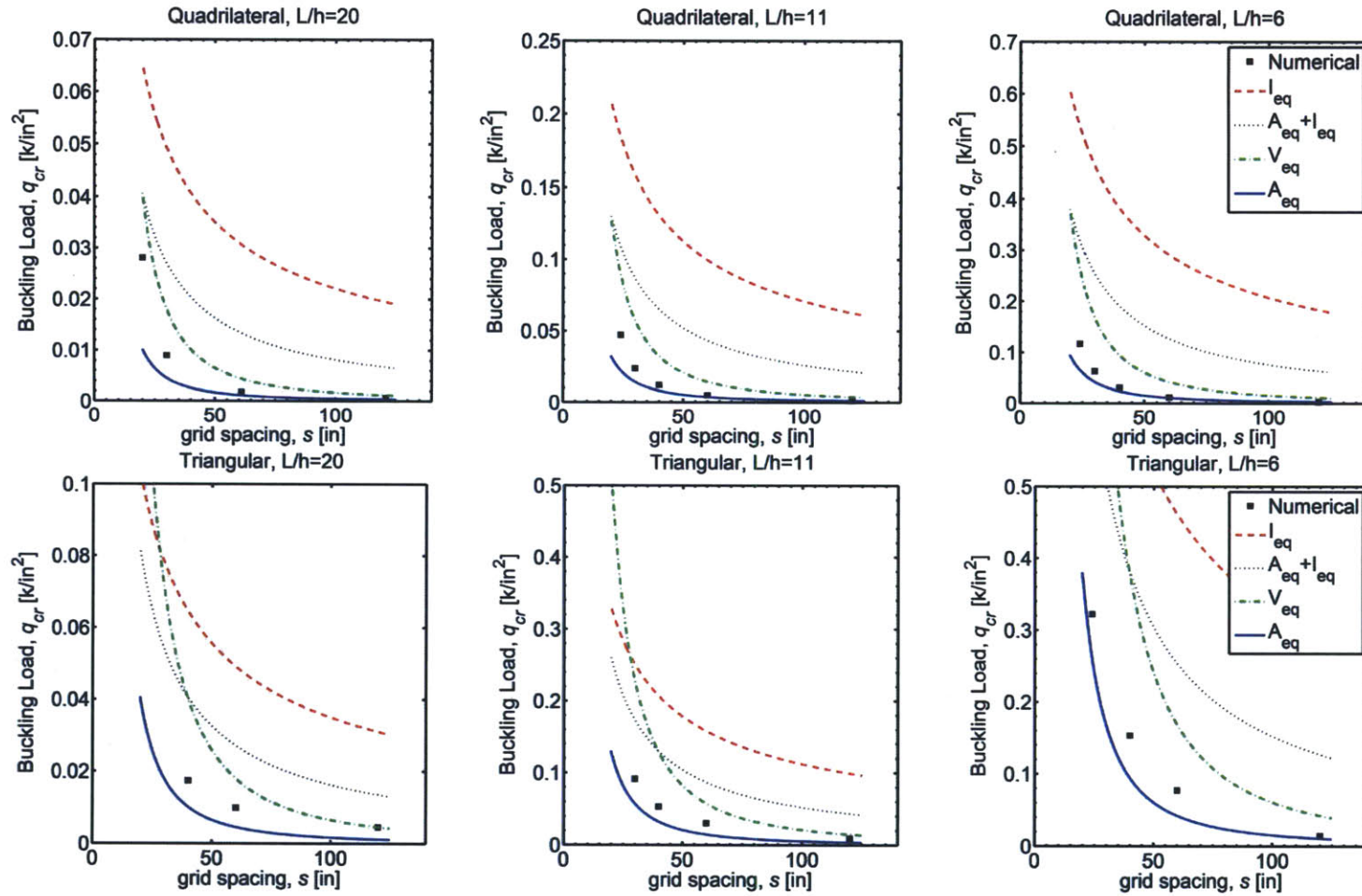


Figure 4.13 – Comparison of analytical and numerical results for the spherical cap grid shell study. The rows from top to bottom represent the topologies quadrilateral and triangular, respectively. The columns from left to right represent decreasing span-to-height ratios.

Chapter 4. Spherical Cap Grid Shell Study

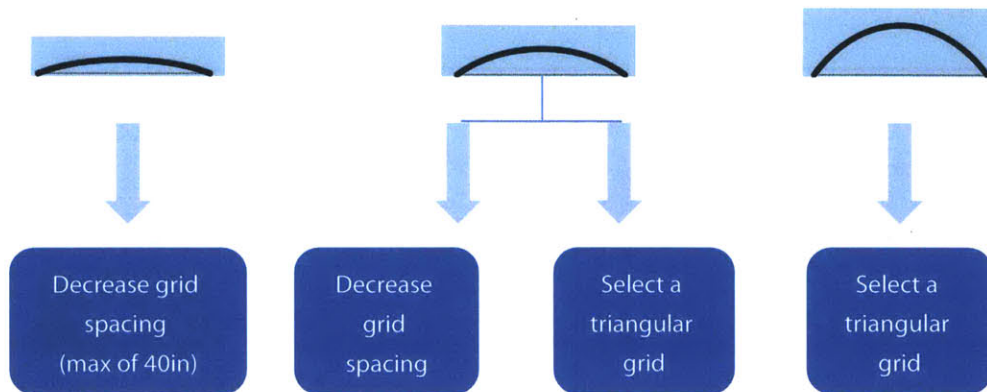


Figure 4.14 – Design guidelines for a spherical cap grid shell. Columns from left to right represent decreasing span-to-height ratio.

lence leads to much closer estimates when compared to the exact numerical solution. The accuracy of the volume equivalence is better for the quadrilateral grid while the combined area/bending equivalence gives better results for triangular meshes.

4.5 Summary

This chapter developed a framework for a quick and accurate assessment of grid shell structural performance by using available closed form solutions of continuous shells. Though the analysis in this chapter is restricted to the spherical cap, the salient features can be extended to more general types of grid shells. By expanding the use of the assessment of simple shell and grid structures to complex ones, an efficient approximation is provided which can immediately impact the design.

The central point of the method is the concept of an equivalent uniform shell where the equivalence is based on the bending or axial rigidity, or both, or volume. This chapter derived and validated multiple equivalent thickness techniques. The area and moment of inertia equivalence establish the upper and lower bounds of the critical failure load.

The vast amount of data compiled and analyzed not only better explains the mechanics of grid shells but also lays the groundwork for providing the following rules of thumb at the start of a grid shell design.

- The effect of topology lessens as the shell become shallower. The more shallow the shell, the less the benefit in using a triangular topology over a quadrilateral.

4.5. Summary

- Steeper shells have a higher capacity than shallow shells.
- Shallower shells require a denser grid to increase the capacity.
- An equivalent continuum defined by area equivalence provides a conservative estimate for the buckling load of a grid shell that can be used in the preliminary stages of design.
- For the quadrilateral grid the upper bound for the buckling load is defined by the equivalent volume. For the triangular grid with spacing greater than 40in, the upper bound is defined by the equivalent volume; for spacing less than 40in the upper bound is the combined area and moment of inertia equivalence.
- Different design configurations of the span-to-height ratio, the spacing and the topology can have the same structural efficiency.

Chapter 5

Corrugated Vault Study

5.1 Introduction

Most grid shell structures have a rectangular footprint leading to the use of a barrel vault shape. Some geometries have gone so far as to add corrugation to the surface as seen in the Japan Pavilion, the Weald and Downland Museum (Figure 5.1). In this chapter, the role of curvature on a barrel vault is studied by gradually introducing double curvature into the geometry.

In Chapter 4, the spherical cap grid shell study provided us with a rapid estimation of grid shell capacity by using the equivalent continuum. In that chapter, the objective was to understand the mechanics while quantifying how the most influencing real design



(a) Weald and Downland



(b) Japan Pavilion

Figure 5.1 – Examples of grid shells with corrugation at the edge and the crown.

5.2. Problem Definition

constraints affect the capacity and efficiency of the structure. In this chapter, the focus is on the role of double curvature for efficiency and capacity. Here the following key questions are asked:

- Is corrugation an effective and efficient means to increase the load-bearing capacity of a barrel vault?
- Can a closed-form solution be derived that accounts for the varied parameters?

To answer these questions, the change in buckling capacity of three corrugated barrel vaults is studied. The varied parameters include the location of corrugation (edge, crown or both), the aspect ratio of corrugation, the span-to-height, and the grid spacing (Figure 5.2).

5.2 Problem Definition

5.2.1 Geometry

The dimensions of the straight edge barrel vault are a span L_1 of 100ft, and a longitudinal length of $2L_2$ of 162ft (Figure 5.3a). The barrel vault has a a parabolic cross section defined

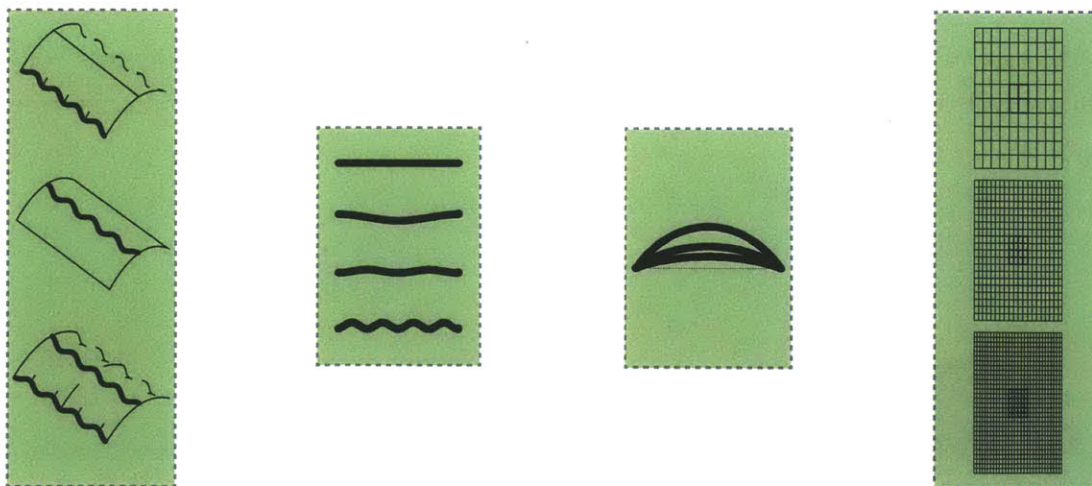


Figure 5.2 – The four groups of parameters: corrugation location, aspect ratio, span-to-height ratio, and grid spacing (left to right).

Chapter 5. Corrugated Vault Study

by Equation 5.1. The span L_1 and the length $2L_2$ are kept constant in all models at 100ft and 162ft respectively. These length values were chosen based on typical values of existing grid shells (Cadji, 2001; Stungo, 2001; Pople, 2002b,a, 2001). The vault is loaded with a uniform pressure and its boundary conditions include no lateral and normal translation along the length of the edges and no longitudinal displacement and rotation about the x axis (Figure 5.3b).

$$z = h \left(1 - \frac{x^2}{x_o^2} \right) \quad (5.1a)$$

$$x_o = \frac{L_1}{2} \quad (5.1b)$$

5.2.2 Parameters

The four groups of parameters defining the parametric space are:

- the corrugation location: at either the edge, the crown or both the edge and the crown (in-phase)
- the aspect ratio of the corrugation: 8 values total
- the span-to-height ratio: $\frac{L}{h}=6, 11, 20$
- the grid spacing: $10 \times 10, 20 \times 20, 30 \times 30$

As in the case of the spherical cap study, every permutation of the parameters was considered, overall there were a total of 390 models. This is illustrated by the hierarchal tree in Figure 5.4.

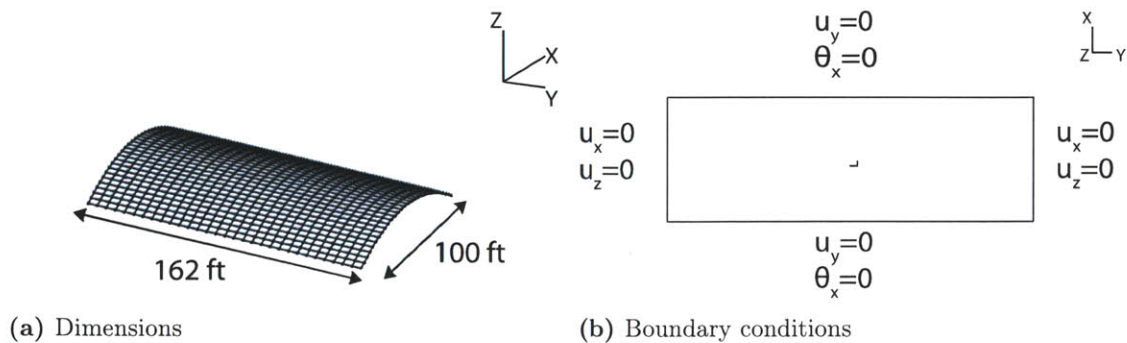


Figure 5.3 – Straight edge barrel vault geometry and boundary conditions

5.2. Problem Definition

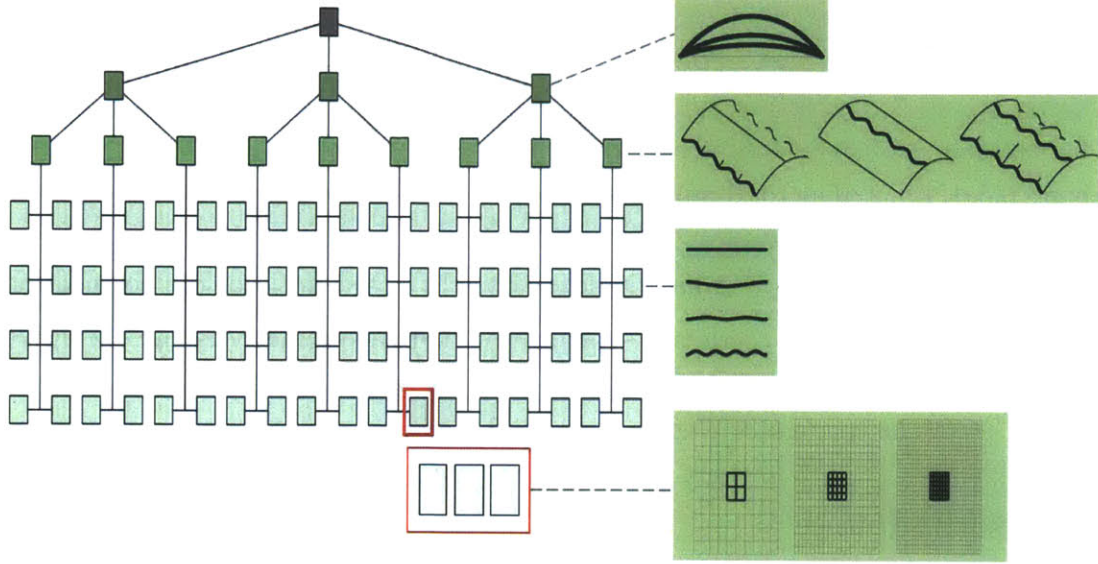


Figure 5.4 – The hierarchal tree illustrating the number of corrugated grid shell models.

The undulations at the edge and crown are defined by a cosine function and the surface is described by Equation 5.2. The two variables defining the undulations are the number of waves n along the length L_2 and the wave amplitudes a_1 and a_2 . The corrugation amplitude at the edge (a_1) is defined as a percentage β_1 of the span; the vault is corrugated at the edge and tapers to a flat crown. The corrugation amplitude at the crown (a_2) is defined as a percentage β_2 of the height; the corrugation is maximum at the crown and tapers to a straight edge at the boundary (Figure 5.5 and Equations 5.3 and 5.4). In the third case where the edge and the crown are corrugated $a_1 \neq a_2$; thus, the corrugation varies along the arclength. The amplitudes are in-phase and this case of corrugation at both the edge and the crown will be referred to as the in-phase case.

$$\begin{aligned} \bar{x} &= x_o + a_1 \cos \frac{2n\pi y}{L_2} \\ z &= \left(h + a_2 \cos \frac{2n\pi y}{L_2} \right) \left(1 - \left(\frac{x}{\bar{x}} \right)^2 \right) \end{aligned} \quad (5.2)$$

$$a_1 = \frac{\beta_1}{100} \left(\frac{L_1}{2} \right) \quad (5.3)$$

Chapter 5. Corrugated Vault Study

$$a_2 = \frac{\beta_2}{100}h \quad (5.4)$$

The two values of β_1 and β_2 are 5% and 10% and the number of waves n per half length are 0.5, 1, 1.5, 2. The total number of combinations of n and β_i is eight and Figure 5.6 illustrates all the combinations. To simplify and minimize the number of parameters, β_i , and n are consumed into $\frac{\lambda}{a_i}$ which is defined as the aspect ratio of the corrugation where $\lambda = \frac{L_2}{n}$. As $\frac{\lambda}{a_i} \rightarrow \infty$ there is no corrugation and the geometry is flat. Multiple combinations of n , and β_i can yield the same $\frac{\lambda}{a_i}$. In Figure 5.7 the change in corrugation in terms of $\frac{\lambda}{a_1}$ for the corrugated edge is illustrated.

5.2.3 Methodology

To tackle this complicated problem, the study is split into two sections. The first is to study the role of curvature on the continuous shell and to validate the modeling techniques used. The second part is to repeat the analysis for grid shells. The procedural steps for both the continuous and grid shell are outlined below, beginning with the definition of the geometry and parameters and concluding with the analysis of the numerical models. In all of these studies the numerical results help identify the structural trends while contributing to the understanding of the mechanics behind grid shells.

Procedural Steps

Continuous Shell:

1. Present the theoretical buckling load of a barrel vault with straight edges.

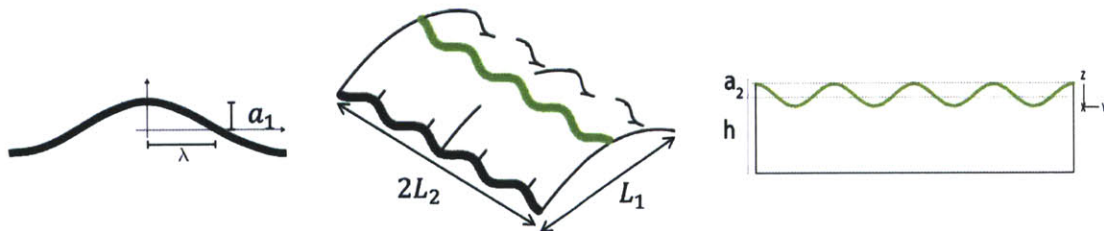


Figure 5.5 – Corrugated barrel vault geometry.

5.2. Problem Definition

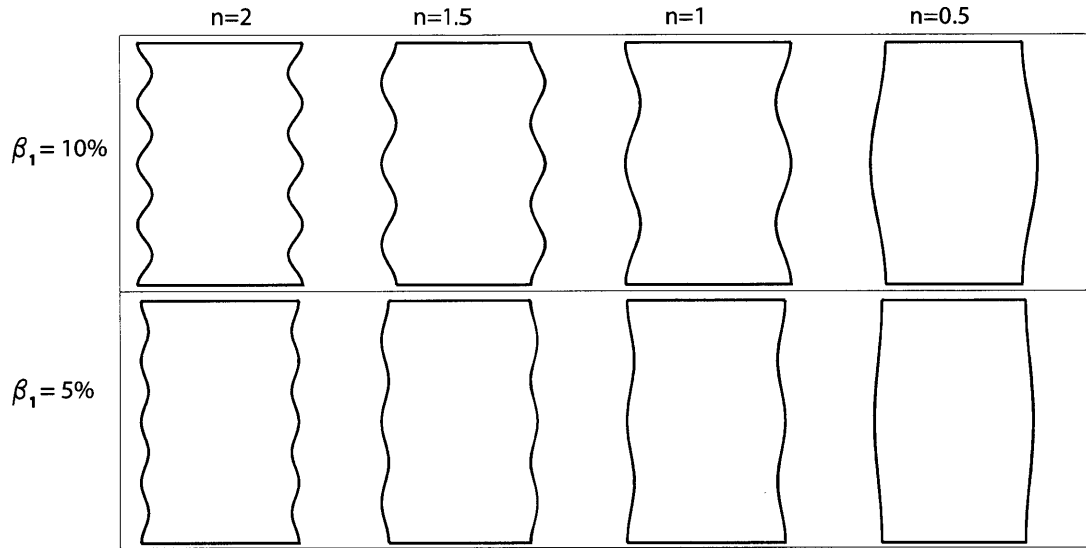


Figure 5.6 – Illustration of the eight combinations of n and β_i for the corrugated edge.

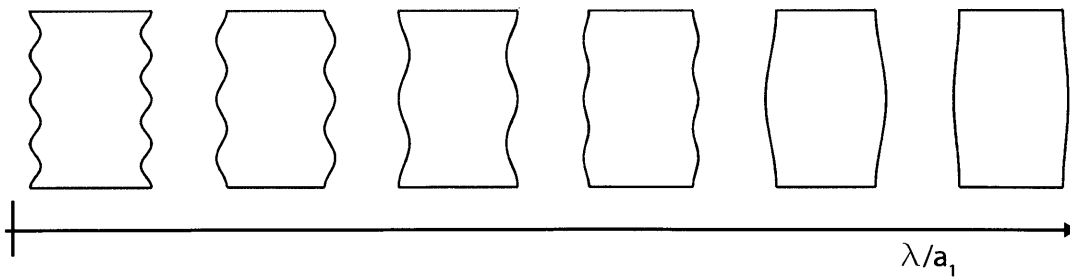


Figure 5.7 – Geometric representation of the corrugated edge as a function of $\frac{\lambda}{a_1}$.

Chapter 5. Corrugated Vault Study

2. Identify parameters describing the double curvature.
3. Construct the continuous shell finite element model of the basic barrel vault.
4. Run the buckling analysis and compare to the analytical solution.
5. Run the collapse analysis and compare to the linearized buckling load.
6. Construct the 100 finite element models in the parametric study.
7. Run the buckling analysis.
8. Plot and analyze results.

Grid Shell:

1. Establish the parameters and ranges that define the grid shell curvature and topology.
2. Define the dimensions based on an equivalent volume between the continuous and the grid shell.
3. Validate the straight edge grid shell with the analytical solution.
4. Proceed with the parametric study constructing 300 grid shell models.
5. Plot and analyze the results.

5.2.4 Analytical Models

In preparation for processing the numerical results, the mathematical representation of the variables affecting the capacity are discussed. No closed form solutions have been derived for the corrugated barrel vault. Here an attempt is made to build an analytical model starting from the plane strain analysis of the straight edge barrel vault.

A plane strain analysis is typically used for structures long in one direction such as a dam. The structure can be simplified to a slice of unit thickness because the strain components ϵ_{yy} , γ_{zy} , and γ_{yz} are zero with the axes defined in Figure 5.8. In the case of the barrel vault, the unit slice is a parabolic arch, as the one studied extensively in Chapter 3.

5.2. Problem Definition

Because the barrel vault span-to-height ratios are relatively shallow, the unit slice is expected to fail by buckling. Thus the arch buckling equation presented in Chapter 3 is modified to a force per unit area in Equation 5.5. The lateral strain is accounted for using Poisson's ratio.

$$q_{cr|barrelvault} = \frac{EI}{R^3} \left(\frac{\pi^2}{\alpha^2} - 1 \right) \left(\frac{1}{b(1-\nu^2)} \right) \quad (5.5)$$

While Equation 5.5 is accurate for a basic barrel vault, the corrugated vault requires more modification. By corrugating the vault the cross-section becomes curved (Figure 5.9) and the moment of inertia is different from the flat section. Thus Equation 5.5 is modified to Equation 5.6 where the moment of inertia for the corrugated section I_{eff} is derived in Equation 5.7. As the amplitude decreases to zero ($a_i \rightarrow 0$), the geometry of the cross-section becomes rectangular and $I_{eff} = I_{rectangle}$. Although the actual corrugation is a cosine function, here the moment of inertia is approximated by using a parabolic function. The ratio of the buckling load of the corrugated vault with I_{eff} to the basic vault can be simplified to Equation 5.8.

$$q_{cr|barrelvault} = \frac{EI_{eff}}{R^3} \left(\frac{\pi^2}{\alpha^2} - 1 \right) \left(\frac{1}{b(1-\nu^2)} \right) \quad (5.6)$$

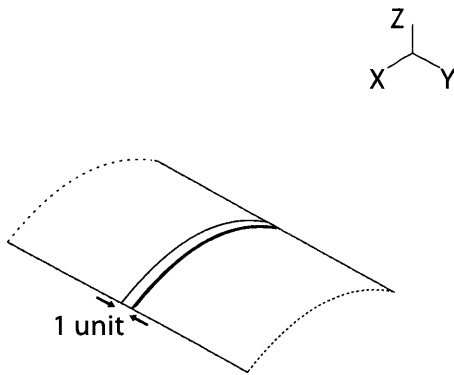


Figure 5.8 – Plane strain condition.

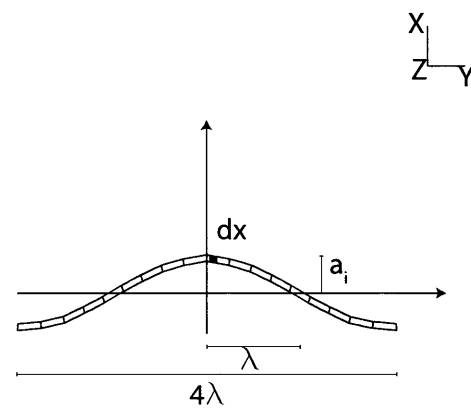


Figure 5.9 – Corrugated shell cross-section.

Chapter 5. Corrugated Vault Study

$$\begin{aligned}
 I_{eff} &= \int_0^\lambda y^2 dA \\
 &= \int_0^\lambda \left(h \left(1 - \left(\frac{x}{\lambda} \right)^2 \right) \right)^2 t dx \\
 &= \frac{2}{5} a_i^2 t \lambda + \frac{2}{3} \left(\frac{t}{2} \right)^3 \lambda \\
 \lim_{a_i \rightarrow 0} I_{eff} &= I_{rectangle} \tag{5.7}
 \end{aligned}$$

$$\begin{aligned}
 \frac{q_{cr}}{q_{cr|straight}} &= \frac{1 + \xi}{\lambda} \\
 \xi &= 5 \left(\frac{a_1}{t} \right)^2 \tag{5.8}
 \end{aligned}$$

As mentioned earlier the moment of inertia varies along the arclength. Timoshenko derived the expression in Equation 5.9 that accounts for a larger moment of inertia at the crown than the edge. The variables I_o and I_1 are the moment of inertias at the crown and the edge respectively, and m is a numerical factor depending on α , the angle of openness and the ratio $\frac{I_1}{I_o}$. The numerical factor m is plotted in Figure 5.10. As the moment of inertia goes to zero at the edge, the capacity decreases. In other words, if the arch became thinner at the supports the arch is weakened and the capacity decreases.

$$\begin{aligned}
 I &= I_o \left[1 - \left(1 - \frac{I_1}{I_o} \right) \frac{\theta}{\alpha} \right] \\
 q_{cr} &= m \frac{EI_o}{\alpha^2 R^3} \tag{5.9}
 \end{aligned}$$

5.2.5 Numerical Models

The mechanics of the corrugated vaults are first studied using continuous shell models of 1 inch thickness. This validates the analytical approach explained earlier as well as the computational modeling techniques.

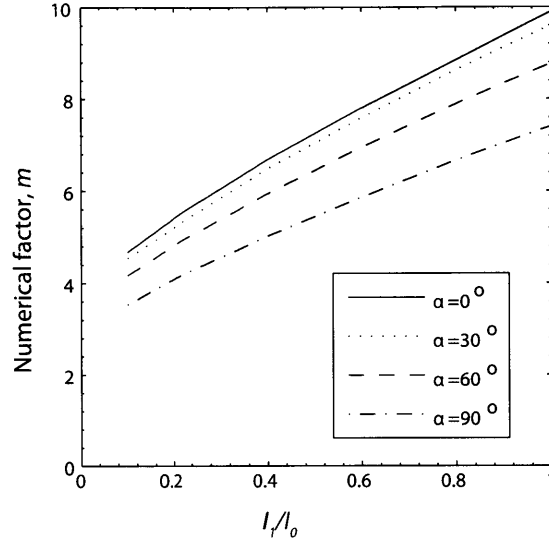


Figure 5.10 – The effect of a varied moment of inertia on the numerical factor m for the buckling load.

Continuous Shell

The FEM of the continuous shell is built using a program by the author (Appendix A) that requires the input of the geometric parameters and outputs a point cloud defining the surface. The surface grid is then imported into ADINA where the surface is created by connecting the control points with a quadrilateral polygonal mesh (Engineering, 2010). A less dense point cloud will produce a less smooth surface, and the surface becomes approximately equal to that of Equation 5.2.

Within the ADINA interface, the surface is meshed using shell elements. As shown earlier in Figure 5.3b, the boundary conditions include no lateral and normal translation along the length of the edges and no longitudinal displacement and rotation about the x axis. Because shell elements are prone to boundary layers due to incompatible boundary conditions, the selection of proper boundary conditions was carefully considered (Chapelle and Bathe, 2011). Finally, a surface pressure is applied, and a linearized buckling analysis is used to calculate the buckling load as was done in Chapters 3 and 4.

Chapter 5. Corrugated Vault Study

Grid Shell

In the grid shell studies three grid densities are considered: 10x10, 20x20, and 30x30 (Figure 5.11). The grid shells are defined to be equivalent in volume to its continuous shell geometric counterpart. The width and longitudinal spacing between the units are denoted as s_x and s_y respectively. The member dimensions are shown in Figure 5.12. To have an equivalent volume to the continuous and because the grid shell members are solid squares, the cross-section dimensions are calculated using Equation 5.10 for the quadrilateral topology. The calculated member thicknesses for an equivalent volume are also provided in Figure 5.11; when the grid becomes finer the member thickness decreases. As in the case of the spherical cap, sources of error in calculating the equivalent thickness include: counting for the volume at the member intersection twice, disregarding the half units at the boundaries, and using a planar projection for calculating the spacing.

$$t_1|_{quad} = t_2|_{quad} \simeq \sqrt{\frac{s_x s_y t}{s_x + s_y}} \quad (5.10)$$

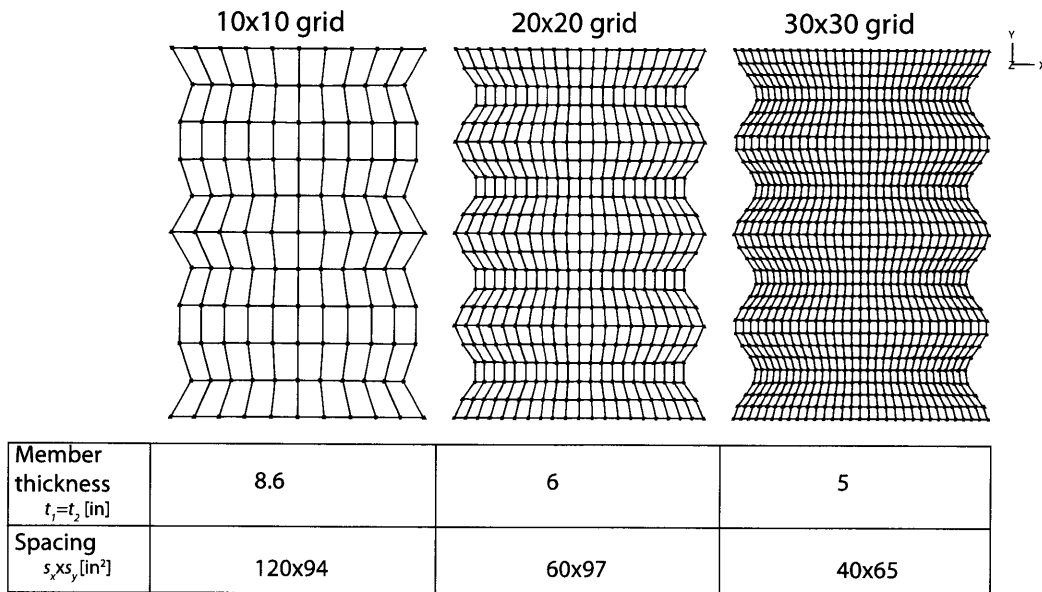


Figure 5.11 – The three grid shell densities used in the corrugated vault study (10x10, 20x20, 30x30).

5.3. Results

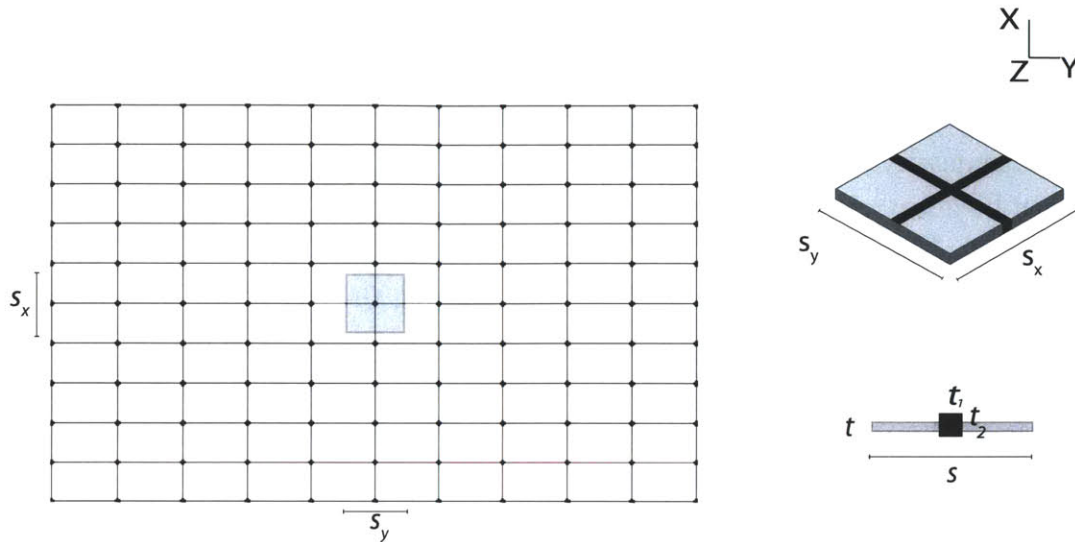


Figure 5.12 – Dimensions of the grid spacing and the overlay of the repeating unit of the grid shell cruciform and the square continuous shell.

The finite element models of the grid shells are created using a Matlab program written by the author and provided in Appendix A. The program defines the FEM by redefining the nodes and element connectivity of the continuous shell to that of the joints and members of the grid shell. The model is then imported into ADINA, and a linearized buckling analysis is used to calculate the buckling load.

5.3 Results

The results are presented in the following subsections:

- **Model Validation:** the straight edge numerical models of both the continuous and the grid shell are compared to the plane strain analysis.
- **Continuous Shell:** the gain in capacity by using corrugation is measured and the results are compared to the analytical model.
- **Grid Shell:** the role of curvature, spacing and topology is analyzed using the numerical results.

Chapter 5. Corrugated Vault Study

5.3.1 Model Validation

First the continuous shell of the basic barrel vault is validated. The buckling load predicted by the numerical models is plotted against the analytical plane strain solution (Figure 5.13). The numerical results coincide with the analytical. Also, the first buckling mode (magnified by a factor of 400 in Figure 5.14) is axisymmetric as is the assumed shape in the analytical derivation.

The grid shell model is also first validated by plotting the analytical plane strain to the numerical for all three grid densities as a function of the shell heights (Figure 5.15). The buckling modes for each grid density are plotted in Figure 5.16 with a magnification factor of 1000. As in the case for the analytical and the continuous shell, the first mode is axisymmetric.

5.3.2 Continuous Shell

The continuous shell results are presented separately by the corrugation locations. To quantify the gains in adding curvature the buckling load of the corrugated barrel vaults is normalized to the buckling load of the basic barrel vault. After the presentation of the numerical results of each corrugation location, the analytical models are discussed. Lastly, all three cases are compared in terms of the cost in volume. In all three cases

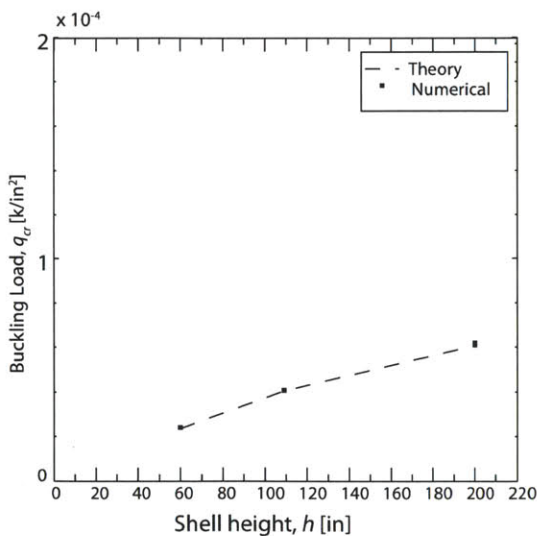


Figure 5.13 – Plane strain validation for the continuous shell.

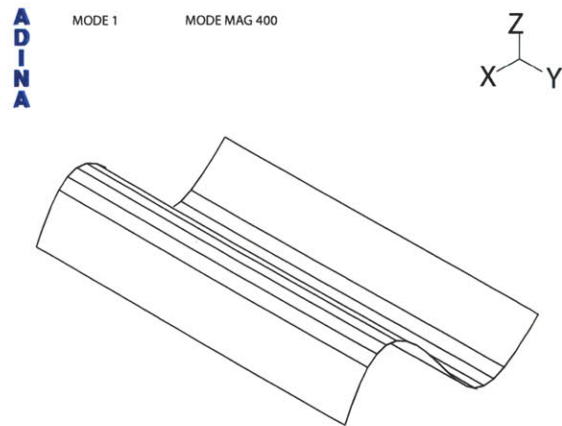


Figure 5.14 – The buckling mode for the continuous shells magnified by a factor of 400.

5.3. Results

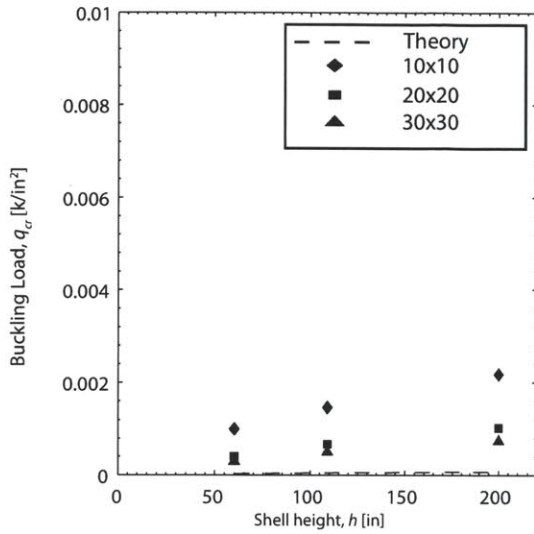


Figure 5.15 – Plane strain validation for the grid shell.

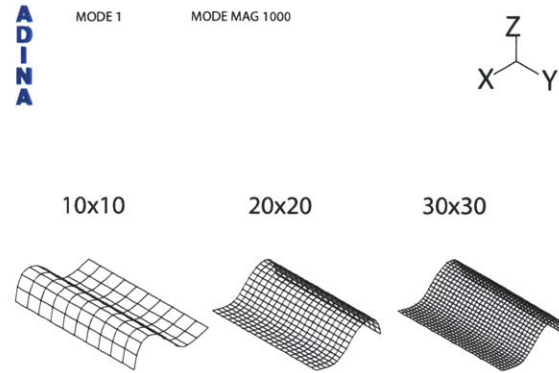


Figure 5.16 – The first buckling mode of the straight vault for each of the three grid shell densities (magnified by a factor of 1000).

there are significant gains by introducing double curvature.

Corrugated Edge: The gain in capacity of the corrugated edge is plotted as a function of the aspect ratio $\frac{\lambda}{a_1}$ in Figure 5.17. First consider the two extremes of the x-axis. As $\frac{\lambda}{a_1}$ approaches infinity the corrugation is non-existent and it becomes a straight edge vault. Thus, the gain in capacity (normalized by the straight edge capacity) converges to unity. At the other extreme when $\frac{\lambda}{a_1}$ approaches zero, the corrugation is “tight” and the gain in capacity ranges from 13 to 35 times the capacity of the straight edge as the span-to-height ratio varies.

In between the two extremes, there is a clear inverse power trend in the data. To understand this trend, in Figure 5.19 the buckling modes (magnified by a factor of 500) are plotted. From top to bottom the aspect ratio of corrugation decreases. All the vaults exhibit the axisymmetric mode as seen in the basic barrel vault. However, it is evident that as the amount of corrugation increases the vault develops a shorter effective length. In essence, the vault maintains the same radius of curvature but the angle of openness α , becomes smaller and smaller as the vault decreases its aspect ratio.

The relationship between the effective angle α_{eff} can be calculated from Equation 5.11 using the numerical data and was plotted as a function of the aspect ratio $\frac{\lambda}{a_1}$. A curve

Chapter 5. Corrugated Vault Study

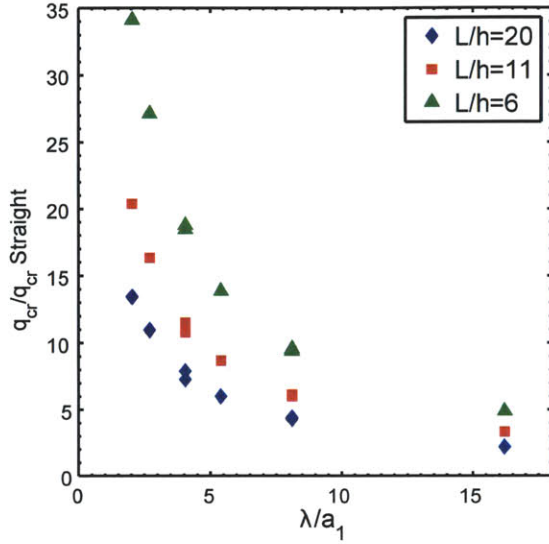


Figure 5.17 – Gain in capacity from the straight barrel vault by corrugating the edge of the continuous shell.

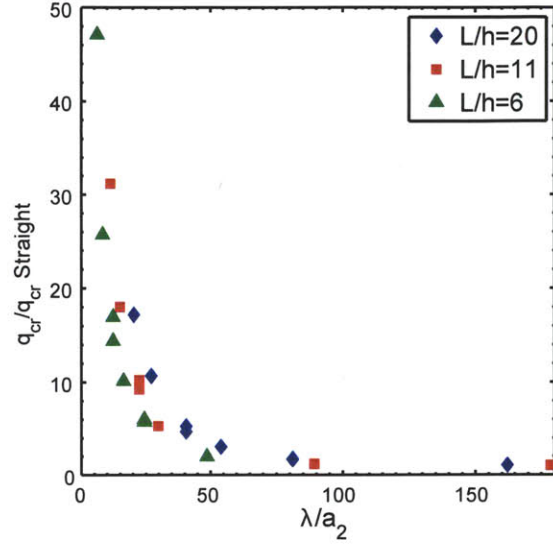


Figure 5.18 – Gain in capacity from the straight barrel vault by corrugating the crown for the continuous shell.

was fit to the data for each of the span-to-height ratios and the fitted equations are given in Table 5.1. These equations can be used for calculated the buckling load of a corrugated edge shell. If the span-to-height ratio is known as well as the desired aspect ratio, the effective angle can be calculated and plugged back into Equation 5.12 to calculate the buckling load.

$$\alpha_{eff} = \frac{\pi}{\sqrt{q_{cr} \left(\frac{12R^3(1-\nu^2)}{Et^3} \right) + 1}} \quad (5.11)$$

$$q_{cr|edge} = \frac{EI}{R^3} \left(\frac{\pi^2}{\alpha_{eff}^2} - 1 \right) \left(\frac{1}{b(1-\nu^2)} \right) \quad (5.12)$$

Corrugated Crown: For the corrugated crown, the gain in capacity is plotted as a function of $\frac{\lambda}{a_2}$, the aspect ratio of the corrugation at the crown (Figure 5.18). As $\frac{\lambda}{a_2}$ approaches infinity, the geometry approaches a straight barrel vault and the gain in capacity approaches unity. As $\frac{\lambda}{a_2}$ approaches zero, the gain in capacity ranges from 20 to 50 times the capacity of the straight vault as the span-to-height ratio varies from 20 to 6 respectively.

In-Phase: The final case considers the vault corrugated at both the crown and the edge.

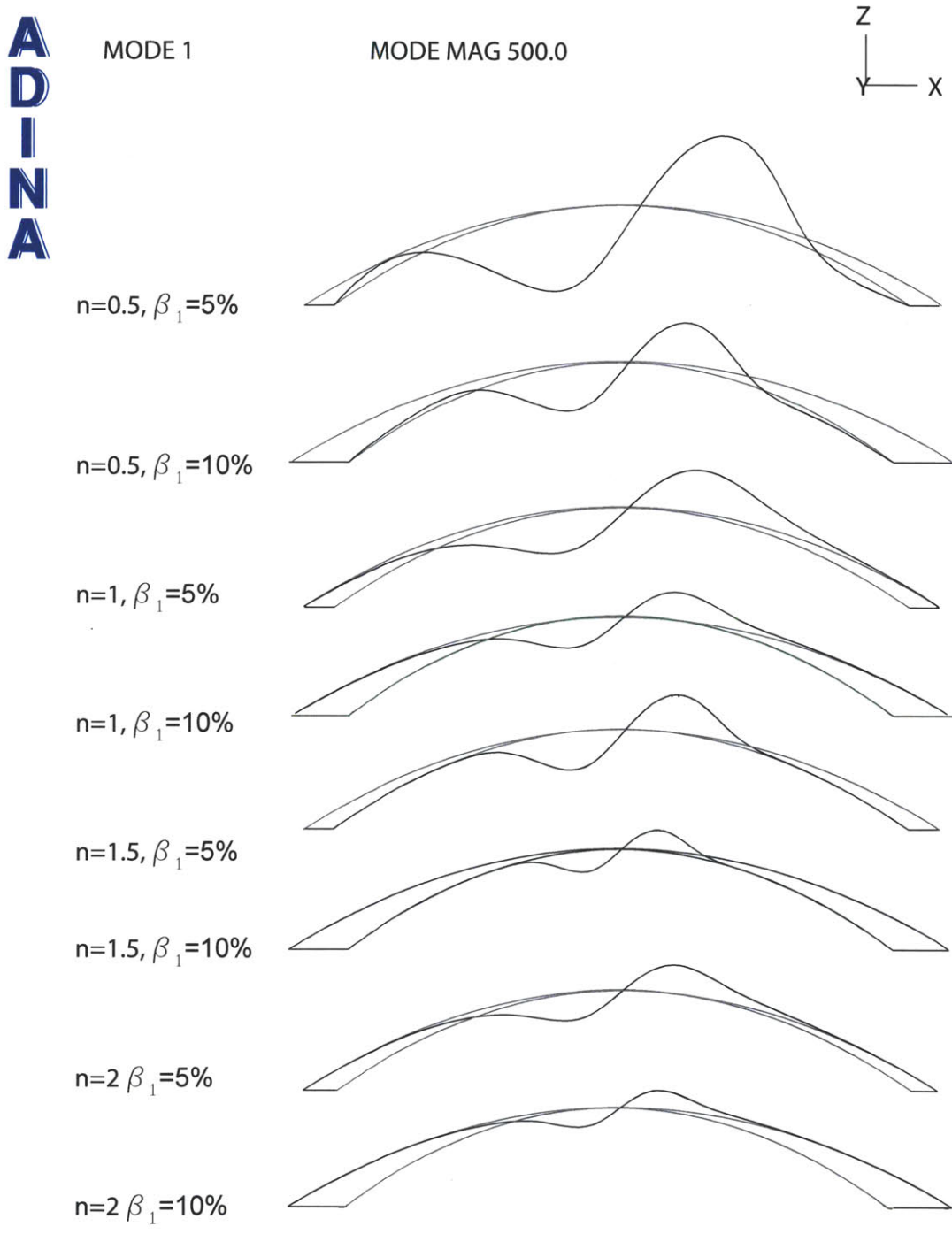


Figure 5.19 – First buckling mode for the corrugated edge case with increasing corrugation from top to bottom (magnified by a factor of 500).

Chapter 5. Corrugated Vault Study

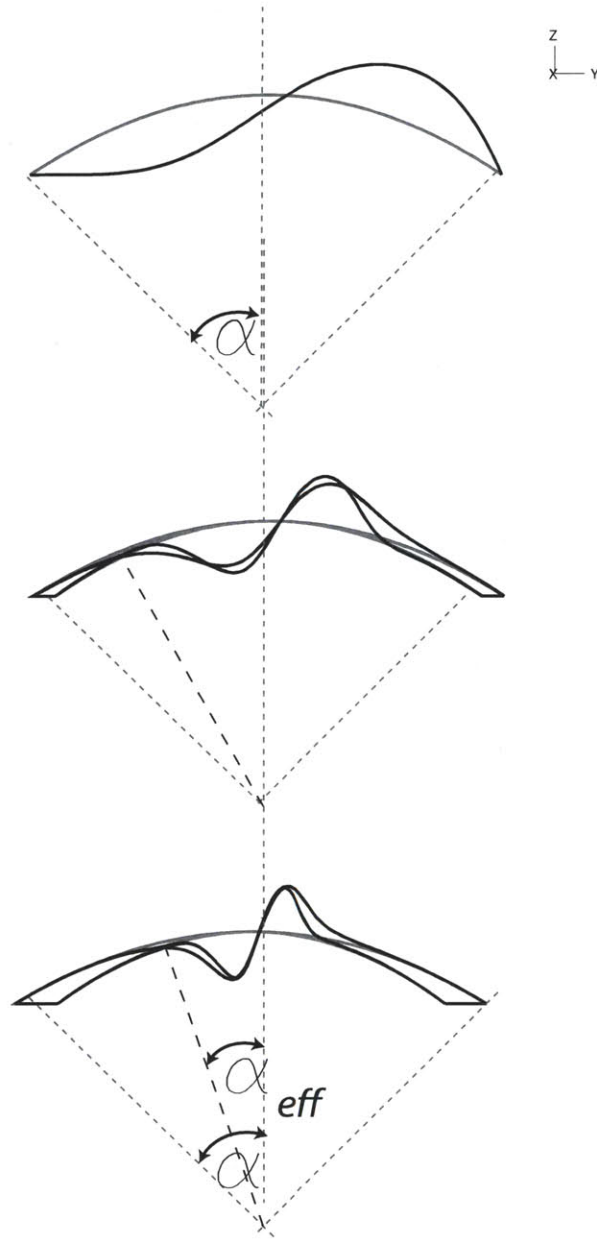


Figure 5.20 – Illustration of the effective arclength α_{eff} .

5.3. Results

Table 5.1 – Equations for calculating α_{eff} given a span-to-height ratio and an aspect ratio of corrugation.

$\frac{L}{h}$	α_{eff}
20	$-0.002\left(\frac{\lambda}{a_1}\right)^2 + 0.23\left(\frac{\lambda}{a_1}\right) + 2.24$
11	$-0.005\left(\frac{\lambda}{a_1}\right)^2 + 0.41\left(\frac{\lambda}{a_1}\right) + 3.08$
6	$-0.006\left(\frac{\lambda}{a_1}\right)^2 + 0.60\left(\frac{\lambda}{a_1}\right) + 4.1$

The gain in capacity is plotted in Figure 5.21 and is measured as a function of the ratio of corrugation amplitudes at the edge and the crown ($\frac{a_1}{a_2}$). As $\frac{a_1}{a_2} \rightarrow \infty$, the corrugated edge is approached and the gain in capacity decreases.

In the matrix plot of Figure 5.21, the rows represent the wave amplitude β_i where row one is $\beta_i = 10\%$ and the second is $\beta_i = 5\%$. The columns represent the number of waves with column 1 at $n = 2$ to column 4 with $n = 0.5$. The plots geometrically match up with Figure 5.6. The presentation of the plots in a matrix shows that having a higher number of waves n is more beneficial than a higher wave amplitude β_i . In other words, it is more beneficial to have a shorter wavelength than to increase the amplitude.

Unlike the corrugated edge case, the buckling modes for the corrugated crown and in-phase all differ. However the mechanics of the structure can still be understood. The weakest point of the straight vault is the flat crown where the point of inflection occurs. If the cross-section at the crown is changed, the difference in capacity can be explained by the increase in the moment of inertia because $q_{cr} \propto I$.

In Figure 5.22 the gain in capacity is calculated analytically using Equation 5.8. Mathematically the behavior is changed by I_{eff} . The plot shows good agreement especially for the in-phase condition. This is because the analytical derivation assumes that the cross-section geometry is the same at the crown and the edge when in fact they vary. To reduce the error, the moment of inertia should be re-derived to take into account its variation along the arclength.

Case Comparison: Having validated that adding double curvature greatly strengthens the barrel vault, the best location to add curvature is measured as a function of the percent increase in volume from the basic barrel vault. In Figure 5.23 all three cases are

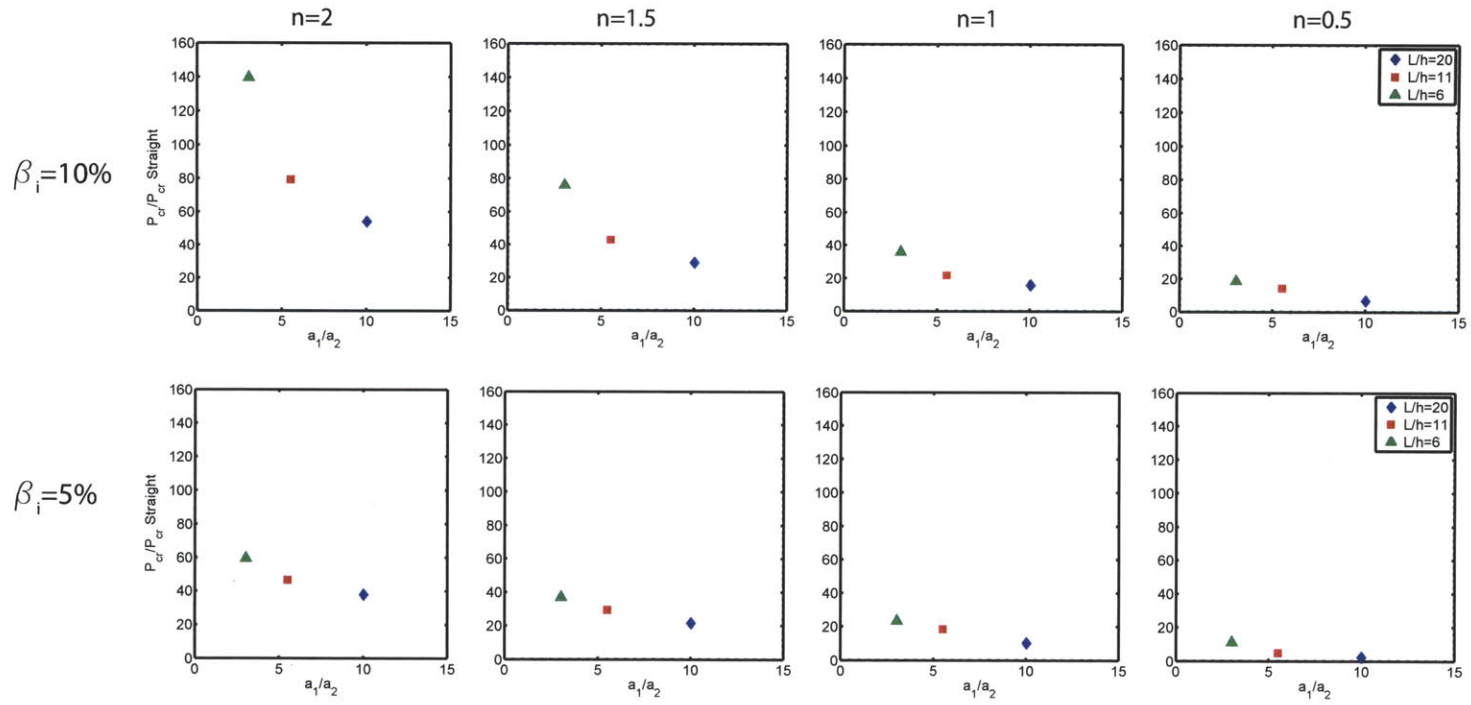


Figure 5.21 – A matrix of plots highlighting the gain in capacity from the straight barrel vault by using in-phase corrugation for the continuous shell. The rows represent the increase in corrugation amplitude by β_i and the columns represent the number of waves n .

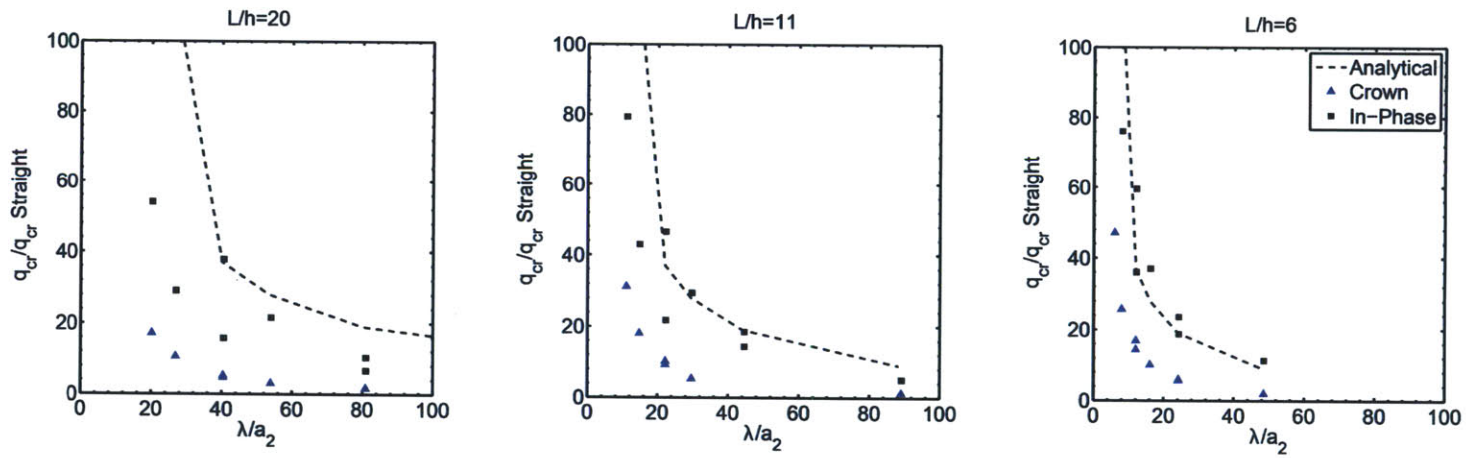


Figure 5.22 – Comparison of the numerical results of the corrugated crown and the in-phase to the analytical (Equation 5.8) for the continuous shell.

Chapter 5. Corrugated Vault Study

plotted as a function of the percent increase in volume for all three span-to-height ratios. For the corrugated edge, for a 1% increase in volume, the capacity is increased by a factor of 40. For the corrugated crown, a 1% increase in volume yields a gain in capacity of a factor of 50. However, the best option is the in-phase corrugation. For the same 1% increase in volume, the in-phase case yields a gain in capacity by a factor of 80.

Collapse Analysis

Before proceeding to the grid shell studies, the linearized buckling analysis is compared to the collapse analysis. The collapse analysis accounts for the prebuckling rotations and nonlinear behavior.

The collapse analysis was performed for an in-phase geometry. Both a normally distributed load and a vertically distributed load was considered and the results are plotted in Figure 5.24. First, both the normal load and vertical load are comparable to each other. Second, the collapse load is approximately three times higher than the buckling load; thus, the buckling load is a conservative estimate and appropriate to use for this parametric study.

5.3.3 Grid Shell

Having gained insight into the behavior of the corrugated continuous shell, the grid shell results are presented next. The same plots used in the continuous shell study are repeated.

Corrugated Edge: First consider only the 30x30 grid shell. For the corrugated edge, the buckling load is normalized by the buckling load of the basic (cylindrical) 30x30 grid shell barrel vault as a function of the aspect ratio $\frac{\lambda}{a_1}$ (Figure 5.25a). The three lines represent the three different span-to-height ratios. Corrugating the edge can increase the capacity up to 5 times that of the straight edge barrel vault. The amount of increase in capacity is proportional to $(\frac{\lambda}{a_1})^{-2}$ as was seen in the continuous shell.

In Figure 5.25b the buckling load is plotted as a function of the shell height. The multiple lines represent the different values of the aspect ratio from 2 to 16. The relationship between the buckling load and the height is linear for a given edge aspect ratio $\frac{\lambda}{a_1}$ and steeper shells are stronger. While increasing the corrugation in the grid shell does benefit the gain in capacity, the amount of gain is not of the same magnitude as seen in the continuous shell.

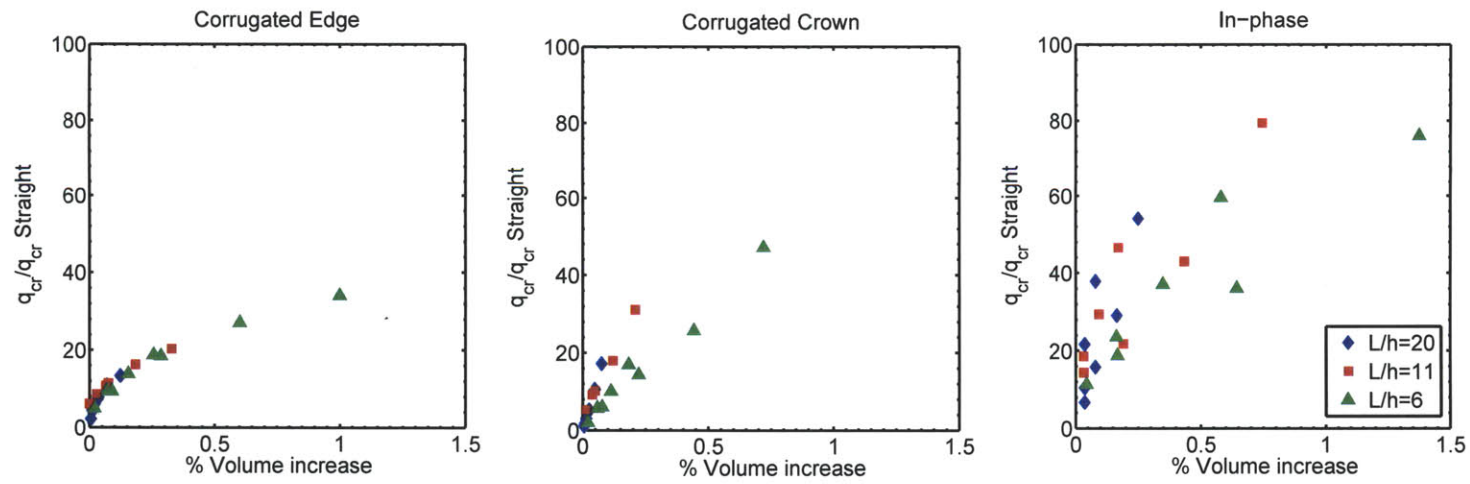


Figure 5.23 – Comparison of the gain in capacity in terms of the percent volume increase from the straight vault for the continuous shell.

Chapter 5. Corrugated Vault Study

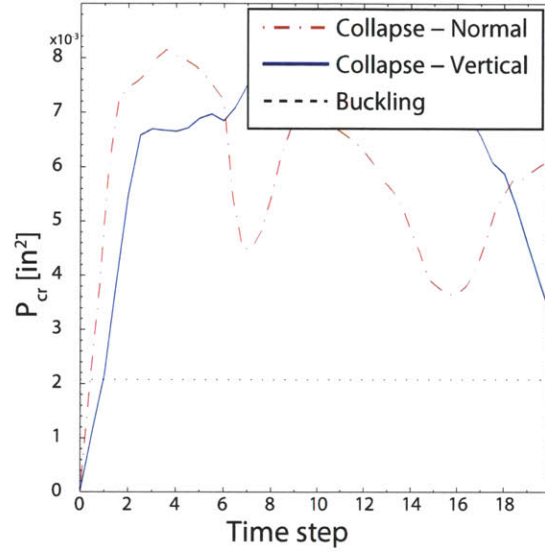


Figure 5.24 – Comparison of the collapse load and the buckling load for a normally distributed load (N) and a vertically distributed load (V) for the in-phase continuous shell.

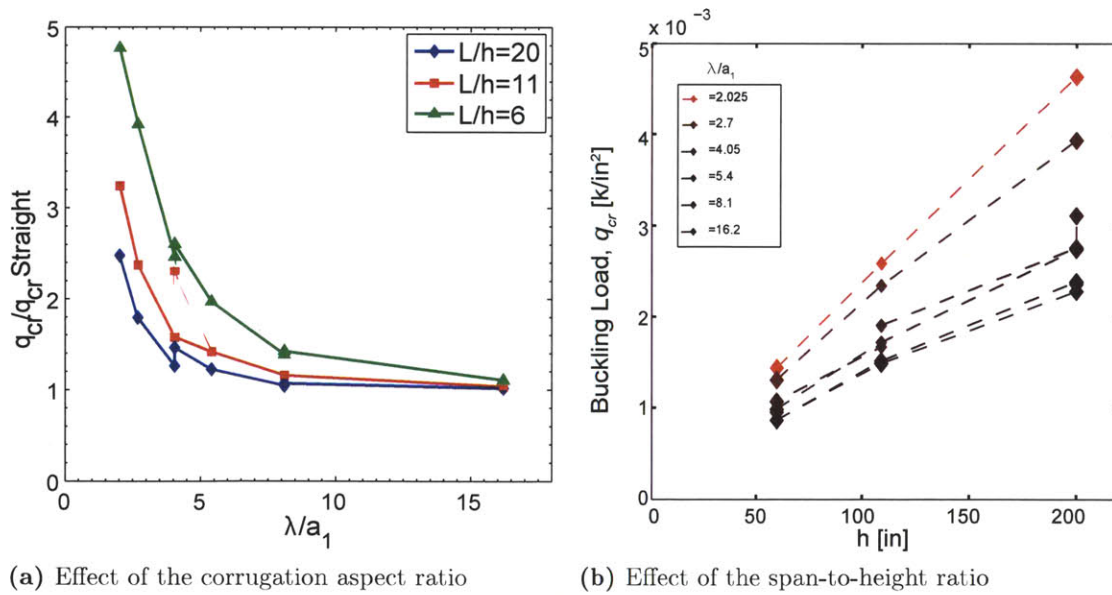


Figure 5.25 – Gain in capacity by corrugating the edge of the 30x30 grid shell.

5.3. Results

Next consider the effect of three grid densities (10x10, 20x20, 30x30) on the capacity for the corrugated edge grid shell. In Figure 5.26 the gain in capacity is plotted for all three grid densities as a function of the aspect ratio. Depending on the grid density, the gain in capacity can reach a maximum of 5 for the densest grid and tallest shell. Table 5.2 lists the maximum allowable corrugation $\frac{\lambda}{a_1}$ to increase the capacity by at least 50%. The denser the grid, the less corrugation is needed to increase the capacity by at least 50%. The effect of grid density is more prominent the steeper shell. Also, the steeper the shell the less corrugation is needed to increase the capacity from a straight vault. Because corrugating the 10x10 grid does not improve the capacity significantly from its straight edge counter part and because for the same amount of volume the 20x20 and 30x30 grid have the same increase in capacity, only a 30x30 grid will be considered in the remaining results.

Corrugated Crown: The same trends seen in the corrugated crown for the continuous shell are exhibited in the grid shell (Figure 5.27). The effect of crown corrugation is only significant if the crown's aspect ratio is $\frac{\lambda}{a_2} \leq 15$. Unlike the corrugated edge, the gain in capacity is less pronounced as the shell height changes; the data points are not easily separated by their height. In total the gain in capacity can quadruple by corrugating the crown.

In-Phase: In Figure 5.28, the grid shell results for the in-phase case are subplotted in a matrix. The rows represent from top to bottom $\beta_i=10\%$ and $\beta_i = 5\%$. The columns from left to right represent the number of waves $n=2$, and 1 respectively. As in the case of the continuous shell, it is more beneficial to increase the number of waves n than to increase the amplitude β_i to increase the gain in capacity; a shorter wavelength is more desirable.

Table 5.2 – Maximum value of $\frac{\lambda}{a_1}$ to increase the capacity of the corrugated edge by at least 50%.

Grid Density	$\frac{L}{h}=20$	$\frac{L}{h}=11$	$\frac{L}{h}=6$
10x10	not possible	2.7	4
20x20	2.7	4	5
30x30	4	4.5	8

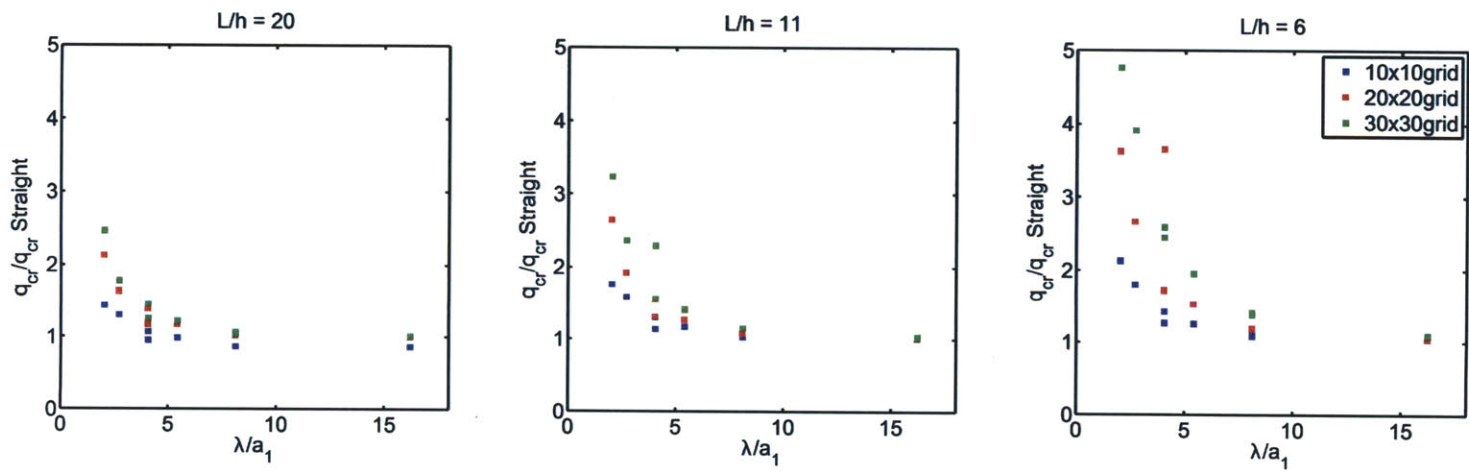


Figure 5.26 – The effect of varying the grid density for the corrugated edge grid shell.

5.3. Results

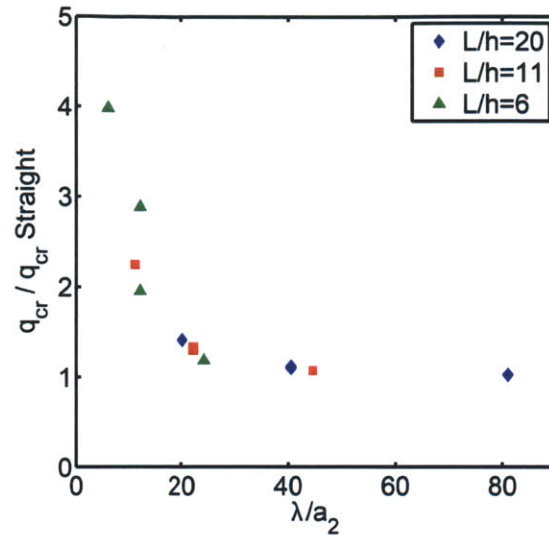


Figure 5.27 – Gain in capacity by corrugating the crown of the 30x30 grid shell.

Case Comparison: Table 5.3 lists the amount of corrugation needed at either the edge or the crown to increase the capacity by 50% for each height. For the corrugated crown, the same increase in capacity can be achieved for a looser corrugation than that at the edge. In Figure 5.29, the three corrugation cases are plotted against each other in terms of the percent increase in volume. For the corrugated edge and the in-phase, the maximum percent increase in volume is 3% but yield a gain in capacity up to five and eight times, respectively. For a less than 1% increase in volume by corrugating the crown, the capacity is quadrupled. As evident in the plots, there is a quicker return on using a corrugated crown.

Table 5.3 – Maximum values of $\frac{\lambda}{a_1}$ and $\frac{\lambda}{a_2}$ to increase the capacity by 50% for the 30x30 grid shell.

Corrugation Case	$\frac{L}{h}=20$	$\frac{L}{h}=11$	$\frac{L}{h}=6$
Edge $\frac{\lambda}{a_1} \leq$	4	4.5	8
Crown $\frac{\lambda}{a_2} \leq$	21	24	19

Chapter 5. Corrugated Vault Study

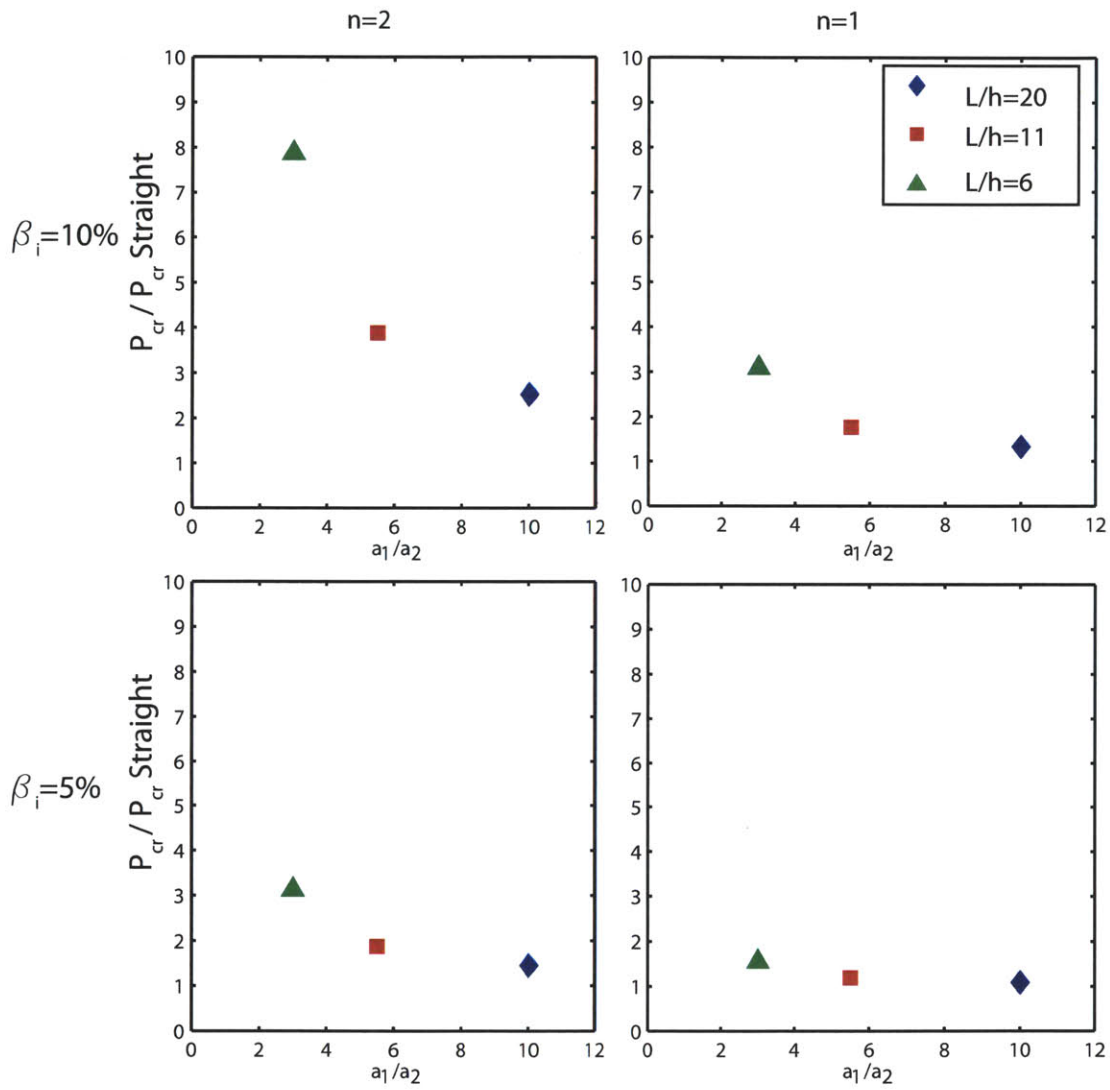


Figure 5.28 – Gain in capacity by in-phase corrugation of the 30x30 grid shell.

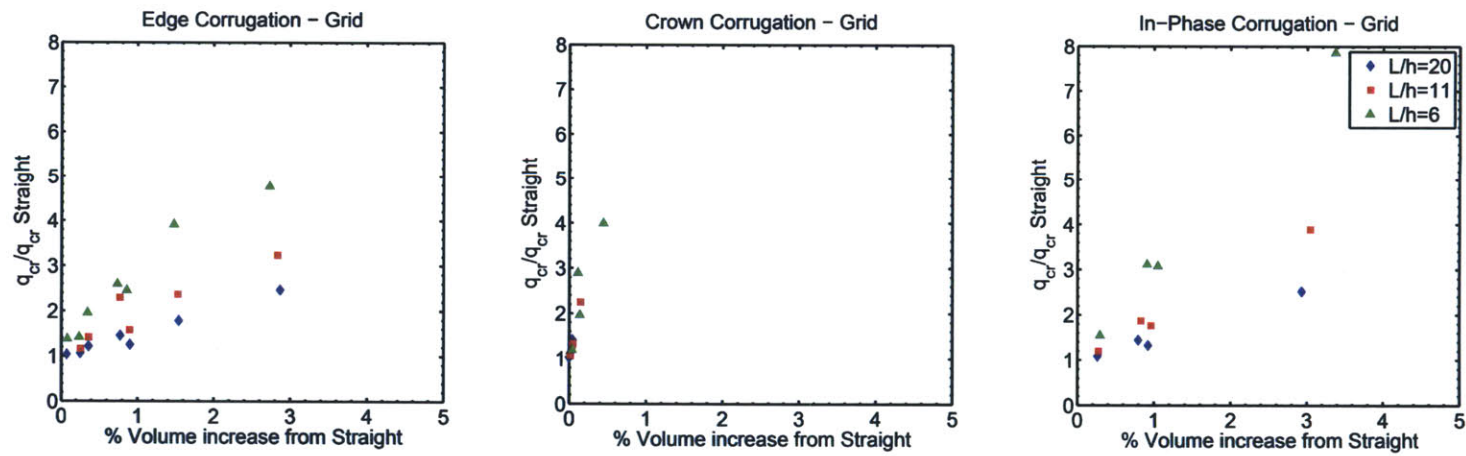


Figure 5.29 – Comparison of the gain in capacity in terms of percent volume increase from straight vault for the grid shell for all three corrugation locations (edge, crown and in-phase).

5.4 Discussion

Corrugated grid shells have many advantages over their continuous counterpart. The discretization and topology provides an articulated, dramatic space. Their openings allow for more design options to be used in terms of lighting, and ventilation. The corrugation provides not only an interesting aesthetic but has a dramatic effect on the capacity, increasing it by a maximum factor of 8 for an increase in volume less than 5%.

The corrugated vault's behavior can be built from considering a plane strain analysis. Physically, corrugation at different locations create different mechanical behavior. For the corrugated edge, the increase corrugation creates an effective length and shortens the arclength that is more susceptible to buckling. For the corrugated crown, the behavior is that of adding a stiffened longitudinal beam to a vault. And lastly the in-phase case changes the cross-section geometry and hence the moment of inertia, increasing the bending stiffness.

In all cases decreasing the span-to-height ratio (becoming steeper) improves the capacity of the vault. However, the amount of improvement in the corrugated crown case is independent of the shell height. The aspect ratio between the edge and the crown differ greatly. To increase the capacity by at least 50%, the corrugated crown can have a looser corrugation by a factor of six than the edge.

Finally, the grid spacing needs to be dense enough to pick up the extra stiffness of curvature, but there is a limiting return. Making the grid denser eventually approaches a continuous shell and the case for designing a grid shell over a continuous lessens. However, as shown in the following design guidelines, increasing the grid density has a small impact when compared to the other factors.

The conclusions made in this study are summarized in a set of design guidelines shown in Figure 5.30 to be used in the early stage of design. The guidelines are organized by the three corrugation locations: the edge, the crown, and at both edge and crown (in-phase). In order to increase the buckling capacity, if the designer is considering edge corrugation, the most effective change would be to increase the height of the shell, and in turn creating a shorter effective arclength.

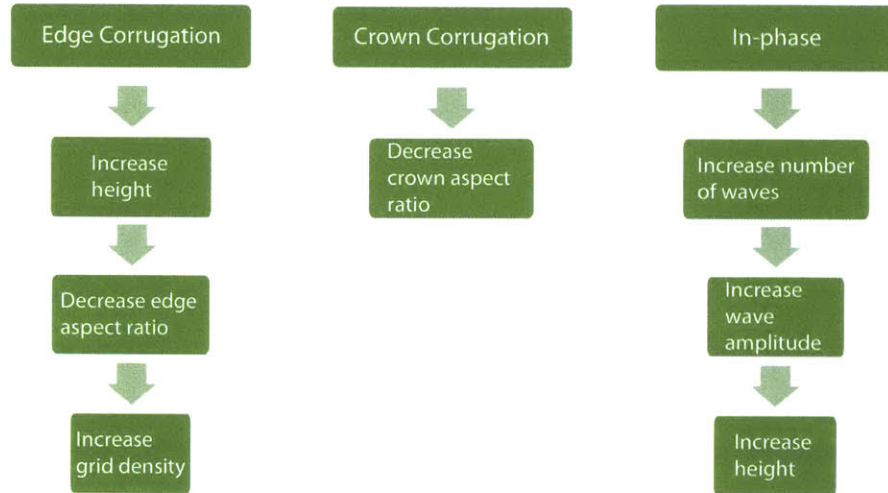


Figure 5.30 – Set of design guidelines to be used in the early stages of design of a corrugated grid shell vault.

5.5 Summary

In this chapter the benefits of corrugating a vault, and varying the grid spacing and span to height ratio are investigated and quantified. Corrugating a vault is an efficient and effective way to increase the load-bearing capacity of a barrel vault. Adding double curvature to the barrel vault has significant gains in capacity up to 8 times for less than a 3% increase in volume. Closed-form solutions for calculating the buckling load were also derived to account for the varied grid shell parameters. A plane strain analysis of a barrel vault was modified to account for an effective arclength when corrugating the edge, and an effective moment of inertia when corrugating the crown. Lastly a set of design guidelines were developed for use in the early stage of design of corrugated grid shells.

Chapter 6

Conclusions

6.1 Summary of Contributions

The goals of this body of work were:

- to calculate the change in load-bearing capacity of grid shells due to their curvature and topology using numerical and analytical methods,
- to provide a set of design guidelines that can contribute to maximize the mechanical performance of grid shells during early design stages.

The goals were achieved by conducting a parametric study varying the topology and topography of grid shells and calculating the change in load-bearing capacity using both numerical and analytical methods. The main contributions are as follows:

- *Parametric Study:* The roles of curvature, and topology on the load-bearing capacity of grid shells were assessed using a parametric study. The parametric study was framed within the context of real design constraints and contained over 400 finite element models. The generation of the spherical cap and corrugated vault finite element models were programmed and inputted into ADINA. The buckling capacity of the finite element models for both the grid shells and the continuous shells was calculated. It was found that:
 - Corrugation is an effective and efficient means to strengthen the barrel vault.
 - Corrugation on a grid shell increases capacity up to 8 times for less than a 3% increase in volume. Corrugation on a continuous shell increases the capacity up to 80 times for a 1.5% volume increase.

6.2. Future Work

- Triangular grid are better for steeper shells (spherical cap).
 - Shallower shells require a denser grid to increase the capacity.
 - Different design configurations of the span-to-height ratio, the spacing and the topology can have the same structural efficiency.
- *Mechanics of Grid Shells:* To describe the mechanics of grid shells, closed form solutions were derived for calculating the buckling load of grid shells. Multiple equivalent continuum approaches were defined and validated and helped distinguish grid shell behavior from being membrane dominated to bending dominated. An equivalent continuum defined by area equivalence is a conservative estimate for the buckling load and can be used the preliminary stages of design.

The first study on the role of double curvature on barrel vaults for both continuous shells and grid shells was completed and the mechanical behavior of the corrugated barrel vault was validated using a plane strain analysis. It was found that corrugating the edge produces an effective arclength, while corrugating the crown increases the moment of inertia.

- *Design Guidelines:* This dissertation developed rules of thumb to be used in the initial design for assessing the behavior of grid shells as a function of their shape, topology, curvature and grid spacing. The parameters of interest were pulled from the literature on the design process of existing grid shells. Simple analytical methods for calculating the buckling load of both spherical cap and corrugated vault grid shells were derived. The guidelines are classified in terms of the main design constraints driving the design process.

6.2 Future Work

The exploration of the mechanics of grid shells have herein contributed towards a better understanding of these complicated structures, but also motivates numerous areas of continued research:

- *Analytical Modeling:* With a better understanding of the collapse analysis and the analytical models developed herein, new analytical models for other surfaces can be developed.

Chapter 6. Conclusions

- *Software Tools*: Having established the significant relationships between the design parameters, the results are to be implemented into a software tool to allow designers and engineers to play with varying the parameters while simultaneously observing their effects on the capacity and volume of material.
- *Joint Design*: Often the cost of grid shells has been affected by the difficulties of the joint design. Future work will account for the trade offs between having more members at the nodes (increasing grid density and capacity) with the complications that arise from designing a joint shared by more members.

Appendix A

MATLAB Code

A.1 Spherical Cap - Quadrilateral Grid

```
1 %The following code creates the finite element ADINA input file a ...
   spherical cap grid shell with a QUADRILATERAL grid
2 clear all
3 delete linecheck15.in
4
5 [headline,geometryData]=hdrload('geometryData.txt');
6 Rvector=geometryData(:,5);
7 hvector=geometryData(:,3);
8 centervector=geometryData(:,2);
9 [d1 d2]=size(Rvector);
10 for(k=1:d1)
11     %Mesh Density
12     uvector=[10;20;30;40;50;60];
13     [u1 u2]=size(uvector);
14     for(l=1:u1)
15         u=uvector(l,1);
16         v=uvector(l,1);
17
18         %% INPUTS
19
20         %Global Geometry
21         L=1200;
22
23
24         h=hvector(k,1); %arc height
25         R=Rvector(k,1); %radius of sphere
26
27         %center of sphere
28         Xo=0;
29         Yo=0;
30         Zo=centervector(k,1);
```

Appendix A. MATLAB Code

```
31
32     %Cross section
33     t1=5; %width of rectangular cross section
34     t2=5; %height of rectangular cross section
35
36     dx=(L)/u; %same as spacing
37     dy=(L)/v;
38
39     ndiv=floor((dx/(2*t1)));%the mesh density per line
40     %% CALCULATING Pcr THEORETICAL
41     %p_crTheoretical
42     %% CREATING THE MESH GRID
43     [X,Y] = meshgrid(-L/2:dx:L/2, -L/2:dy:L/2);
44
45     %to remove point outside of circle
46     %radius that describes the boundary circle on the plane ...
47     (R-h+- Zo)
48     CBR=X.^2+Y.^2;
49     index=find(CBR>(L/2)^2);
50     X(index) = [];
51     Y(index) = [];
52     X=X';
53     Y=Y';
54     %plot(X,Y)
55
56     %to add points that are with the xi, or yi coordinate but sit ...
57     on the circle
58     YcirclePos=((L/2)^2-X.^2).^0.5;
59     XcirclePos=((L/2)^2-Y.^2).^0.5;
60     YcircleNeg=-((L/2)^2-X.^2).^0.5;
61     XcircleNeg=-((L/2)^2-Y.^2).^0.5;
62
63     %check plot
64     %plot(XcirclePos,Y,'bo',XcircleNeg,Y,'m*')
65     %plot(X,YcirclePos,'ks', X,YcircleNeg,'g*')
66
67     %add the circlce boundary points to the mesh grid so we can ...
68     find the z
69     %values at those point
70     Xnew=vertcat(X,XcirclePos, XcircleNeg,X,X);
71     Ynew=vertcat(Y,Y,Y,YcirclePos, YcircleNeg);
72
73     %plot(Xnew,Ynew,'k. ');
74     points=[Xnew Ynew];
75     %points=[X Y];%un comment the line above when i add back the ...
76     circle points
77     %plot(points(:,1),points(:,2),'go');
78     pointsFinal=unique(sortrows(points),'rows');
79     %plot(pointsFinal(:,1),pointsFinal(:,2),'go');
```

A.1. Spherical Cap - Quadrilateral Grid

```

78     X=pointsFinal(:,1);
79     Y=pointsFinal(:,2);
80
81     %need to change the - zo to + if zo is negative
82     if(Zo<0)
83         Z=(R^2-(X-Xo).^2-(Y-Yo).^2).^0.5+Zo;
84     else
85         Z=(R^2-(X-Xo).^2-(Y-Yo).^2).^0.5-Zo;
86     end
87
88     %plot3(X,Y,Z,'ko')
89     pointID=[1:size(X,1)]';
90     PointBLOCK=[pointID X Y Z zeros(size(X))];
91     % if(Zo<0)
92     % axis([-600 600 -600 600 R-h+Zo R+Zo]);
93     % else
94     % axis([-600 600 -600 600 R-h-Zo R-Zo]);
95     % end
96     PointBLOCKOriginal=PointBLOCK;
97
98     %                                     %
99     %   ADD THE AUXILIARY NODES         %
100    %                                     %
101    auxPoints=[PointBLOCK(:,1)+5000,PointBLOCK(:,2:3),...
102               PointBLOCK(:,4)-1,PointBLOCK(:,5)];
103    %append the auxiliary point coordinates to the point block
104    PointBLOCK=[PointBLOCK; auxPoints];
105
106    %% GET THE LINE CONNECTIVITY
107    Xvector=[-L/2:dx:L/2]';
108    Yvector=[-L/2:dy:L/2]';
109    LineBlockFinal=[];
110    for(i=1:size(Xvector,1))
111        indices1=find(X==Xvector(i,1));
112        if(size((indices1),1)>1)
113            LineBlock=[indices1 indices1+1];
114            LineBlock(end,:)=[];
115            LineBlockFinal=vertcat(LineBlockFinal,LineBlock);
116        else
117            end
118    end
119    for(j=1:size(Yvector,1))
120        indices2=find(Y==Yvector(j,1));
121        if(size((indices2),1)>1)
122            indicesA=indices2;
123            indicesA(end,:)=[];
124
125            indicesB=indices2;
126            indicesB(1,:)=[];
127
128            LineBlock=[indicesA indicesB];

```

Appendix A. MATLAB Code

```
129         LineBlockFinal=vertcat (LineBlockFinal,LineBlock);
130     else
131     end
132 end
133 %% ISOLATE THE BOUNDARY NODES
134 CBR=X.^2+Y.^2;
135 tolerance=1e-7;
136 %index3=find(CBR==(L/2)^2);
137 index4=find((1-tolerance)*(L/2)^2<=CBR);%≤(1+tolerance)*(L/2)^2);
138 boundaryPoints=[index4];
139 %SORT BOUNDARY POINTS BASED ON THETA
140 boundaryPointsCoords=[index4 zeros(size(index4))];
141 %more complicated calculation of theta
142 for(i=1:size(index4,1))
143     if(X(index4(i,1))>0)
144         boundaryPointsCoords(i,2)=...
145             atan(Y(index4(i,1))/X(index4(i,1)));
146     end
147
148     if((X(index4(i,1))<0)&& Y(index4(i,1))≥0)
149         boundaryPointsCoords(i,2)=...
150             atan(Y(index4(i,1))/X(index4(i,1)))+pi;
151     end
152
153     if((X(index4(i,1))<0)&& Y(index4(i,1))<0)
154         boundaryPointsCoords(i,2)=...
155             atan(Y(index4(i,1))/X(index4(i,1)))-pi;
156     end
157
158     if((X(index4(i,1))==0)&& Y(index4(i,1))>0)
159         boundaryPointsCoords(i,2)=pi/2;
160     end
161
162     if((X(index4(i,1))==0)&& Y(index4(i,1))<0)
163         boundaryPointsCoords(i,2)=-pi/2;
164     end
165
166     if((X(index4(i,1))==0)&& Y(index4(i,1))==0)
167         boundaryPointsCoords(i,2)=0;
168     end
169
170 end
171
172 sortedboundaryPoints=sortrows(boundaryPointsCoords,2);
173 %get P1 and P2 for boundary lines
174 P1=sortedboundaryPoints(:,1);
175 P2=P1;
176 P2= P2([2:end 1]);
177 boundaryLines=[P1 P2];
178
179 %add boundary lines to line block
```

A.1. Spherical Cap - Quadrilateral Grid

```

180 LineBlockFinal=vertcat (LineBlockFinal,boundaryLines);
181 %
182 %% WRITE THE POINT BLOCK
183 fid=fopen('linecheck15.in','at');
184 fprintf(fid, '*\nMASTER ANALYSIS=STATIC MODEX=EXECUTE ...
      TSTART=0.00000000000000 IDOF=0,\nNOVALIZAT=NONE ...
      FLUIDPOT=AUTOMATIC CYCLICPA=1 IPOSIT=STOP,\nREACTION=YES ...
      INITIALS=NO FSINTERA=NO IPRINT=DEFAULT ...
      CMASS=YES,\nSHELLNDO=AUTOMATIC AUTOMATI=OFF ...
      SOLVER=SPARSE,\nCONTACT=CONSTRAINT-FUNCTION ...
      TRELEASE=0.00000000000000,\nRESTART=NO FRACTURE=NO ...
      LOAD-CAS=NO LOAD-PEN=NO ...
      SINGULAR=YES,\nSTIFFNES=0.000100000000000000 ...
      MAP-OUTP=NONE MAP-FORM=NO,\nNODAL-DE=''' POROUS-C=NO ...
      ADAPTIVE=0 ZOOM-LAB=1 AXIS-CYC=0,\nPERIODIC=NO ...
      VECTOR-S=GEOMETRY EPSI-FIR=NO ...
      STABILIZ=NO,\nSTABFACT=1.0000000000000000E-10 ...
      RESULTS=PORTHOLE FEFCORR=NO,\nBOLTSTEP=1 EXTEND-S=YES ...
      CONVERT=NO DEGEN=YES TMC-MODE=NO,\nENSIGHT=NO');
185 fprintf(fid, '\n*\nCOORDINATES POINT SYSTEM=0\n@CLEAR');
186 fprintf(fid, '\n%d %d %d %d %d',PointBLOCK');
187 %% WRITE THE LINE BLOCK
188 LineID=[1:size(LineBlockFinal,1)];
189 LineBlockFinal2=[LineID LineBlockFinal];
190
191 fprintf(fid, '\n*\nLINE STRAIGHT NAME=%d P1=%d ...
      P2=%d',LineBlockFinal2');
192 fclose(fid);
193
194 %% DEFINE BOUNDARY CONDITIONS
195 %GET POINT IDS OF POINTS THAT NEED TO BE PINNED
196 %Define pinned condition
197 fid=fopen('linecheck15.in','at');
198 fprintf(fid, '\n*\n FIXITY ...
      NAME=PINNED\n@CLEAR\n'X-TRANSLATION'...
      '\n'Y-TRANSLATION'\n'Z-TRANSLATION'\n'OVALIZATION''');
199
200
201 % APPLY BOUNDARY CONDITIONS TO POINTS
202 fprintf(fid, '\n@\n*\n FIXBOUNDARY POINTS FIXITY=PINNED\n@CLEAR');
203 fprintf(fid, '\n%d 'PINNED'', boundaryPoints);
204 fprintf(fid, '\n@');
205
206 %APPLY BOUNDARY CONDITIONS TO LINES
207 fprintf(fid, '\n@\n*\n FIXBOUNDARY LINES FIXITY=PINNED\n@CLEAR');
208 fprintf(fid, '\n%d 'PINNED'', ...
      LineBlockFinal2((end+1-size(boundaryLines)):end,1));
209 fprintf(fid, '\n@');
210 fclose(fid);
211
212 %% CALCULATE LINE LENGTH

```

Appendix A. MATLAB Code

```

213     %this is used to calculate if the rigid end length is greater ...
        than the
214     %line length. here we separate the lines that will have a ...
        rigid end
215     %length and those that will not.
216
217     indexP1=LineBlockFinal2(:,2);
218     indexP2=LineBlockFinal2(:,3);
219
220     length=sqrt((PointBLOCKOriginal(indexP1,2)-...
221                 PointBLOCKOriginal(indexP2,2)).^2+...
222                 (PointBLOCKOriginal(indexP1,3)-...
223                 PointBLOCKOriginal(indexP2,3)).^2+...
224                 (PointBLOCKOriginal(indexP1,4)-...
225                 PointBLOCKOriginal(indexP2,4)).^2);
226     length((end+1-size(boundaryLines)):end,1)=0;
227     %set boundary line lengths to zero so that it won't come up ...
        in rigid end
228     %search
229     indexLength=find((length/ndiv)>=t1);
230
231     indexNOLength=LineID;
232     indexNOLength(indexLength)=[];
233
234     %% WRITE REST OF INPUT FILE
235     %% WRITE MATERIAL BLOCK%
236     fid=fopen('linecheck15.in','at');
237     %below is for elastic material
238     %fprintf(fid,'\n*\nMATERIAL ELASTIC NAME=1 E=29000 NU=0.3, ...
        DESNITY=2.83e-4 ALPHA=0 MDESCRIP='STEEL\''');
239
240     %below is for bilinear material (so that we can enter a ...
        sigma_y yield
241     %stress)
242     fprintf(fid,'\n*\nMATERIAL PLASTIC-BILINEAR NAME=1 ...
        HARDENIN=ISOTROPIC,\nE=29000.0000000000 ...
        NU=0.3000000000000000 ...
        YIELD=50.00000000000000,\nET=50.00000000000000 ...
        EPA=0.0000000000000000 ...
        STRAINRA=0,\nDENSITY=0.000283000000000000 ...
        ALPHA=0.0000000000000000,\nTREF=0.0000000000000000 ...
        DEPENDEN=NO ...
        TRANSITI=0.000100000000000000,\nep-STRAI=0.0000000000000000 ...
        BCURVE=0 ...
        BVALUE=0.0000000000000000,\nXM-INF=0.0000000000000000 ...
        XM0=0.0000000000000000,\nETA=0.0000000000000000 ...
        MDESCRIP='STEEL\''');
243     fclose(fid);
244     %% WRITE CROSS SECTION BLOCK
245     fid=fopen('linecheck15.in','at');

```

A.1. Spherical Cap - Quadrilateral Grid

```

246 fprintf(fid, '\n@\n*\nCROSS-SECTIO RECTANGULAR NAME=1 ...
      WIDTH=%d, \n HEIGHT=%d SC=0 TC=0, \n TORFAC=1 ...
      SSHEARF=0.8333, \n TSHEARF=0 ISHEAR=NO SQUARE=NO', t1, t2);
247 %% DEFINE ELEMENT TYPE
248 fprintf(fid, '\n*\nEGROUP BEAM NAME=1 SUBTYPE=THREE-D ...
      DISPLACE=DEFAULT MATERIAL=1 RINT=5, \n SINT=DEFAULT ...
      TINT=DEFAULT RESULTS=STRESSES INITIALS=NONE, \n ...
      CMASS=DEFAULT RIGIDEND=INFINITE MOMENT-C=NO RIGIDITY=1, \n ...
      MULTIPLY=1000000.00000000 RUPTURE=ADINA OPTION=NONE, \n ...
      BOLT-TOL=0.0000000000000000000000000000000000, \n ...
      PRINT=DEFAULT SAVE=DEFAULT TBIRTH=0.0000000000000000, \n ...
      TDEATH=0.0000000000000000 SPOINT=4 ...
      BOLTFORC=0.0000000000000000, \n BOLINCUR=0 TMC-MATE=1 ...
      BOLT-NUM=0 BOLT-LOA=0.0000000000000000, \n WARP=NO');
249 fclose(fid);
250 %% APPLY LOADS
251 % Apply Point loads to Points on Edge and in middle of ...
      interesecting
252 LoadedPoints=PointBLOCKOriginal(:,1);
253 LoadedPoints([boundaryPoints])=[];
254 [d1 d2]=size(LoadedPoints);
255 forceLabel=(1:1:d1)';
256 fid=fopen('linecheck15.in', 'at');
257 fprintf(fid, '\n*\n LOAD FORCE NAME=1 MAGNITUD= 1 ...
      FX=0.0000000000000000, \nFY=0.0000000000000000 ...
      FZ=-1.0000000000000000');
258 fprintf(fid, '\n*\n APPLY-LOAD BODY=0\n@CLEAR');
259 fprintf(fid, '\n*d ''FORCE'' 1 ''POINT'' %d 0 1 0 0 -1 0 0 0 ...
      ''NO'', \n 0 0 1 0 ''MID'', [forceLabel(:,1) ...
      LoadedPoints(:,1)]');
260 fclose(fid);
261 noLoadedPoints=d1;
262 %% MESH DENSITY
263 %insert here Line Labels
264 fid=fopen('linecheck15.in', 'at');
265 fprintf(fid, '\n*\nSUBDIVIDE LINE NAME=1 MODE=DIVISIONS ...
      NDIV=%d RATIO=1.0000000000000000, \n PROGRESS=GEOMETRIC ...
      CBIAS=NO\n@CLEAR', ndiv);
266 fprintf(fid, '\n*d ', LineBlockFinal2(:,1));
267 fprintf(fid, '\n@');
268 fclose(fid);
269 %% CREATE MESH
270 fid=fopen('linecheck15.in', 'at');
271 auxPointonLine=[LineBlockFinal2(:,2)+5000 LineBlockFinal2(:,1)];
272 %print to file the auxiliary point
273 fprintf('\nauxpoint %d line %d', auxPointonLine')
274 %insert here line labels
275 fprintf(fid, '\n*\nGLINE NODES=2 AUXPOINT=%d NCOINCID=ENDS ...
      NCENDS=12, \n NCTOLERA=1.0000000000000000E-05 SUBSTRUC=0 ...
      GROUP=1 MIDNODES=CURVED\n @CLEAR \n*d\n@', auxPointonLine');

```

Appendix A. MATLAB Code

```

276     fprintf('\nauxpoint %d line %d',[auxPointonLine(:,2) ...
        lineLabel]')
277     fclose(fid);
278     fid=fopen('linecheck15.in','at');
279     fprintf(fid,'\n*\n');
280     fclose(fid);
281     %% ELEMENT DATA
282     t1Vector(1:size(LineBlockFinal2),1)=t1;
283     %to include rigid end lengths
284     fid=fopen('linecheck15.in','at');
285     fprintf(fid,'EDATA SUBSTRUC=0 GROUP=1 ...
        UNDEFINE=IGNORE\n@CLEAR\n@\n');
286     fprintf(fid,'EDATA SUBSTRUC=0 GROUP=1 ...
        UNDEFINE=IGNORE\n@STARTMODIFY\n@CHAROW           1           ...
        101           101');
287     fprintf(fid,'\n%d 1 1 0 ''DEFAULT'' ''DEFAULT'' ...
        0.000000000000000 0.000000000000000 0,\n0.000000000000000 %d ...
        %d\n', [LineBlockFinal2(:,1) t1Vector t1Vector]);
288     %put rigid ends on elements that are long enough
289     firstElement=(ndiv).*LineBlockFinal2(indexLength,1)-(ndiv-1);
290     lastElement=(ndiv).*LineBlockFinal2(indexLength,1);
291
292     noOfElement=(1:ndiv*size(LineBlockFinal2,1))';
293     noOfElement([firstElement,lastElement])=[];
294
295     fprintf(fid,'\n%d 1 1 0 ''DEFAULT'' ''DEFAULT'' ...
        0.000000000000000 0.000000000000000 0,\n0.000000000000000 %d ...
        0',[firstElement t1Vector(indexLength,1)]');
296     fprintf(fid,'\n%d 1 1 0 ''DEFAULT'' ''DEFAULT'' ...
        0.000000000000000 0.000000000000000 0,\n0.000000000000000 0 ...
        %d',[lastElement t1Vector(indexLength,1)]');
297     %make NO rigid ends on elements whose length are not long enough
298     fprintf(fid,'\n%d 1 1 0 ''DEFAULT'' ''DEFAULT'' ...
        0.000000000000000 0.000000000000000 0,\n0.000000000000000 0 ...
        0',noOfElement);
299     %
300     fprintf(fid,'\n@ENDMODIFY\n*\nEDATA SUBSTRUC=0 GROUP=1 ...
        UNDEFINE=IGNORE\n@STARTMODIFY\n@ENDMODIFY');
301     fclose(fid);
302     %% COPY INPUT FILE TO FILE WITH THE HEIGHT AND MESH DENSITY ...
        IDENTIFIED
303     copyfile('linecheck15.in',['inputFiles/Height_' num2str(h) ...
        '_' num2str(u) 'x' num2str(u) '.in'])
304     delete linecheck15.in
305     end
306 end

```


A.2 Spherical Cap - Triangular Grid

```

1 %The following code creates the finite element input file for a spherical
2 %cap grid shell with a TRIANGULAR grid
3 clear all
4 %% INPUTS
5 %Global Geometry
6 L=1200;
7 h=200;%hvector(k,1); %arc height
8 R=1000%Rvector(k,1); %radius of sphere
9 %center of sphere
10 Xo=0;
11 Yo=0;
12 Zo=-200;%centervector(k,1);
13 %Cross section
14 t1=5; %width of rectangular cross section
15 t2=5; %height of rectangular cross section
16 %mesh density
17 u=50;
18 v=50;
19 dx=(L)/u;
20 dy=(L)/v;
21
22 ndiv=floor((dx/(2*t1)));%the mesh density per line
23 %% MESH GENERATOR
24 figure
25 fd=inline('sqrt(sum(p.^2,2))-600','p');
26 [p,t]=distmesh2d(fd,@huniform,dx,[-600,-600;600,600],[]);
27 % p contains the nodal points, need to insert the nodal label, and ...
   put in a
28 % z coordinate of 0, and a coordinate system of 0;
29 %% edit info from mesh generator
30 % t contains teh element connectivity, but need to insert the element ...
   label
31 % [d1 d2]= size(t)
32 % elemid=[1:1:d1]';
33 % elemconn=[elemid, t(:,1), t(:,2), t(:,3)];
34
35 % Get POINT coordinates
36 [d1 d2]=size(p);
37 pointid=[1:1:d1]';
38 X=p(:,1);
39 Y=p(:,2);
40 Z=zeros(d1,1);
41 coordsys=zeros(d1,1);
42 pointBlock1=[pointid X Y Z coordsys];
43 %% CALCULATING THE Z VALUE
44 %need to change the - zo to + if zo is negative
45 if(Zo<0)

```

Appendix A. MATLAB Code

```
46     Z=(R^2-(X-Xo).^2-(Y-Yo).^2).^0.5+Zo;
47 else
48     Z=(R^2-(X-Xo).^2-(Y-Yo).^2).^0.5-Zo;
49 end
50
51 pointBlock(:,4)=Z;
52 pointBlock=pointBlock1;
53 PointBLOCKOriginal=pointBlock;
54 %% GET THE ELEMENT CONNECTIVITY
55 elemConnectivity=t;
56 [d1 d2]=size(elemConnectivity);
57 for (i=1:d1)
58     j=3*i-2;
59     lineBlock(j,1:2)=[elemConnectivity(i,1) elemConnectivity(i,2)];
60     lineBlock(j+1,1:2)=[elemConnectivity(i,2) elemConnectivity(i,3)];
61     lineBlock(j+2,1:2)=[elemConnectivity(i,3) elemConnectivity(i,1)];
62 end
63 %clean up the line block to get rid of repeating lines
64 lineBlock(:, :);
65 lineblockorig=lineBlock;
66 [d1 d2]=size(lineBlock);
67 for (i=2:d1)
68     for (j=i+1:d1)
69         pair1=[lineBlock(i,1) lineBlock(i,2)];
70         pair2=[lineBlock(j,2) lineBlock(j,1)];
71
72         if(pair2==pair1)
73             lineBlock(j,:)=[];
74
75             [d1 d2]=size(lineBlock);
76             break
77         else
78             end
79     end
80 end
81 lineLabel=(1:1:d1)';
82 lineBLOCKFINAL=[lineLabel, lineBlock];
83
84 %%
85 %     START TO WRITE INPUT BLOCKS FOR ADINA FILE
86 %
87 %% INSERTING COMMON INFO INTO THE ADINA INPUT FILE
88 % WRITE THE POINT BLOCK
89 auxPoints=[pointBlock(:,1)+5000,pointBlock(:,2:3),pointBlock(:,4)-1,...
90     pointBlock(:,5)]
91 pointBlockFINAL=[pointBlock; auxPoints]
92 %
93 %% WRITE THE POINT BLOCK
94 fid=fopen('linecheck15.in','at');
95 fprintf(fid, '*\nMASTER ANALYSIS=STATIC MODEX=EXECUTE ...
    TSTART=0.000000000000 IDOF=0,\noVALIZAT=NONE FLUIDPOT=AUTOMATIC ...
```

A.2. Spherical Cap - Triangular Grid

```

CYCLICPA=1 IPOSIT=STOP,\nREACTION=YES INITIALS=NO FSINTERA=NO ...
IRINT=DEFAULT CMASS=YES,\nSHELLNDO=AUTOMATIC AUTOMATI=OFF ...
SOLVER=SPARSE,\nCONTACT-=CONSTRAINT-FUNCTION ...
TRELEASE=0.00000000000000,\nRESTART-=NO FRACTURE=NO LOAD-CAS=NO ...
LOAD-PEN=NO SINGULAR=YES,\nSTIFFNES=0.000100000000000000 ...
MAP-OUTP=NONE MAP-FORM=NO,\nNODAL-DE='' POROUS-C=NO ADAPTIVE=0 ...
ZOOM-LAB=1 AXIS-CYC=0,\nPERIODIC=NO VECTOR-S=GEOMETRY EPSI-FIR=NO ...
STABILIZ=NO,\nSTABFACT=1.0000000000000000E-10 RESULTS=PORTHOLE ...
FEFCORR=NO,\nBOLTSTEP=1 EXTEND-S=YES CONVERT-=NO DEGEN=YES ...
TMC-MODE=NO,\nENSIGHT-=NO');
96 fprintf(fid, '\n*\nCOORDINATES POINT SYSTEM=0\n@CLEAR');
97 fprintf(fid, '\n%d %d %d %d %d',pointBlockFINAL);
98 fclose(fid);
99 %% WRITE THE LINE BLOCK
100 fid=fopen('linecheck15.in','at');
101 fprintf(fid, '\n*\nLINE STRAIGHT NAME=%d P1=%d P2=%d',lineBLOCKFINAL);
102 fclose(fid);
103 %define the auxiliary point for each line, this will be used later
104 auxPointonLine=[lineBLOCKFINAL(:,1),lineBLOCKFINAL(:,2)+5000]
105 %% Find boundary lines and points
106 index1=find((599<=Z) & (Z<=601));
107 boundarypoints=pointBlockFINAL(index1,1);
108 %% WRITE BOUNDARY BLOCK
109 %GET POINT IDS OF POINTS THAT NEED TO BE PINNED
110 %Define pinned condition
111 fid=fopen('linecheck15.in','at');
112 fprintf(fid, '\n*\n FIXITY NAME=PINNED\n@CLEAR\n'X-TRANSLATION'...
113 '\n'Y-TRANSLATION'\n'Z-TRANSLATION'\n'OVALIZATION''');
114 %APPLY BOUNDARY CONDITIONS TO POINTS
115 fprintf(fid, '\n@\n*\n FIXBOUNDARY POINTS FIXITY=PINNED\n@CLEAR');
116 fprintf(fid, '\n%d 'PINNED'', boundarypoints);
117 fprintf(fid, '\n@');
118 fclose(fid);
119 %% WRITE REST OF ADINA FILE
120 %
121 %%% WRITE MATERIAL BLOCK%
122 fid=fopen('linecheck15.in','at');
123 %below is for elastic material
124 fprintf(fid, '\n*\nMATERIAL ELASTIC NAME=1 E=29000 NU=0.3, ...
125 DESNITY=2.83e-4 ALPHA=0 MDESCRIP='STEEL\''');
126 %below is for bilinear material (so that we can enter a sigma_y yield
127 %stress)
128 %fprintf(fid, '\n*\nMATERIAL PLASTIC-BILINEAR NAME=1 ...
129 HARDENIN=ISOTROPIC,\nE=29000.000000000000 NU=0.3000000000000000 ...
130 YIELD=50.00000000000000,\nET=50.00000000000000 ...
131 EPA=0.0000000000000000 STRAINRA=0,\nDENSITY=0.000283000000000000 ...
132 ALPHA=0.0000000000000000,\nTREF=0.0000000000000000 DEPENDEN=NO ...
133 TRANSITI=0.000100000000000000,\nEP-STRAI=0.0000000000000000 ...
134 BCURVE=0 BVALUE=0.0000000000000000,\nXM-INF=0.0000000000000000 ...
135 XM0=0.0000000000000000,\nETA=0.0000000000000000 MDESCRIP='STEEL\''');
128 fclose(fid);

```

Appendix A. MATLAB Code

```
129 %% WRITE CROSS SECTION BLOCK
130 fid=fopen('linecheck15.in','at');
131 fprintf(fid,'\n*\n\CROSS-SECTIO RECTANGULAR NAME=1 WIDTH=%d,\n ...
    HEIGHT=%d SC=0 TC=0,\n TORFAC=1 SSHEARF=0.8333,\n TSHEARF=0 ...
    ISHEAR=NO SQUARE=NO',t1,t2);
132 %% DEFINE ELEMENT TYPE
133 fprintf(fid,'\n*\nEGROUP BEAM NAME=1 SUBTYPE=THREE-D DISPLACE=DEFAULT ...
    MATERIAL=1 RINT=5,\n SINT=DEFAULT TINT=DEFAULT RESULTS=STRESSES ...
    INITIALS=NONE,\n CMASS=DEFAULT RIGIDEND=INFINITE MOMENT-C=NO ...
    RIGIDITY=1,\n MULTIPLY=1000000.00000000 RUPTURE=ADINA ...
    OPTION=NONE,\n BOLT-TOL=0.0000000000000000 DESCRIPT='NONE' ...
    SECTION=1,\n PRINT=DEFAULT SAVE=DEFAULT ...
    TBIRTH=0.0000000000000000,\n TDEATH=0.0000000000000000 SPOINT=4 ...
    BOLTFORC=0.0000000000000000,\n BOLTNCUR=0 TMC-MATE=1 BOLT-NUM=0 ...
    BOLT-LOA=0.0000000000000000,\n WARP=NO');
134 fclose(fid);
135 %% APPLY LOADS
136 % Apply Point loads to Points on Edge and in middle of interesecting
137 LoadedPoints=pointBlock(:,1);
138 LoadedPoints([boundarypoints])=[];
139 [d1 d2]=size(LoadedPoints);
140 forceLabel=(1:1:d1)';
141 fid=fopen('linecheck15.in','at');
142 fprintf(fid,'\n*\n LOAD FORCE NAME=1 MAGNITUD= 1 ...
    FX=0.0000000000000000,\nFY=0.0000000000000000 FZ=-1.0000000000000000');
143 fprintf(fid,'\n*\n APPLY-LOAD BODY=0\n@CLEAR');
144 fprintf(fid,'\n%d ''FORCE'' 1 ''POINT'' %d 0 1 0 0 -1 0 0 0 ...
    ''NO'',\n 0 0 1 0 ''MID'',[forceLabel(:,1) LoadedPoints(:,1)]');
145 fclose(fid);
146 noLoadedPoints=d1;
147 %% MESH DENSITY
148 %insert here Line Labels
149 fid=fopen('linecheck15.in','at');
150 fprintf(fid,'\n*\nSUBDIVIDE LINE NAME=1 MODE=DIVISIONS NDIV=%d ...
    RATIO=1.0000000000000000,\n PROGRESS=GEOMETRIC CBIAS=NO\n@CLEAR',ndiv);
151 fprintf(fid,'\n%d ', lineBLOCKFINAL(:,1));
152 fprintf(fid,'\n@');
153 fclose(fid);
154 %% CREATE MESH
155 fid=fopen('linecheck15.in','at');
156 auxPointonLine=[lineBLOCKFINAL(:,2)+5000 lineBLOCKFINAL(:,1)];
157 %print to file the auxiliary point
158 fprintf('\nauxpoint %d line %d',auxPointonLine)
159 %insert here line labels
160 fprintf(fid,'\n*\nGLINE NODES=2 AUXPOINT=%d NCOINCID=ENDS ...
    NCENDS=12,\n NCTOLERA=1.0000000000000000E-05 SUBSTRUC=0 GROUP=1 ...
    MIDNODES=CURVED\n @CLEAR \n%d\n@',auxPointonLine);
161 fprintf('\nauxpoint %d line %d',[auxPointonLine(:,2) lineLabel]')
162 fclose(fid);
163 fid=fopen('linecheck15.in','at');
164 fprintf(fid,'\n*\n');
```

A.2. Spherical Cap - Triangular Grid

```

165 fclose(fid);
166 %% isolate boundary, copied this from quad grid
167 %ISOLATE THE BOUNDARY NODES
168 CBR=X.^2+Y.^2;
169 tolerance=1e-7;
170 %index3=find(CBR==(L/2)^2);
171 index4=find((1-tolerance)*(L/2)^2<=CBR);%<=(1+tolerance)*(L/2)^2);
172 boundaryPoints=[index4];
173 %SORT BOUNDARY POINTS BASED ON THETA
174 boundaryPointsCoords=[index4 zeros(size(index4))];
175 %more complicated calculation of theta
176 for(i=1:size(index4,1))
177     if(X(index4(i,1))>0)
178         boundaryPointsCoords(i,2)=atan(Y(index4(i,1))/X(index4(i,1)));
179     end
180
181     if((X(index4(i,1))<0)&& Y(index4(i,1))>=0)
182         boundaryPointsCoords(i,2)=atan(Y(index4(i,1))/X(index4(i,1)))+pi;
183     end
184
185     if((X(index4(i,1))<0)&& Y(index4(i,1))<0)
186         boundaryPointsCoords(i,2)=atan(Y(index4(i,1))/X(index4(i,1)))-pi;
187     end
188
189     if((X(index4(i,1))==0)&& Y(index4(i,1))>0)
190         boundaryPointsCoords(i,2)=pi/2;
191     end
192
193     if((X(index4(i,1))==0)&& Y(index4(i,1))<0)
194         boundaryPointsCoords(i,2)=-pi/2;
195     end
196
197     if((X(index4(i,1))==0)&& Y(index4(i,1))==0)
198         boundaryPointsCoords(i,2)=0;
199     end
200
201 end
202
203 sortedboundaryPoints=sortrows(boundaryPointsCoords,2);
204 %get P1 and P2 for boundary lines
205 P1=sortedboundaryPoints(:,1);
206 P2=P1;
207 P2= P2([2:end 1]);
208 boundaryLines=[P1 P2];
209 %         LineBlockFinal=vertcat(LineBlockFinal,boundaryLines);
210
211 %% CALCULATE LINE LENGTH
212 %this is used to calculate if the rigid end length is greater than the
213 %line length. here we separate the lines that will have a rigid end
214 %length and those that will not.
215

```

Appendix A. MATLAB Code

```

216 indexP1=lineBLOCKFINAL(:,2);
217 indexP2=lineBLOCKFINAL(:,3);
218
219 length=sqrt((PointBLOCKOriginal(indexP1,2)-...
220 PointBLOCKOriginal(indexP2,2)).^2+...
221 (PointBLOCKOriginal(indexP1,3)-...
222 PointBLOCKOriginal(indexP2,3)).^2+...
223 (PointBLOCKOriginal(indexP1,4)-PointBLOCKOriginal(indexP2,4)).^2);
224 length((end+1-size(boundaryLines):end,1)=0;
225 %set boundary line lengths to zero so that it won't come up in rigid end
226 %search
227 indexLength=find((length/ndiv)>=t1);
228
229 LineID=lineLabel; %this was edited for the triangle case
230 indexNOLength=LineID;
231 indexNOLength(indexLength)=[];
232 %% ELEMENT DATA
233 t1Vector(1:size(lineBLOCKFINAL,1))=t1;
234 %to include rigid end lengths
235 fid=fopen('linecheck15.in','at');
236 fprintf(fid,'EDATA SUBSTRUC=0 GROUP=1 UNDEFINE=IGNORE\n@CLEAR\n@\n');
237 fprintf(fid,'EDATA SUBSTRUC=0 GROUP=1 ...
        UNDEFINE=IGNORE\n@STARTMODIFY\n@CHAROW          1          101          ...
        101');
238 %fprintf(fid,'\n%d 1 1 0 'DEFAULT' 'DEFAULT' 0.000000000000000 ...
        0.000000000000000 0,\n0.000000000000000 %d %d\n', ...
        [LineBlockFinal2(:,1) t1Vector t1Vector]);
239 %put rigid ends on elements that are long enough
240 firstElement=(ndiv).*lineBLOCKFINAL(indexLength,1)-(ndiv-1);
241 lastElement=(ndiv).*lineBLOCKFINAL(indexLength,1);
242
243 noOfElement=(1:ndiv*size(lineBLOCKFINAL,1))';
244 noOfElement([firstElement,lastElement])=[];
245
246 fprintf(fid,'\n%d 1 1 0 'DEFAULT' 'DEFAULT' 0.000000000000000 ...
        0.000000000000000 0,\n0.000000000000000 %d 0',[firstElement ...
        t1Vector(indexLength,1)]');
247 fprintf(fid,'\n%d 1 1 0 'DEFAULT' 'DEFAULT' 0.000000000000000 ...
        0.000000000000000 0,\n0.000000000000000 0 %d',[lastElement ...
        t1Vector(indexLength,1)]');
248 %make NO rigid ends on elements whose length are not long enough
249 fprintf(fid,'\n%d 1 1 0 'DEFAULT' 'DEFAULT' 0.000000000000000 ...
        0.000000000000000 0,\n0.000000000000000 0 0',noOfElement);
250 %
251 fprintf(fid,'\n@ENDMODIFY\n*\nEDATA SUBSTRUC=0 GROUP=1 ...
        UNDEFINE=IGNORE\n@STARTMODIFY\n@ENDMODIFY');
252 fclose(fid);
253 %
254 %% COPY INPUT FILE TO FILE WITH THE HEIGHT AND MESH DENSITY IDENTIFIED
255 % copyfile('linecheck15.in',['inputFiles/Height_' num2str(h) '_' ...
        num2str(u) 'x' num2str(u) '.in'])

```

A.2. Spherical Cap - Triangular Grid

```
256 % delete linecheck15.in
```

Appendix A. MATLAB Code

A.3 Corrugated Vault - Continuous Shell

```
1 %the following file is used to create the input ADINA data (points, ...
   surface
2 %grids etc) that is then used to create the CONTINUOUS Barrel Vault ...
   shell.
3 %user inputs the geometrical parameters that define the corrugated vault
4 clear all
5 hold on
6
7 % INPUTS - INCHES, KIPS
8 L1=1200; %L1 is the full width
9 L2=972; %L2 is HALF the length
10 h=109; %h is the height of the arch
11
12 %INSERT as a percent of the length and width used in the amplitude, I ...
   dividt
13 %by 100 later.
14 %to be OUT OF PHASE put one of the beta's as negative
15 beta1=0 %PERCENT
16 beta2=10%PERCENT
17
18 %a1 is the amplitude of the edge curve (so at z==0)
19 a1=(beta1/100)*(L1/2);
20 %a2 is the amplitude of the top undulation (so at z==h)
21 a2=(beta2/100)*(h);
22
23 %n is the number of waves on half the length, so in total there are 2*n
   %waves
24 n=1.5
25
26 %steps refers to the remaking of the mesh grid, and how many steps we ...
   take
27 %in the x direction
28 %THIS needs to be MORE FINE to get the curvature
29 steps=40;
30 %THIS MAKES THE NUMBER OF ROWS DIFFERENT (S1)
31
32 %redefining the parameters
33 xo=L1/2;%half the width
34 if n==0;
35     A=0;
36 else
37     A=a1;
38 end
39
40 l=L2;
41 %dx=L1/50;
42 dx=(xo+A)/50;
43 if (n<=3)
```


A.3. Corrugated Vault - Continuous Shell

```
44     dy=L2/20; %dy doesn't need to be as fine as dx, %NOT TRUE FOR ...
        WHEN n=5;
45 else
46     dy=L2/50
47 end
48 %%
49 [X1,Y1]=meshgrid(0:dx:xo+A,-l:dy:l);
50 XX=X1(:);
51 YY=Y1(:);
52 plot(XX,YY,'y. ');
53
54 %maybe need to add boundary points
55 xb=(xo+A*cos(2*n*pi*YY/l));
56 plot(xb,YY,'k. ');
57 XX=vertcat(XX,xb);
58 YY=vertcat(YY,YY);
59 plot(XX,YY,'gs ');
60
61 points2=[XX YY];
62 points3=unique(points2,'rows');
63
64 XX=points3(:,1);
65 YY=points3(:,2);
66 plot(XX,YY,'b. ');
67
68 dd=(xo+A*cos(2*n*pi*YY/l))-XX;
69
70 XXX=XX;
71 YYY=YY;
72 indices=find(dd<0);
73 XXX(indices)=[];
74 YYY(indices)=[];
75 plot(XXX,YYY,'cd ');
76
77 XFINAL=vertcat(XXX,-1*XXX);
78 YFINAL=vertcat(YYY,YYY);
79 plot(XFINAL,YFINAL,'k+ ');
80 %%
81 %clear X Y xlin ylin Input inputy inputsub
82 Yvalues=unique(YFINAL);
83 [y1 y2]=size(Yvalues)
84
85 X=[];
86 Y=[];
87 Input=[];
88
89 for(i=1:y1)
90     indices=find(YFINAL==Yvalues(i,1));
91     xlin1=linspace(0,max(XFINAL(indices)),(steps))';
92     xlin2=sortrows(vertcat(-1*xlin1,xlin1));
93
```

Appendix A. MATLAB Code

```
94     ind=find(xlin2==0);
95     xlin2(ind(1,1))=[]
96     xlin=xlin2;
97
98     X=vertcat(X,xlin);
99     [s1 s2]=size(xlin)
100
101     ylin(1:s1)=Yvalues(i,1);
102     Y=vertcat(Y,ylin');
103
104     inputy(1:s1)=i;
105     inputsub=[1:1:s1; inputy]';
106     Input=vertcat(Input,inputsub);
107 end
108 Z=(h+a2.*cos(2*n*pi.*Y./l)).*[1-((X.^2)./(xo+A.*cos(2*n*pi.*Y./l)).^2)];
109
110 POINTS=[X Y Z];
111 %reorder
112 POINTS2=sortrows(POINTS,2);
113 plot3(POINTS2(:,1), POINTS2(:,2), POINTS2(:,3),'m*');
114 X=POINTS2(:,1);
115 Y=POINTS2(:,2);
116 Z=POINTS2(:,3);
117
118 [z1 z2]=size(Z);
119 label=[1:1:z1]';%
120 %points=[label p zeros(d1,1)]
121 points=[label X Y Z zeros(z1,1)];
122 points2=[X Y Z];
123 InputFinal= [Input(:,2) Input(:,1) label];
124
125 %steps
126 noRows = size(Yvalues) %becomes 3 of rows
127 noCols=s1 %becomes # of cols
128
129 polylinePoint1=(noCols+1)/2;
130 polylinePoint2=polylinePoint1+(noCols)*(noRows-1)
131 Δ=noCols
132 a1
133 a2
134 dlmwrite('PointsToimport.txt', points,'delimiter', '\t');
135 dlmwrite('SurfaceGridToimport.txt', InputFinal,'delimiter', '\t');
136
137 %% using MyCrust to plot the delauney triangulation
138 % Author:Giaccari Luigi
139 % Last Update: 28/01/2009
140 % Created: 15/4/2008
141 % MYCRUST - makes a surface out of nonuniform grid data
142 % Input:
143 %           p is a Nx3 array containing the 3D set of points
144 % Output:
```

A.3. Corrugated Vault - Continuous Shell

```
145 %           t are points id contained in triangles nx3 array .
146 addpath('D:\Smalek\Desktop\RESEARCH SPRING ...
           2011\MATLAB\MyCrustOpen070909');
147 figure
148 [t]=MyCrustOpen(points2);
149 trisurf(t,points2(:,1),points2(:,2),points2(:,3),'facecolor','c',...
150         'edgecolor','b');%plot della superficie;
151 shading interp;
152 colormap(gray);
153 figure
154 trimesh(t,points2(:,1),points2(:,2),points2(:,3),'facecolor','c',...
155         'edgecolor','b');%plot della superficie;
```

Appendix A. MATLAB Code

A.4 Corrugated Vault - Quadrilateral Grid

```
1 clear all
2 % the following code takes the element connectivity of QUAD SHELL ...
   ELEMENTS
3 % and gives them a line id # and the points/nodes that connect them
4 %rewrite data into line #, point 1, point 2 of ADINA Block portion
5
6 % INPUT FILES
7 %read in data
8 %file name "archQUADElements.txt" - is the exported data from adina ...
   that contains
9 %the element connectivity
10 %file name "archQUADnodes.txt" - is teh exported data from adina that
11 %contains the nodal points and their coordinates
12
13 % OUTPUT FILES
14 %this program writes all the adina commands into one file called
15 %"adinaINPUTQUAD.in"
16
17 % INPUT PARAMETERS TO EDIT
18 % NDIV = which is the number of elements to mesh each beam member into
19 ndiv=3;
20 %ALSO - delete the adinaINPUTQUAD.in file when rerunning this. ...
   otherwise it
21 %will append the new info to the old input file.
22
23 %Cross section
24 t1=4.98; %width of rectangular cross section
25 t2=4.98; %height of rectangular cross section
26 %% INSERTING COMMON INFO INTO THE ADINA INPUT FILE
27 %specifically CMASS=Yes, allows the option to print the mass and ...
   volume of
28 %the model
29 fid=fopen('adinaINPUTQUAD.in','at');
30 fprintf(fid, '*\nMASTER ANALYSIS=STATIC MODEX=EXECUTE ...
   TSTART=0.00000000000000 IDOF=0,\nNOVALIZAT=NONE FLUIDPOT=AUTOMATIC ...
   CYCLICPA=1 IPOSIT=STOP,\nREACTION=YES INITIALS=NO FSINTERA=NO ...
   IRINT=DEFAULT CMASS=YES,\nSHELLNDO=AUTOMATIC AUTOMATI=OFF ...
   SOLVER=SPARSE,\nCONTACT-=CONSTRAINT-FUNCTION ...
   TRELEASE=0.00000000000000,\nRESTART-=NO FRACTURE=NO LOAD-CAS=NO ...
   LOAD-PEN=NO SINGULAR=YES,\nSTIFFNES=0.000100000000000000 ...
   MAP-OUTP=NONE MAP-FORM=NO,\nNODAL-DE='' POROUS-C=NO ADAPTIVE=0 ...
   ZOOM-LAB=1 AXIS-CYC=0,\nPERIODIC=NO VECTOR-S=GEOMETRY EPSI-FIR=NO ...
   STABILIZ=NO,\nSTABFACT=1.00000000000000E-10 RESULTS=PTHOLE ...
   FEFCORR=NO,\nBOLTSTEP=1 EXTEND-S=YES CONVERT-=NO DEGEN=YES ...
   TMC-MODE=NO,\nENSIGHT-=NO');
31 %% POINT BLOCK
32 pointBlock1=dlmread('archQUADnodes.txt');
```

A.4. Corrugated Vault - Quadrilateral Grid

```

33 %define the auxiliary points
34 auxPoints=[pointBlock1(:,1)+1000,pointBlock1(:,2:3),pointBlock1(:,4)-1,...
35     pointBlock1(:,5)];
36 pointBlock=[pointBlock1; auxPoints];
37 fprintf(fid, '\n*\nCOORDINATES POINT SYSTEM=0\n@CLEAR');
38 fprintf(fid, '\n%d %d %d %d %d',pointBlock');
39 fclose(fid);
40 %% LINE BLOCK%
41 elemConnectivity=dlmread('archQUADElements.txt');
42 [d1, d2]=size(elemConnectivity);
43 elemConnectivity=elemConnectivity(1:d1,2:5);
44
45 for(i=1:d1)
46     j=4*i-3;
47     lineBlock(j,1:2)=[elemConnectivity(i,1) elemConnectivity(i,2)];
48     lineBlock(j+1,1:2)=[elemConnectivity(i,2) elemConnectivity(i,3)];
49     lineBlock(j+2,1:2)=[elemConnectivity(i,3) elemConnectivity(i,4)];
50     lineBlock(j+3,1:2)=[elemConnectivity(i,4) elemConnectivity(i,1)];
51 end
52
53 %clean up the line block to get rid of repeating lines
54 lineBlock(:,:);
55 [d1 d2]=size(lineBlock);
56 for(i=1:d1)
57     for(j=i:d1)
58         pair1=[lineBlock(i,1) lineBlock(i,2)];
59         pair2=[lineBlock(j,2) lineBlock(j,1)];
60         if(pair2==pair1);
61             lineBlock(j,:)=[];
62             [d1 d2]=size(lineBlock);
63             break
64         end
65     end
66 end
67 lineLabel=(1:1:d1)';
68 lineBLOCKFINAL=[lineLabel, lineBlock];
69 fid=fopen('adinaINPUTQUAD.in','at');
70 fprintf(fid, '\n*\nLINE STRAIGHT NAME=%d P1=%d P2=%d',lineBLOCKFINAL');
71 fclose(fid);
72 %define the auxiliary point for each line
73 auxPointonLine=[lineBLOCKFINAL(:,1),lineBLOCKFINAL(:,2)+1000];
74 %% WRITE MATERIAL BLOCK%
75 fid=fopen('adinaINPUTQUAD.in','at');
76 %below is for elastic material
77 fprintf(fid, '\n*\nMATERIAL ELASTIC NAME=1 E=29000 NU=0.3, ...
78     DESDENSITY=2.83e-4 ALPHA=0 MDESCRIP='STEEL\''');
79
80 %below is for bilinear material (so that we can enter a sigma_y yield
81 %stress)
82 %fprintf(fid, '\n*\nMATERIAL PLASTIC-BILINEAR NAME=1 ...
83     HARDENIN=ISOTROPIC,\nE=29000.0000000000 NU=0.3000000000000000 ...

```

Appendix A. MATLAB Code

```

YIELD=50.00000000000000,\nET=0.0000000000000000 EPA=0.0000000000000000 ...
STRAINRA=0,\nDENSITY=0.00028300000000000000 ...
ALPHA=0.0000000000000000,\nTREF=0.0000000000000000 DEPENDEN=NO ...
TRANSITI=0.00010000000000000000,\nEP-STRAI=0.0000000000000000 ...
BCURVE=0 BVALUE=0.0000000000000000,\nXM-INF=0.0000000000000000 ...
XMO=0.0000000000000000,\nETA=0.0000000000000000 MDESCRIP='STEEL');
82
83 %% WRITE CROSS SECTION BLOCK
84 fprintf(fid,'\n*\nCROSS-SECTIO RECTANGULAR NAME=1 WIDTH=%d,\n ...
    HEIGHT=%d SC=0 TC=0,\n TORFAC=1 SSHEARF=0,\n TSHEARF=0 ISHEAR=NO ...
    SQUARE=YES',t1,t2);
85 %DEFINE ELEMENT TYPE
86 % HERE INSERT IF THE JOINTS ARE RIGID OR NOT "RIGIDEND=INFINITE" OR ...
    "RIGIDEND=NONE"
87 fprintf(fid,'\n*\nEGROUP BEAM NAME=1 SUBTYPE=THREE-D DISPLACE=DEFAULT ...
    MATERIAL=1 RINT=5,\n SINT=DEFAULT TINT=DEFAULT RESULTS=STRESSES ...
    INITIALS=NONE,\n CMASS=DEFAULT RIGIDEND=INFINITE MOMENT-C=NO ...
    RIGIDITY=1,\n MULTIPLY=1000000.0000000000 RUPTURE=ADINA ...
    OPTION=NONE,\n BOLT-TOL=0.0000000000000000 DESCRIPT='NONE' ...
    SECTION=1,\n PRINT=DEFAULT SAVE=DEFAULT ...
    TBIRTH=0.0000000000000000,\n TDEATH=0.0000000000000000 SPOINT=4 ...
    BOLTFORC=0.0000000000000000,\n BOLTNCUR=0 TMC-MATE=1 BOLT-NUM=0 ...
    BOLT-LOA=0.0000000000000000,\n WARP=NO');
88 %% MESH DENSITY
89 %insert here Line Labels
90 fprintf(fid,'\n*\nSUBDIVIDE LINE NAME=103 MODE=DIVISIONS NDIV=1 ...
    RATIO=1.0000000000000000,\n PROGRESS=GEOMETRIC CBIAS=NO\n@CLEAR\n');
91 fprintf(fid,'\n*\nSUBDIVIDE LINE NAME=103 MODE=DIVISIONS NDIV=%d ...
    RATIO=1.0000000000000000,\n PROGRESS=GEOMETRIC ...
    CBIAS=NO\n@CLEAR\n',ndiv);
92 fprintf(fid,'\n %d ', lineLabel);
93 fprintf(fid,'\n@');
94
95 %% CREATE MESH
96 %insert here line labels
97 fprintf(fid,'\n*\nGLINE NODES=2 AUXPOINT=%d NCOINCID=ENDS ...
    NCENDS=12,\n NCTOLERA=1.0000000000000000E-05 SUBSTRUC=0 GROUP=1 ...
    MIDNODES=CURVED\n @CLEAR \n%d \n@ ',[auxPointonLine(:,2) ...
    lineLabel]');
98 fprintf('\nauxpoint %d line %d',[auxPointonLine(:,2) lineLabel]')
99 fclose(fid);
100
101 %% CALCULATE LINE LENGTH
102 %this is used to calculate if the rigid end length is greater than the
103 %line length. here we separate the lines that will have a rigid end
104 %length and those that will not.
105
106 indexP1=lineBLOCKFINAL(:,2);
107 indexP2=lineBLOCKFINAL(:,3);
108
109 length=sqrt((pointBlock1(indexP1,2)-pointBlock1(indexP2,2)).^2+...

```

A.4. Corrugated Vault - Quadrilateral Grid

```

110     (pointBlock1(indexP1,3)-pointBlock1(indexP2,3)).^2+...
111     (pointBlock1(indexP1,4)-pointBlock1(indexP2,4)).^2);
112 %length((end+1-size(boundaryLines)):end,1)=0;
113 %set boundary line lengths to zero so that it won't come up in rigid end
114 %search
115 indexLength=find((length/ndiv)>=t1);
116
117 indexNOLength=lineLabel;
118 indexNOLength(indexLength)=[];
119 %% ELEMENT DATA
120 t1Vector(1:size(lineBLOCKFINAL,1))=t1;
121 %to include rigid end lengths
122 fid=fopen('adinaINPUTQUAD.in','at');
123 fprintf(fid,'EDATA SUBSTRUC=0 GROUP=1 UNDEFINE=IGNORE\n@CLEAR\n@\n');
124 fprintf(fid,'EDATA SUBSTRUC=0 GROUP=1 ...
    UNDEFINE=IGNORE\n@STARTMODIFY\n@CHAROW          1          101          ...
    101');
125 %fprintf(fid,'\n%d 1 1 0 'DEFAULT' 'DEFAULT' 0.000000000000000 ...
    0.000000000000000 0,\n0.000000000000000 %d %d\n', ...
    [LineBlockFinal2(:,1) t1Vector t1Vector]);
126 %put rigid ends on elements that are long enough
127 %place holder
128 firstElement=(ndiv).*lineBLOCKFINAL(indexLength,1)-(ndiv-1);
129 lastElement=(ndiv).*lineBLOCKFINAL(indexLength,1);
130
131 noOfElement=(1:ndiv*size(lineBLOCKFINAL,1))';
132 noOfElement([firstElement,lastElement])=[];
133
134 fprintf(fid,'\n%d 1 1 0 'DEFAULT' 'DEFAULT' 0.000000000000000 ...
    0.000000000000000 0,\n0.000000000000000 %d 0',[firstElement ...
    t1Vector(indexLength,1)]');
135 fprintf(fid,'\n%d 1 1 0 'DEFAULT' 'DEFAULT' 0.000000000000000 ...
    0.000000000000000 0,\n0.000000000000000 0 %d',[lastElement ...
    t1Vector(indexLength,1)]');
136 %make NO rigid ends on elements whose length are not long enough
137 fprintf(fid,'\n%d 1 1 0 'DEFAULT' 'DEFAULT' 0.000000000000000 ...
    0.000000000000000 0,\n0.000000000000000 0 0',noOfElement);
138 %
139 fprintf(fid,'\n@ENDMODIFY\n*\nEDATA SUBSTRUC=0 GROUP=1 ...
    UNDEFINE=IGNORE\n@STARTMODIFY\n@ENDMODIFY');
140 fclose(fid);
141 %% LOADS
142 %Apply Point loads to Points on Edge and in middle of interesecting
143 [d1 d2]=size(pointBlock1);
144 forceLabel=(1:1:d1)';
145 fid=fopen('adinaINPUTQUAD.in','at');
146 fprintf(fid,'\n*\n LOAD FORCE NAME=1 MAGNITUD= 1 ...
    FX=0.000000000000000,\nFY=0.000000000000000 FZ=-1.000000000000000');
147 fprintf(fid,'\n*\n APPLY-LOAD BODY=0\n@CLEAR');
148 fprintf(fid, '\n%d 'FORCE' 1 'POINT' %d 0 1 0 0 -1 0 0 0 ...
    'NO',\n 0 0 1 0 'MID'',[forceLabel(:,1) pointBlock1(:,1)]');

```

Appendix A. MATLAB Code

```
149 fclose(fid);
150 %% collect boundary points
151 boundaryPointsOPENINGS=[find(pointBlock1(:,3)>=971.9); ...
    find(pointBlock1(:,3)<=-971.9)];
152 boundaryPointsBOUNDARIES=[find(pointBlock1(:,4)==0)];
153 %% DEFINE BOUNDARY CONDITIONS
154 %GET POINT IDS OF POINTS THAT NEED TO BE PINNED
155 %Define pinned condition
156 fid=fopen('adinaINPUTQUAD.in','at');
157 fprintf(fid,'\n*\n FIXITY NAME=OPENINGS\n@CLEAR\n'X-ROTATION'\n'...
158     'Y-TRANSLATION'\n'OVALIZATION''');
159 fprintf(fid,'\n*\n FIXITY NAME=BOUNDARIES\n@CLEAR\n'X-TRANSLATION'...
160     '\n'Z-TRANSLATION'\n'OVALIZATION''');
161
162 %Degree(s) of freedom to be fixed. {X-TRANSLATION/Y-TRANSLATION/
163 % Z-TRANSLATION/X-ROTATION/Y-ROTATION/Z-ROTATION/OVALIZATION/
164 % FLUID-POTENTIAL/PORE-FLUID-PRESSURE/BEAM-WARP}
165 % APPLY BOUNDARY CONDITIONS TO POINTS
166 fprintf(fid,'\n@\n*\n FIXBOUNDARY POINTS FIXITY=ALL\n@CLEAR');
167 fprintf(fid,'\n%d ''OPENINGS'', boundaryPointsOPENINGS);
168 fprintf(fid,'\n%d ''BOUNDARIES'', boundaryPointsBOUNDARIES);
169 fprintf(fid,'\n@');
170
171 %           %APPLY BOUNDARY CONDITIONS TO LINES
172 %           fprintf(fid,'\n@\n*\n FIXBOUNDARY LINES ...
    FIXITY=PINNED\n@CLEAR');
173 %           fprintf(fid,'\n%d ''PINNED'', ...
    LineBlockFinal2((end+1-size(boundaryLines)):end,1));
174 %           fprintf(fid,'\n@');
175 fclose(fid);
```


A.5 Corrugated Vault - Triangular Grid

```

1 clear all
2 % the following code takes the element connectivity of Triangular 2D ...
   ELEMENTS
3 % and gives them a line id # and the points/nodes that connect them
4 %rewrite data into line #, point 1, point 2 of ADINA Block portion
5
6 % INPUT FILES
7 %read in data
8 %file name "arch4elements.txt" - is the exported data from adina that ...
   contains
9 %the element connectivity
10 %file name "arch4nodes.txt" - is teh exported data from adina that
11 %contains the nodal points and their coordinates
12
13 % OUTPUT FILES
14 %this program writes all the adina commands into one file called
15 %"adinaINPUTQUAD.in"
16
17 % INPUT PARAMETERS TO EDIT
18 % NDIV = which is the number of elements to mesh each beam member into
19 ndiv=4;
20 %ALSO - delete the adinaINPUTQUAD.in file when rerunning this. ...
   otherwise it
21 %will append the new info to the old input file.
22
23 %Cross section
24 t1=4.1; %width of rectangular cross section
25 t2=4.1; %height of rectangular cross section
26 %read in data
27 %rewrite data into line #, point 1, point 2 of ADINA Block portion
28 %% INSERTING COMMON INFO INTO THE ADINA INPUT FILE
29 %specifically CMASS=Yes, allows the option to print the mass and ...
   volume of
30 %the model
31 fid=fopen('adinaINPUT.in','at');
32 fprintf(fid, '*\nMASTER ANALYSIS=STATIC MODEX=EXECUTE ...
   TSTART=0.000000000000 IDOF=0,\nNOVALIZAT=NONE FLUIDPOT=AUTOMATIC ...
   CYCLICPA=1 IPOSIT=STOP,\nREACTION=YES INITIALS=NO FSINTERA=NO ...
   IRINT=DEFAULT CMASS=YES,\nSHELLNDO=AUTOMATIC AUTOMATI=OFF ...
   SOLVER=SPARSE,\nCONTACT=CONSTRAINT-FUNCTION ...
   TRELEASE=0.000000000000,\nRESTART=NO FRACTURE=NO LOAD-CAS=NO ...
   LOAD-PEN=NO SINGULAR=YES,\nSTIFFNES=0.0001000000000000 ...
   MAP-OUTP=NONE MAP-FORM=NO,\nNODAL-DE='' POROUS-C=NO ADAPTIVE=0 ...
   ZOOM-LAB=1 AXIS-CYC=0,\nPERIODIC=NO VECTOR-S=GEOMETRY EPSI-FIR=NO ...
   STABILIZ=NO,\nSTABFACT=1.000000000000000E-10 RESULTS=PORTHOLE ...
   FEFCORR=NO,\nBOLTSTEP=1 EXTEND-S=YES CONVERT=NO DEGEN=YES ...
   TMC-MODE=NO,\nENSIGHT=NO');

```

Appendix A. MATLAB Code

```
33 %% POINT BLOCK
34 pointBlock1=dlmread('arch4nodes.txt');
35 [ap1 ap2]=size(pointBlock1);
36 %if lines get messed up, revisit the next line where i add 10,000 to the
37 %point id for creating the auxillary nodes. if the geometry has more than
38 %10,000 points then the numbering gets messed up. the 10,000 is the line
39 %below must also match the line further down ...
    %auxPointonLine=[lineBLOCKFINAL(:,1),lineBLOCKFINAL(:,2)+10000];
40
41 auxPoints=[pointBlock1(:,1)+ap1,pointBlock1(:,2:3),pointBlock1(:,4)-1,...
42     pointBlock1(:,5)];
43 pointBlock=[pointBlock1; auxPoints];
44 fprintf(fid, '\n*\nCOORDINATES POINT SYSTEM=0\n@CLEAR');
45 fprintf(fid, '\n%d %d %d %d %d',pointBlock');
46 fclose(fid);
47 %% LINE BLOCK%
48 elemConnectivity=dlmread('arch4elements.txt')
49 [d1, d2]=size(elemConnectivity)
50 elemConnectivity=elemConnectivity(1:d1,2:4)
51
52 for(i=1:d1)
53     j=3*i-2;
54     lineBlock(j,1:2)=[elemConnectivity(i,1) elemConnectivity(i,2)];
55     lineBlock(j+1,1:2)=[elemConnectivity(i,2) elemConnectivity(i,3)];
56     lineBlock(j+2,1:2)=[elemConnectivity(i,3) elemConnectivity(i,1)];
57 end
58
59 %clean up the line block to get rid of repeating lines
60 lineBlock(:,:);
61 [d1 d2]=size(lineBlock);
62 for(i=1:d1)
63     for(j=i:d1)
64         pair1=[lineBlock(i,1) lineBlock(i,2)];
65         pair2=[lineBlock(j,2) lineBlock(j,1)];
66         if(pair2==pair1);
67             lineBlock(j,:)=[];
68             [d1 d2]=size(lineBlock);
69             break
70         end
71     end
72 end
73 lineLabel=(1:1:d1) '
74 lineBLOCKFINAL=[lineLabel, lineBlock]
75 fid=fopen('adinaINPUT.in','at');
76 fprintf(fid, '\n*\nLINE STRAIGHT NAME=%d P1=%d P2=%d',lineBLOCKFINAL');
77 fclose(fid);
78 %define the auxiliary point for each line
79 auxPointonLine=[lineBLOCKFINAL(:,1),lineBLOCKFINAL(:,2)+ap1]
80
81 %% WRITE MATERIAL BLOCK%
82 fid=fopen('adinaINPUT.in','at');
```

A.5. Corrugated Vault - Triangular Grid

```

83 %below is for elastic material
84 fprintf(fid, '\n*\nMATERIAL ELASTIC NAME=1 E=29000 NU=0.3, ...
    DESNITY=2.83e-4 ALPHA=0 MDESCRIP='STEEL\''');
85
86 %below is for bilinear material (so that we can enter a sigma_y yield
87 %stress)
88 %fprintf(fid, '\n*\nMATERIAL PLASTIC-BILINEAR NAME=1 ...
    HARDENIN=ISOTROPIC, \nE=29000.0000000000 NU=0.3000000000000000 ...
    YIELD=50.0000000000000, \nET=0.0000000000000000 EPA=0.0000000000000000 ...
    STRAINRA=0, \nDENSITY=0.0002830000000000000 ...
    ALPHA=0.000000000000000, \nTREF=0.0000000000000000 DEPENDEN=NO ...
    TRANSITI=0.000100000000000000, \nEP-STRAI=0.0000000000000000 ...
    BCURVE=0 BVALUE=0.000000000000000, \nXM-INF=0.0000000000000000 ...
    XM0=0.000000000000000, \nETA=0.0000000000000000 MDESCRIP='STEEL\''');
89 %% WRITE CROSS SECTION BLOCK
90 fprintf(fid, '\n@\n*\n\CROSS-SECTIO RECTANGULAR NAME=1 WIDTH=%d, \n ...
    HEIGHT=%d SC=0 TC=0, \n TORFAC=1 SSHEARF=0, \n TSHEARF=0 ISHEAR=NO ...
    SQUARE=YES', t1, t2);
91 %DEFINE ELEMENT TYPE
92 % HERE INSERT IF THE JOINTS ARE RIGID OR NOT "RIGIDEND=INFINITE" OR ...
    "RIGIDEND=NONE"
93 fprintf(fid, '\n*\nEGROUP BEAM NAME=1 SUBTYPE=THREE-D DISPLACE=DEFAULT ...
    MATERIAL=1 RINT=5, \n SINT=DEFAULT TINT=DEFAULT RESULTS=STRESSES ...
    INITIALS=NONE, \n CMASS=DEFAULT RIGIDEND=INFINITE MOMENT-C=NO ...
    RIGIDITY=1, \n MULTIPLY=1000000.000000000 RUPTURE=ADINA ...
    OPTION=NONE, \n BOLT-TOL=0.0000000000000000 DESCRIP='NONE' ...
    SECTION=1, \n PRINT=DEFAULT SAVE=DEFAULT ...
    TBIRTH=0.000000000000000, \n TDEATH=0.0000000000000000 SPOINT=4 ...
    BOLTFORC=0.000000000000000, \n BOLTNCUR=0 TMC-MATE=1 BOLT-NUM=0 ...
    BOLT-LOA=0.000000000000000, \n WARP=NO');
94 %% MESH DENSITY
95 %insert here Line Labels
96 fprintf(fid, '\n*\nSUBDIVIDE LINE NAME=103 MODE=DIVISIONS NDIV=%d ...
    RATIO=1.000000000000000, \n PROGRESS=GEOMETRIC ...
    CBIAS=NO\n@CLEAR\n', ndiv);
97 fprintf(fid, '\n %d ', lineLabel);
98 fprintf(fid, '\n@');
99 %% CREATE MESH
100 %insert here line labels
101 fprintf(fid, '\n*\nGLINE NODES=2 AUXPOINT=%d NCOINCID=ENDS ...
    NCENDS=12, \n NCTOLERA=1.000000000000000E-05 SUBSTRUC=0 GROUP=1 ...
    MIDNODES=CURVED\n @CLEAR \n%d \n@ ', [auxPointonLine(:,2) ...
    lineLabel]);
102 %fprintf('\nauxpoint %d line %d', [auxPointonLine(:,2) lineLabel])
103 fclose(fid);
104 %% CALCULATE LINE LENGTH
105 %this is used to calculate if the rigid end length is greater than the
106 %line length. here we separate the lines that will have a rigid end
107 %length and those that will not.
108
109 indexP1=lineBLOCKFINAL(:,2);

```

Appendix A. MATLAB Code

```

110 indexP2=lineBLOCKFINAL(:,3);
111
112 length=sqrt((pointBlock1(indexP1,2)-pointBlock1(indexP2,2)).^2+...
113     (pointBlock1(indexP1,3)-pointBlock1(indexP2,3)).^2+...
114     (pointBlock1(indexP1,4)-pointBlock1(indexP2,4)).^2);
115 %length((end+1-size(boundaryLines)):end,1)=0;
116 %set boundary line lengths to zero so that it won't come up in rigid end
117 %search
118 indexLength=find((length/ndiv)>=t1);
119
120 indexNOLength=lineLabel;
121 indexNOLength(indexLength)=[];
122 %% ELEMENT DATA
123 t1Vector(1:size(lineBLOCKFINAL,1))=t1;
124 %to include rigid end lengths
125 fid=fopen('adinaINPUT.in','at');
126 fprintf(fid,'EDATA SUBSTRUC=0 GROUP=1 UNDEFINE=IGNORE\n@CLEAR\n@\n');
127 fprintf(fid,'EDATA SUBSTRUC=0 GROUP=1 ...
        UNDEFINE=IGNORE\n@STARTMODIFY\n@CHAROW          1          101          ...
        101');
128 %fprintf(fid,'\n%d 1 1 0 'DEFAULT' 'DEFAULT' 0.000000000000000 ...
        0.000000000000000 0,\n0.000000000000000 %d %d\n', ...
        [LineBlockFinal2(:,1) t1Vector t1Vector]);
129 %put rigid ends on elements that are long enough
130 %place holder
131 firstElement=(ndiv).*lineBLOCKFINAL(indexLength,1)-(ndiv-1);
132 lastElement=(ndiv).*lineBLOCKFINAL(indexLength,1);
133
134 noOfElement=(1:ndiv*size(lineBLOCKFINAL,1))';
135 noOfElement([firstElement,lastElement])=[];
136
137 fprintf(fid,'\n%d 1 1 0 'DEFAULT' 'DEFAULT' 0.000000000000000 ...
        0.000000000000000 0,\n0.000000000000000 %d 0',[firstElement ...
        t1Vector(indexLength,1)]');
138 fprintf(fid,'\n%d 1 1 0 'DEFAULT' 'DEFAULT' 0.000000000000000 ...
        0.000000000000000 0,\n0.000000000000000 0 %d',[lastElement ...
        t1Vector(indexLength,1)]');
139 %make NO rigid ends on elements whose length are not long enough
140 fprintf(fid,'\n%d 1 1 0 'DEFAULT' 'DEFAULT' 0.000000000000000 ...
        0.000000000000000 0,\n0.000000000000000 0 0',noOfElement);
141 %
142 fprintf(fid,'\n@ENDMODIFY\n*\nEDATA SUBSTRUC=0 GROUP=1 ...
        UNDEFINE=IGNORE\n@STARTMODIFY\n@ENDMODIFY');
143 fclose(fid);
144 %% Apply Point loads to Points on Edge and in middle of interesecting
145 [d1 d2]=size(pointBlock);
146 forceLabel=(1:1:d1)';
147 fid=fopen('adinaINPUT.in','at');
148 fprintf(fid,'\n*\n LOAD FORCE NAME=1 MAGNITUD= 1 ...
        FX=0.000000000000000,\nFY=0.000000000000000 FZ=-1.000000000000000');
149 fprintf(fid,'\n*\n APPLY-LOAD BODY=0\n@CLEAR')

```

A.5. Corrugated Vault - Triangular Grid

```
150 fprintf(fid, '\n%d 'FORCE' 1 'POINT' %d 0 1 0 0 -1 0 0 0 ...
    'NO', \n 0 0 1 0 'MID'', [forceLabel(:,1) pointBlock(:,1)]');
151 fclose(fid);
152 %%
153 %GET POINT IDS OF POINTS THAT NEED TO BE PINNED
154 boundaryPointsOPENINGS=[find(pointBlock(:,3)≥971.9); ...
    find(pointBlock(:,3)≤-971.9)];
155 boundaryPointsBOUNDARIES=[find(pointBlock(:,4)==0)];
156 %% DEFINE BOUNDARY CONDITIONS
157 %GET POINT IDS OF POINTS THAT NEED TO BE PINNED
158 %Define pinned condition
159 fid=fopen('adinaINPUT.in','at');
160 fprintf(fid, '\n*\n FIXITY NAME=OPENINGS\n@CLEAR\n'X-ROTATION'\n'...
    'Y-TRANSLATION'\n'OVALIZATION');
161
162 fprintf(fid, '\n*\n FIXITY NAME=BOUNDARIES\n@CLEAR\n'X-TRANSLATION'...
    '\n'Z-TRANSLATION'\n'OVALIZATION');
163
164
165 %Degree(s) of freedom to be fixed. {X-TRANSLATION/Y-TRANSLATION/
166 % Z-TRANSLATION/X-ROTATION/Y-ROTATION/Z-ROTATION/OVALIZATION/
167 % FLUID-POTENTIAL/PORE-FLUID-PRESSURE/BEAM-WARP}
168 % APPLY BOUNDARY CONDITIONS TO POINTS
169 fprintf(fid, '\n@\n*\n FIXBOUNDARY POINTS FIXITY=ALL\n@CLEAR');
170 fprintf(fid, '\n%d 'OPENINGS'', boundaryPointsOPENINGS);
171 fprintf(fid, '\n%d 'BOUNDARIES'', boundaryPointsBOUNDARIES);
172 fprintf(fid, '\n@');
173 fclose(fid);
```

Appendix B

Equivalent Continuum

1. Reduce the equation of equilibrium and compatibility into a couple set of two homogeneous equations in w and f .

$$D\nabla^4 w + \frac{1}{R}\nabla^4 f + \frac{1}{2}p_e R \nabla^2 w = 0 \quad (\text{B.1a})$$

$$\nabla^4 f = \frac{Eh_a}{R}\nabla^2 w \quad (\text{B.1b})$$

where f must satisfy the compatibility condition and h_a is the thickness from to axial rigidity.

2. Use the solutions of w and f derived by (Hutchinson, 1967) and solve for B_1 .

$$w = \cos\left(\kappa_x \frac{X}{R}\right) \cos\left(\kappa_y \frac{Y}{R}\right) \quad (\text{B.2a})$$

$$f = B_1 \cos\left(\kappa_x \frac{X}{R}\right) \cos\left(\kappa_y \frac{Y}{R}\right) \quad (\text{B.2b})$$

where B_1 is a constant and κ_x and κ_y are wavelength parameters.

3. Substitute Equations B.2a into Equations B.1a.

$$B_1 = -\frac{Eh_a R}{\kappa_x^2 + \kappa_y^2} \quad (\text{B.3})$$

4. Substitute B_1 and the bending rigidity D into Equation B.1a and solve for p_e .

$$D = \frac{Eh_b^3}{12(1-\nu^2)} \quad (\text{B.4a})$$

$$p_e = \frac{2E}{R} \left[\frac{h_b^3 (\kappa_x^2 + \kappa_y^2)}{12R^2(1 - \nu^2)} + \frac{h_a}{\kappa_x^2 + \kappa_y^2} \right] \quad (\text{B.4b})$$

where h_b is the thickness from to the bending rigidity.

5. Find the minimum of $\kappa_x^2 + \kappa_y^2$ to solve for the buckling load.

$$\frac{\partial}{\partial (\kappa_x^2 + \kappa_y^2)} p_e = 0 \quad (\text{B.5a})$$

$$\kappa_x^2 + \kappa_y^2 = \sqrt{\frac{12R^2 h_a}{h_b^3}} p_{cr} = \frac{2E}{\sqrt{3(1 - \nu^2)}} \frac{\sqrt{h_b^3 h_a}}{R^2} \quad (\text{B.5b})$$

Bibliography

- (2007). Ripple effect: Glenn howells architects in windsor great park. *Architecture today*, (175):72–78. 18
- Adriaenssens, S., Ney, L., Bodarwe, E., and Williams, C. (2010). Dutch maritime museum: Form-finding of an irregular faceted skeletal shell - part b. p. 1356-1366. 26, 28
- Anderson, R. (2000). *The Great Court at the British Museum*. British Museum Press, London. 26, 28
- Balut, N. and Gioncu, V. (2000). The influence of geometrical tolerances on the behaviour of space structures. *International Journal of Space Structures*, 15(3):189. 29
- Bathe, K.-J. (1996). *Finite element procedures*. Prentice Hall, Englewood Cliffs, N.J. 43
- Bernard, E. S., Coleman, R., and Bridge, R. Q. (1999). Measurement and assessment of geometric imperfections in thin-walled panels. *Thin-Walled Structures*, 33(2):103–126. 55
- Blachut, J. and Galletly, G. D. (1995). Buckling strength of imperfect steel hemispheres. *Thin-Walled Structures*, 23(14):1–20. 55
- Bouhaya, L., Baverel, O., and Caron, J.-F. (2010). Mapping two-way continuous elastic grid on an imposed surface: Application to grid shells. p. 989-998. 28
- Buchert, K. (1965). Buckling of framed domes. *AISC Engineering Journal*, 2(4):120. 29, 32
- Bulenda, T. and Knippers, J. (2001). Stability of grid shells. *Computers & Structures*, 79(12):1161–1174. 29
- Cadji, M. (2001). Wood work: Weald and downland timber gridshell. *RIBA journal*, 108(2):78–79. RW: Cadji, Miriam. 66
- Calladine, C. R. (1995). Understanding imperfection-sensitivity in the buckling of thin-walled shells. *Thin-Walled Structures*, 23(14):215–235. 29, 55

Bibliography

- Chapelle, D. and Bathe, K.-J. (2011). *The finite element analysis of shells*. Springer, Berlin ; Heidelberg, 2 edition. 73
- Chriss, S. and Wright, D. (1978). Analysis of square reticular pattern for hypars. *Journal of Boston Society of Civil Engineers Section, American Society of Civil engineers*, 64(4):149. 30
- Day, A. (1965). An introduction to dynamic relaxation. *The Engineer*, 219. 28
- Delay, T., Famer, S., and Jennings, T. (2009). Executive summary: Building the future, today. Technical Report CTC766, The Carbon Trust. 17
- Douthe, C., Baverel, O., and Caron, J. F. (2006). Form-finding of a grid shell in composite materials. *Journal of the International Association for Shell and Spatial Structures*, 47(150):53. 14
- Engineering, I. A. (2010). *AUI Command Reference Manual*, volume 1. Watertown, MA. 23, 73
- Forman, S. E. and Hutchinson, J. W. (1970). Buckling of reticulated shell structures. *International Journal of Solids and Structures*, 6(7):909–932. 30, 31, 32, 52, 53
- Gioncu, V. (1985). Instability problems in space structures. *International Journal of Space Structures*, 1(3):169–183. 29, 32
- Gioncu, V. (1995). Buckling of reticulated shells. state-of-the-art. *International Journal of Space Structures*, 10(1):1–1. 29, 30
- Hanaor, A. (1995). Design and behaviour of reticulated spatial structural systems. *International Journal of Space Structures*, 10(3):139–149. Compilation and indexing terms, Copyright 2010 Elsevier Inc.; M1: Compendex; undefined; undefined; undefined; undefined; undefined. 29
- Happold, E. and Liddell, W. I. (1975). Timber lattice roof for the mannheim bundesgartenschau. *The Structural Engineer*, 53(3). 15
- Harris, R., Haskins, S., and Roynon, J. (2008). The savill garden gridshell: design and construction. *The Structural Engineer*, 86(17):27–34. 9, 22, 28
- Harris, R., Romer, J., Kelly, O., and Johnson, S. (2003). Design and construction of the downland gridshell. *Building Research & Information*, 31(6):427–454. M3: Article. 28
- Hart, S. (2001). A brilliant shell game at the british museum. *Architectural Record*, 189(3):149–154. PD: Illustration. 28
- Holgate, A. (1997). *The art of structural engineering: the work of Jrg Schlaich and his team*. Edition Axel Menges, Stuttgart. 49

Bibliography

- Hutchinson, J. (1967). Imperfection sensitivity of externally pressurized spherical shells. *Journal of Applied Mechanics*, 34:49. 126
- Keuning, D. (2011). Sander and ney cover two historic buildings with glazed roofs. 28
- Kollar, L. and Dulacska, E. (1984). *Buckling of shells for engineers*. Akademiai Kiado ; Wiley, Budapest; Chichester [W. Sussex]; New York. 31, 32, 52
- Lpez, A., Puente, I., and Serna, M. A. (2007). Numerical model and experimental tests on single-layer latticed domes with semi-rigid joints. *Computers & Structures*, 85(7-8):360–374. 29
- Ouroussoff, N. (2007). A delicate glass roof with links to the past. 28
- Parliament, U. K. (2008). The climate change act. 17
- Persson, P. O. and Strang, G. (2004). A simple mesh generator in matlab. *SIAM Review*, 46(2):329–345. 50
- Pople, N. (2001). Worth the weight: Weald and downland gridshell. *RIBA journal*, 108(9):80–81. RW: Pople, Nicolas. 66
- Pople, N. (2002a). Off the grid: Weald and downland gridshell. *RIBA journal*, 109(5):36–44. RW: Pople, Nicolas. 18, 66
- Pople, N. (2002b). The other gridshell: Goethean science centre, pishwanton scotland. *RIBA journal*, 109(8):54–55. 66
- Schlaich, J. and Schober, H. (1996). Glass-covered grid-shells. *Structural Engineering Internatinoal*, 6(2):88. 26
- Singer, J. and Abramovich, H. (1995). The development of shell imperfection measurement techniques. *Thin-Walled Structures*, 23(14):379–398. 29, 55
- Stansfield, K. (2007). Gridshell covers courtyard formed by historic buildings. 28
- Stungo, N. (2001). Timber talk: Weald and downland timber gridshell. *RIBA journal*, 108(7):60–61. RW: Stungo, Naomi. 66
- Sumec, J. and Sumec, J. m. d. a. s. (1990). *Regular lattice plates and shells*. Elsevier, Amsterdam ; New York. Jozef Sumec.; Translation of: Regulrne mriezkov dosky a skrupiny.; Bibliography: Includes bibliographical references and indexes. 29, 32
- Thornton, J. A. (2000). The new parliamentary building - portcullis house. *The Structural Engineer*, 78(18):17. 28
- Timoshenko, S. (1961). *Theory of elastic stability*. McGraw-Hill, New York, 2d edition. 39, 52

Bibliography

- Vyzantiadou, M. A., Avdelas, A. V., and Zafirooulos, S. (2007). The application of fractal geometry to the design of grid or reticulated shell structures. *Computer-Aided Design*, 39(1):51–59. 29
- Wells, M. (2001). Taking shape: on site at weald and downland. *RIBA journal*, 108(4):75–76. RW: Wells, Matthew. 15
- Williams, C. J. K. (2001). *The analytic and numerical definition of the geometry of the British Museum Great Court Roof*, pages 434–440. Mathematics & design 2001. Deakin University, Geelong, Victoria, Australia. Proceedings of the the Third International Conference on Mathematics & Design, MD-2001. Deakin University, Geelong, Australia, July 3-5, 2001. 26, 28, 29
- Wright, D. T. (1965). Membrane forces and buckling in reticulated shells. *American Society of Civil Engineers Proceedings, Journal of the Structural Division*, 91:173–201. 30, 31, 32, 52